Synthesis and characterization of pure and doped ZnO thin films by colloidal solution route

A Thesis submitted to Gujarat Technological University

for the Award of

Doctor of Philosophy

in

Physics

by

Vipul Jagdishchandra Shukla

149997674005

under supervision of

Dr. Amitkumar J. Patel

GUJARAT TECHNOLOGICAL UNIVERSITY

AHMEDABAD

April-2022

Synthesis and characterization of pure and doped ZnO thin films by colloidal solution route

A Thesis submitted to Gujarat Technological University

For the Award of

Doctor of Philosophy

in

Physics

by

Vipul Jagdishchandra Shukla

149997674005

under supervision of

Dr. Amitkumar J. Patel

GUJARAT TECHNOLOGICAL UNIVERSITY

AHMEDABAD

April-2022

DECLARATION

I declare that the thesis entitled **Synthesis and characterization of pure and doped ZnO thin films by colloidal solution route** submitted by me for the degree of Doctor of Philosophy is the record of research work carried out by me during the period from 18/5/2015 to 20/12/2021 under the supervision of **Dr. Amitkumar J Patel** and this has not formed the basis for the award of any degree, diploma, associate ship, fellowship, titles in this or any other University or other institution of higher learning.

I further declare that the material obtained from other sources has been duly acknowledged in the thesis. I shall be solely responsible for any plagiarism or other irregularities, if noticed in the thesis.

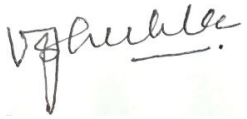

Signature of the Research Scholar: Date: 30/4/2022

Name of Research Scholar: Vipul Jagdishchandra Shukla

Place: Ahmedabad.

CERTIFICATE

I certify that the work incorporated in the thesis **Synthesis and characterization of pure and doped ZnO thin films by colloidal solution route** submitted by **Shri Vipul Jagdishchandra Shukla** was carried out by the candidate under my supervision/guidance. To the best of my knowledge: (i) the candidate has not submitted the same research work to any other institution for any degree/diploma, Associateship, Fellowship or other similar titles (ii) the thesis submitted is a record of original research work done by the Research Scholar during the period of study under my supervision, and (iii) the thesis represents independent research work on the part of the Research Scholar.

Signature of Supervisor:  Date: 30/4/2022

Name of Supervisor: **Dr. Amitkumar J Patel**

Place: Ahmedabad.

Course-work Completion Certificate

This is to certify that **Mr. Vipul Jagdishchandra Shukla** enrolment no. **149997674005** is a PhD scholar enrolled for PhD program in the branch **Physics** of Gujarat Technological University, Ahmedabad.

(Please tick the relevant option(s))

☐ He/She has been exempted from the course-work (successfully completed during M.Phil Course)

☐ He / She has been exempted from Research Methodology Course only (successfully completed during M.Phil Course)

☑ He / She has successfully completed the PhD course work for the partial requirement for the award of PhD Degree. His/ Her performance in the course work is as follows-

Grade Obtained in Research Methodology (PH001)	Grade Obtained in Self Study Course (Core Subject) (PH002)
BC	**BB**

Supervisors Sign:

Name of Supervisor: **Dr. Amitkumar J Patel**

Originality Report Certificate

It is certified that PhD Thesis titled **Synthesis and characterization of pure and doped ZnO thin films by colloidal solution route** by **Vipul Jagdishchandra Shukla** has been examined by us. We undertake the following:

a. Thesis has significant new work / knowledge as compared already published or are under consideration to be published elsewhere. No sentence, equation, diagram, table, paragraph or section has been copied verbatim from previous work unless it is placed under quotation marks and duly referenced.

b. The work presented is original and own work of the author (i.e. there is no plagiarism). No ideas, processes, results or words of others have been presented as Author own work.

c. There is no fabrication of data or results which have been compiled / analysed.

d. There is no falsification by manipulating research materials, equipment or processes, or changing or omitting data or results such that the research is not accurately represented in the research record.

e. The thesis has been checked using https://www.urkund.com (copy of originality report attached) and found within limits as per GTU Plagiarism Policy and instructions issued from time to time (i.e. permitted similarity index <10%).

Signature of the Research Scholar: Date: 30/4/2022

Name of Research Scholar: **Vipul Jagdishchandra Shukla**

Place: Ahmedabad.

Signature of Supervisor: Date: 30/4/2022

Name of Supervisor: **Dr. Amitkumar J Patel**

Place: Ahmedabad.

Curiginal

Document Information

Analyzed document	Vipul J Shukla_PhD_Thesis.docx (D123233736)
Submitted	2021-12-20T15:04:00.0000000
Submitted by	
Submitter email	vipuljshukla317@gmail.com
Similarity	3%
Analysis address	vipuljshukla317.gtuni@analysis.urkund.com

Sources included in the report

W	URL: https://ijisrt.com/assets/upload/submitted_files/1567228217.pdf Fetched: 2021-02-03T07:38:58.6800000	2
W	URL: https://www.researchgate.net/publication/272402893_Effects_of_Na_content_on_structural_and_optical_properties_of_Na-doped_ZnO_thin_films_prepared_by_sol-gel_method Fetched: 2021-09-22T19:16:15.7400000	1
W	URL: https://www.mdpi.com/2079-6412/9/3/202/htm Fetched: 2020-04-04T15:36:32.8100000	2
W	URL: https://www.researchgate.net/publication/248178195_Structural_and_magnetic_property_of_Co-doped-ZnO_thin_films_prepared_by_pulsed_laser_deposition Fetched: 2021-06-12T13:28:13.1300000	2
W	URL: https://www.researchgate.net/publication/263970503_Characterization_of_Dilute_Magnetic_Semiconducting_Transition_Metal_Doped_ZnO_Thin_Films_by_Sol-Gel_Spin_Coating_Method Fetched: 2021-09-11T07:39:08.5200000	1
W	URL: https://www.academia.edu/7876726/Effect_of_fluorine_doping_on_structural_electrical_and_optical_properties_of_ZnO_thin_films Fetched: 2021-12-18T06:17:52.8030000	1
W	URL: https://davidpublisher.com/Public/uploads/Contribute/5ee3395c4b765.pdf Fetched: 2021-12-20T12:31:45.7300000	1
W	URL: https://www.researchgate.net/publication/264461023_Characterization_and_optical_studies_of_pure_and_Sb_doped_ZnO_nanoparticles Fetched: 2019-10-25T13:25:44.2500000	2
J	URL: 02d0c278-6878-480c-b5c2-0ac7a0f98227 Fetched: 2020-02-26T19:54:49.7630000	1
J	URL: 9bd8d0ba-a756-41f2-93f4-fc4ad8e171ee Fetched: 2020-02-26T19:54:47.2370000	2
W	URL: https://www.hindawi.com/journals/ijp/2020/1627498/ Fetched: 2020-12-08T08:52:43.9930000	1
	URL: a5c57af1-642a-4a01-b95b-bac8840f0504	

PhD THESIS Non-Exclusive License to GUJARAT TECHNOLOGICAL UNIVERSITY

In consideration of being a PhD Research Scholar at GTU and in the interests of the facilitation of research at GTU and elsewhere, I, **Vipul Jagdishchandra Shukla** (Full Name of the Research Scholar) having (Enrollment No.) **149997674005** hereby grant a non-exclusive, royalty free and perpetual license to GTU on the following terms:

a) GTU is permitted to archive, reproduce and distribute my thesis, in whole or in part, and/or my abstract, in whole or in part (referred to collectively as the "Work") anywhere in the world, for non-commercial purposes, in all forms of media;

b) GTU is permitted to authorize, sub-lease, sub-contract or procure any of the acts mentioned in paragraph (a);

c) GTU is authorized to submit the Work at any National / International Library, under the authority of their "Thesis Non-Exclusive License";

d) The Universal Copyright Notice (©) shall appear on all copies made under the authority of this license;

e) I undertake to submit my thesis, through my University, to any Library and Archives.

Any abstract submitted with the thesis will be considered to form part of the thesis.

f) I represent that my thesis is my original work, does not infringe any rights of others, including privacy rights, and that I have the right to make the grant conferred by this non-exclusive license.

g) If third party copyrighted material was included in my thesis for which, under the terms of the Copyright Act, written permission from the copyright owners is required, I have obtained such permission from the copyright owners to do the acts

mentioned in paragraph (a) above for the full term of copyright protection.

h) I retain copyright ownership and moral rights in my thesis, and may deal with the copyright in my thesis, in any way consistent with rights granted by me to my University in this non-exclusive license.

i) I further promise to inform any person to whom I may hereafter assign or license my copyright in my thesis of the rights granted by me to my University in this non-exclusive license.

j) I am aware of and agree to accept the conditions and regulations of PhD including all policy matters related to authorship and plagiarism.

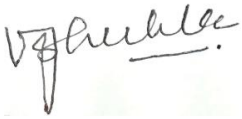

Signature of the Research Scholar: _____

Name of Research Scholar: **Vipul Jagdishchandra Shukla**

Date: 30/4/2022 Place: **Ahmedabad**

Signature of Supervisor:_ _____

Name of Supervisor: **Dr. Amitkumar J Patel**

Date: 30/4/2022 Place: **Ahmedabad**

Seal:

Thesis Approval Form

The viva-voce of the PhD Thesis submitted by Shri. **Vipul Jagdishchandra Shukla**. (Enrollment No.149997674005) entitled **Synthesis and characterization of pure and doped ZnO thin films by colloidal solution route** was conducted on **Saturday, 30th April 2022** (day and date) at Gujarat Technological University.

(Please tick any one of the following option)

☑ The performance of the candidate was satisfactory. We recommend that he/she be awarded the PhD degree.

☐ Any further modifications in research work recommended by the panel after 3 months from the date of first viva-voce upon request of the Supervisor or request of Independent Research Scholar after which viva-voce can be re-conducted by the same panel again.

(Briefly specify the modifications suggested by the panel)

☐ The performance of the candidate was unsatisfactory. We recommend that he/she should not be awarded the PhD degree.

(The panel must give justifications for rejecting the research work)

30-4-2022
Dr. Amit Kumar J. Patel
Asst. Professor (Physics)
Humanities & Sciences
Govt. Engg. College, Godhra
Name and Signature of Supervisor with Seal

Dr. Dimple Shah
1) (External Examiner 1) Name and Signature

2) (External Examiner 2) Name and Signature
Dr. Savita Dixit

30/04/2022
Dr. Nishant N. Patel
3) (External Examiner 3) Name and Signature

ABSTRACT

ZnO, a II-VI group semiconductor having a direct wide band gap (3.37 eV) and large exciton binding energy (60 meV), has great attention of researchers because of its electrical and optical properties which makes it an important material in various applications. ZnO thin film exhibits hexagonal wurtzite crystal structure. High excitonic binding energy, high resistivity against radiation, high breakdown voltage, sensitivity to visible light, and easy wet chemical stability are some of the interesting features of this material. ZnO is mostly being deposited using two ways: vacuum deposition and chemical route. The main drawback of vacuum deposition is the requirement of expensive vacuum equipments. Additionally the throughput of this method is less compared to chemical (colloidal) one. The present work focuses the Chemical Bath Deposition (CBD) method due to its simplicity in requirements. Another advantage of the CBD method over other methods is that the film can be deposited on substrates of different shapes and size. Influence of multiple layering of pure ZnO thin films on the structural, morphological and optical properties are studied. The films of various thicknesses and particle size are prepared by varying the concentration of $ZnCl_2$ as precursor material from 0.1M to 0.5M. Structural, morphological, optical and electrical properties of pure zinc oxide (ZnO) thin films grown by CBD and dip coating method on glass substrates and effect of doping various materials such as copper (Cu: ZnO), sodium (Na: ZnO) and potassium (K: ZnO) on the properties of ZnO thin films grown by CBD on glass substrates are investigated.

Acknowledgement

I would like to express my heartfelt gratitude to everyone who contributed to my thesis and supported me in some way during this incredible journey since without any of them, this research work would not have been possible. I would like to express my sincere appreciation to everyone, some of whom deserve special mention here.

First and foremost, I would like to express my sincere gratitude to my beloved research supervisor **Dr. Amitkumar J Patel**, Assistant Professor (Physics) Government Engineering college, Godhra. Throughout my research period, his continuous guidance, encouragement, inspiration, and concern were astounding. With his unwavering support and constant motivation, the research was successfully finished on schedule and with complete satisfaction. He has been always with me, giving a lot of help with his cordial heart.

My sincere and deep appreciation also goes to **Dr. G. K. Solanki**, Professor, Department of Physics, Sardar Patel University, Vallabh Vidyanagar, a member of my doctoral progress committee (DPC). He gave his valuable suggestions generously and took a keen interest in my research work. My sincere and profound gratitude also goes to **Dr. S. H. Chaki**, Professor, Department of Physics, Sardar Patel University, Vallabh Vidyanagar., who is my other DPC member for always being supportive and encouraging. His critical remarks and insightful comments on how to improve my research work were thoughtful and informative.

Above all, I thank God Almighty, who enabled me with philosophy, perception, and motivation. Last but not least, I would like to say a heartfelt thanks to my family and friends for their unconditional support, care and always being beside me.

Vipul J Shukla

Date: 30/4/2022

Place: Ahmedabad

Table of Content

List of Symbols

Symbol	Meaning
λ	Wavelength
d	Interatomic spacing
θ	Diffraction edge
Å	Angstrom
D	Crystallite or molecular size
β	Full width at half maximum intensity
T	Transmittance
A	Absorbance
R	Optical reflectance
α	Absorption coefficient
Γ_{opt}	Optical phonons at Γ point
R_H	Hall coefficient
V_H	Hall voltage
t	Thickness of the film
I	Electric current
B	Magnetic field
ρ	Resistivity
S	Thermoelectric power
k_B	Boltzmann constant
E_c	Energy of the conduction band edge
E_v	Energy of the valence band edge
E_F	Energy of Fermi level
E_0	Low temperature limit
γ	Temperature coefficient
σ	Electrical conductivity
K	Shape factor
δ	Dislocation density
ε	Micro strain
h	Planck's constant
n	Refractive index
k	Extinction coefficient
ε_r	Real part of dielectric constant
ε_i	Imaginary part of dielectric constant
E_g	Band gap
E_a	Activation energy
η	Carrier concentration
μ	Mobility

List of Figures

List of Tables

CHAPTER 1

Introduction

1.1 Zinc oxide and its properties

Transparent conducting oxide (TCO) thin film has been an impressive study topic in the area of material science in past years. Among the researches on different TCOs, study of zinc oxide (ZnO) has been favored due to its provocative structural, chemical, optical, electrical, etc. properties. The primitive commercially produced semiconducting materials belong to II-VI compounds. Synthesis and characterization of ZnO and ZnO-based alloys (such as Cu: ZnO, Na: ZnO, K: ZnO, Co: ZnO, Mn: ZnO, etc.) are being promoted in research work more and more in recent past. Additionally, ZnO is one of the most significant materials that we notice in our everyday lives. Zinc white is utilized as a basic dye in paints and in preparing layer for paper. Some of the affirmative forms of ZnO integrate its radiation hardness, abundance in nature, nontoxicity, biocompatibility, admirable piezoelectric and semiconducting properties among many others [1].

ZnO thin film presents investigating optical, acoustical and electrical properties with relevant scope of uses in the areas of gadgets, optoelectronics and sensors. ZnO thin film shows optical transmittance property which is high in the visible range so it is practiced to the transparent conductive thin film as well as to the solar cell devices. In the most recent years, low size (Nano, micro) materials have curious consideration due to their size dependent properties and wide scope utilization in distinct fields such as industry, health and environment [2-5]. ZnO is an example of the II-VI semiconductors which gives direct wide band gap (3.37 eV), excitation energy (60 meV) [6,7], and has incredible consideration for researchers due to its electrical and optical properties which support it to be a significant material in many applications such as solar cell, chemical sensors, electroluminescent devices and ultraviolet laser diodes [8-9].

From a more chemical aspects, the lattice can be depicted as two associated hexagonal close packed Zn and O lattices, arranged in that way where each Zn^{+2} and O^{-2} ions are coordinated by four O^{-2} and Zn^{+2} ions respectively in a tetrahedral arrangement. The sp^3 hybridized bonds present in the lattice and are of almost equally ionic and covalent character. Also a few familiar properties of ZnO cover large radiation firmness, active non-linear optical behavior and large thermal conductivity, which prepare the material fascinating for space operations, non-linear optical matters and thermoelectric alternators respectively.

Likewise ZnO have been focused as the dynamic medium in assembling and advancement of transistors due to its n-type electric properties [10]. ZnO thin film can be prepared by numerous chemical preparations, for example, chemical bath deposition (CBD), chemical vapor deposition (CVD), sol–gel spin coating, doctor blade, printing deposition, and electrochemical deposition (ED). These chemical processes are low-cost, simple, and easy to be adjusted or doped by different elements [11, 12]

ZnO seems anisotropic in crystal structure and shows strong absorption in the ultraviolet range. Accordingly it has a few potential applications in windows for photovoltaic solar cell and heterojunction solar cell, IR reflective coatings, piezo-electric and guided optical wave devices, surface acoustic wave (SAW) devices, blue and UV light emitting diodes, phosphors, solid state gas sensors and transducers [13-20]. In transparent conducting oxide structure, the material have applications in solid state display devices, resistors, selective absorber components in solar collectors and in a number of electronic and opto-electronic gadgets [21].

1.2 Thin films of pure and doped ZnO

Zinc oxide is a semiconductor with a wide direct band gap that has appropriateness in certain scientific and industrial areas. ZnO is a main extensively studied semiconductor oxide, as a result of its many versatile and attractive properties, for example, high chemical and thermal stability, non-toxicity [22], ease of preparation, tunable direct wide band gap (3.4 eV), and high transparency in visible range [23]. These properties shows ZnO thin films formulated for different modern industrial applications, for example, in optoelectronic devices [24], lasers, gas sensors, and ultraviolet (UV) light emitters [25], and as defensive surface coatings [26]. ZnO thin film can be reasonably applied in numerous fields, and it likewise has numerous functions such as UV light emitters, hydrophobic coating, and transparent thin film in electronic devices, piezoelectric material, transducers and gas-sensing. ZnO assumes

significant aspect in a number of solar cell systems, such as silicon-based solar cells (first-generation), thin films (second generation), and organic multi-junction, dye-sensitized (third-generation) systems, either as a transparent conductive oxide (TCO) or as a terminal for exciton division [27].

Undoped ZnO is n-type in view of the "intrinsic" shallow donors such as Zn interstitial (Zni) [28], Zni-related complexes [29], hydrogen (H) [30], and H-related complexes [31] inside ZnO. Besides, it has been hypothetically determined that the formation energy of the intrinsic donors in ZnO, such as Zni and oxygen vacancy (VO), is lot of lower than that of the intrinsic acceptors in ZnO, such as oxygen interstitial (Oi) and Zn vacancy (VZn) [32]. So, it is hard to get reliable p-type ZnO because of asymmetrical formation energies between the intrinsic donors and acceptors and the aforementioned intrinsic shallow donors in ZnO, in spite of the fact that analysts have been investigating on the p-type ZnO for many years [33]. Distinctive dopants have been attempted to obtain p-type ZnO materials, such as group-I elements (Li, Na, Ag, and Cu) and group-V elements (N, P, As, Sb, and Bi). Li and Na could be shallow acceptors in ZnO in case they are in substitutional states for Zn sites [32] notwithstanding, these elements favor interstitial states in ZnO due to their moderately small atom sizes, which become donors' states. Among all these potential acceptor competitors, N, P, As, and Sb appear to have better opportunities to obtain p-type doping in ZnO and working gadgets.

Zinc oxide thin films is one of the most contemplated group II-VI semiconducting materials that have gained interest and consideration of many analysts globally due to its extraordinary properties. The little formation energy and large ionisation energy of Cu cause a quick diffusing contamination into ZnO. In addition, copper is familiar as a outstanding luminescent catalyst and forms localized phase in the band gap of ZnO which improves the green luminescent band [34-35]. Cu increases more consideration when used as a dopant because of its ferromagnetism at room-temperature, profound acceptor level, gas sensitivity, improved green luminescence [36-37]. The diffused Cu into ZnO can give rise to the development of complex centres and it is conceivable that Cu atoms can take over Zn atoms either substitutional or interstitial(Cu) in the ZnO lattice making structural deformations, thereby influencing the optical, electrical, chemical, structural and morphological properties of ZnO fundamentally [38].

1.3 Techniques for thin film deposition

Any entity with one of its physical quantity (length, breadth and height) not as much as that of the other two is called a thin film. A deposition technique is considered as the basic key for the preparedness of new thin film materials to fulfill the ever-expanding need from industries for adaptable and multi-dynamics materials. The deposition techniques as shown in Fig.1.1, decide for all intents and purposes all the properties of a thin film and can also be used to vary the existing properties.

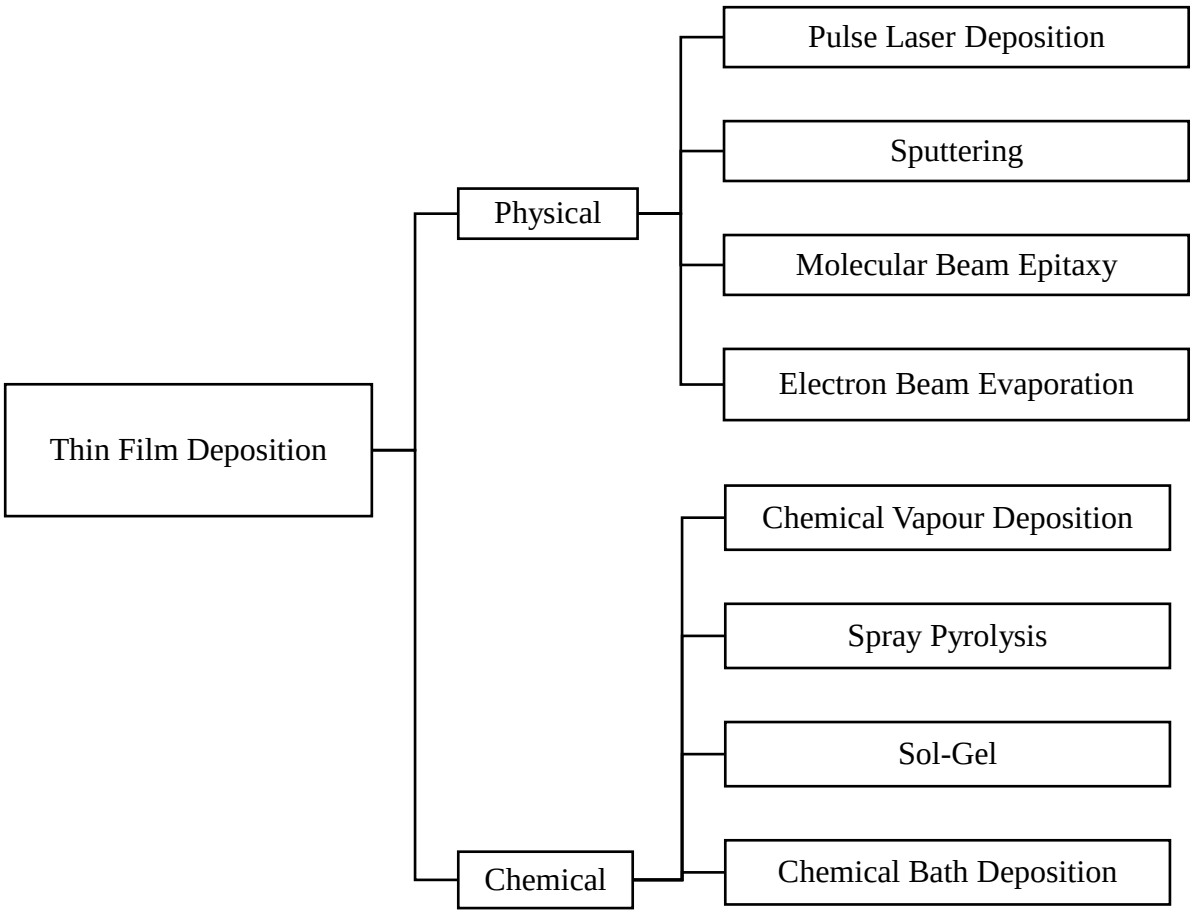

FIGURE 1.1 Types of deposition techniques

Proper consideration should be given to the deposition techniques relying upon the area of utilization in light of the fact that not all the deposition techniques result into the identical properties such as microstructure, surface morphology, tribological, electrical, biocompatibility, optical, corrosion and hardness [39]. ZnO thin films have been prepared

by various deposition techniques, such as pulsed laser deposition [40], r.f. sputtering [41], molecular beam epitaxy [42], electron beam evaporation [43], chemical vapor deposition [44] and spray pyrolysis [45].

Pulsed Laser Deposition (PLD):

Pulsed laser deposition (PLD) is for many reasons a flexible technique. Since with this method the energy source is situated outside the chamber, the utilization of ambient gas as well as ultrahigh vacuum (UHV) is conceivable. Pulsed laser deposition (PLD) is a physical vapor deposition method in which high power pulsed laser beam strikes over a target of the desired composition. The vaporized material deposits as a thin film on a substrate facing the target. This process can take place in ultra-high vacuum or within the sight of a background gas, such as oxygen when depositing films of oxides. During PLD, many trial parameters can be altered, which at that point strongly affect the film properties [40]. An ordinary arrangement for PLD is schematically demonstrated in Fig. 1.2,

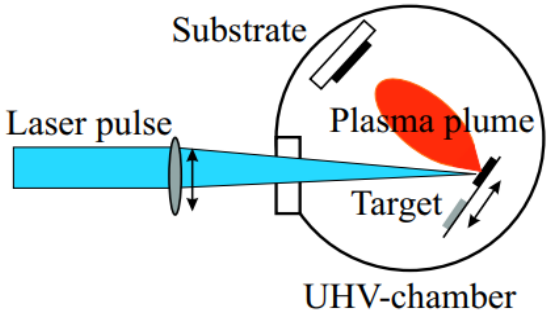

FIGURE 1.2 Schematic diagram of a typical laser deposition set-up

Sputtering:

The general sputtering method is utilized to synthesize a variety of materials, for example, metals, insulators, semiconductors and so forth. Also this method has the favor of simple apparatus, large coating surface, easy to govern and solid adhesion. Sputtering techniques are generally utilized in commercial process since high quality films can be gained at low temperature substrates. The magnetron sputtering technique offers extraordinary favorable circumstances like uniform, homogeneity, and incredible adhesion deposition over the similarly large area, facility to select the substrate material and target material with extremely high melting points, high deposition rate, and also ease to control thickness [46].

However, several disadvantages of reactive sputtering for example target toxicity, poor deposition rates, and arcing causing defects in the thin film [47].

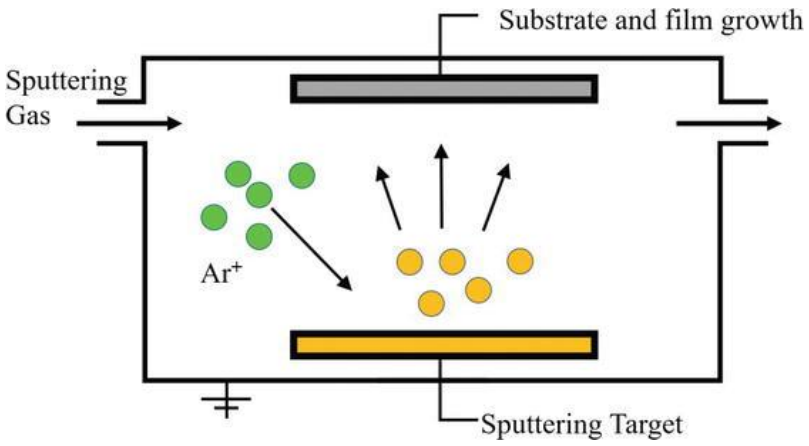

FIGURE 1.3 Schematic diagram of DC sputtering

Molecular Beam Epitaxy (MBE):

Molecular Beam Epitaxy (MBE) is a flexible technique to explore various materials and heterostructures in various substrate combinations. MBE is a laboratory technique used for layer-by-layer development of growth in thin films of various quantum materials. Molecular beam epitaxy is extraordinary in two regards: it is executed in UHV, and it depends on the reaction of atomic as well as molecular beams with a crystalline surface, depending on kinetic processes such as adsorption, desorption, dissociation, migration, reaction, and incorporation. These emphasizes allow real-time in situ monitoring and control during the substrate formation and film growth, to assure the best conditions for stoichiometry and epitaxy [42].

Electron beam evaporation:

Electron beam deposition technique is using electron beams produced in a vacuum from an electron source to irradiate an evaporant material, and heating and vaporizing it with the goal that the vaporized material structures a thin film on a substance, for example, a substrate or a lens. The deviation type electron source that is introduced in a vacuum device is utilized in a wide scope of fields, and we will present the deviation type electron source here. Else ways, the direct-type electron sources are large and powerful, enabling rapid vaporization, and are also utilized for deposition onto long films and large area substrates [43].

Chemical vapour deposition (CVD):

Chemical vapour deposition is a technique where at least one volatile precursors are moved through the vapour phase to the reaction chamber, where they deteriorate on a heated substrate. It is a complicated method of depositing solid materials at a high temperature because of a chemical reaction. This deposition shapes a special type of material usually known as ordered crystal grown from vapour. Numerous materials may be deposited using CVD and related methods. It is the responsive procedures that differentiate CVD process from physical vapour deposition processes, such as physical evaporation process, sputtering and sublimation processes. Chemical vapor deposition is a generally used materials-processing technique. The most of its applications include deposition of solid thin-films on surfaces, however it is additionally used to produce powders and high-purity mass materials, as well as formulating complex materials through infiltration techniques. It has been utilized to deposit an exceptionally wide scope of materials [44].

Spray pyrolysis:

The paralysis implies the decay of chemical compounds or solutions under the presence of heat at very high temperature. In reality, paralysis word is originated from pyro means (heat) and lysis means (breaking). Accordingly, pyrolysis means change under the activity of heat. The splitting of part of complex molecule into simple units by the utilization of heat is called paralysis. It has numerous preferences, such as low processing temperature, high homogeneity and purity of products, etc. The spray paralysis technique is a magnificent technique in material science. A basic and reasonable technique for getting ready thin and thick films, ceramic coatings, and metal and metal oxide powders in large scale is spray paralysis. Spray pyrolysis represents an extremely basic and generally financially savvy handling technique [45].

FIG. 1.4 shows general schematic of a spray pyrolysis deposition process. Spray pyrolysis does not require high-quality substrates or chemicals. The method has been selected for the deposition of thick films, permeable films, and for powder production. Indeed, even multilayered films can be easily prepared utilizing this adaptable technique. Spray pyrolysis is utilized in different gadgets such as fuel cells of solid oxide, sensors and solar units [48].

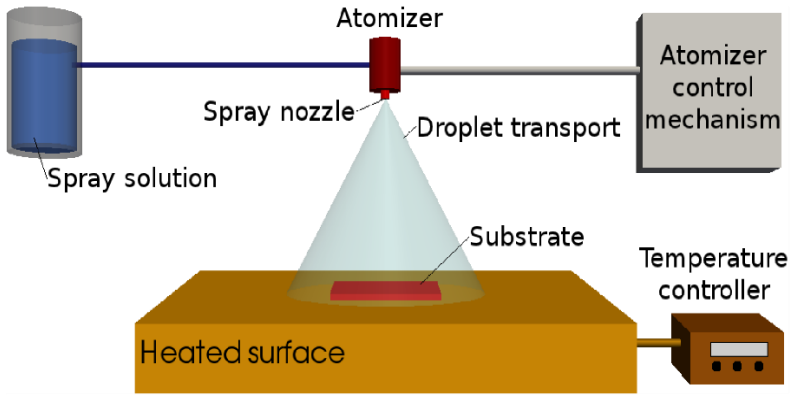

FIGURE 1.4 General schematic of a spray pyrolysis deposition process

1.4 The technique of colloidal solution route

There are three basic types of mixtures – solution, suspension and colloid. Particle size in colloid is intermediate between solutions and suspensions i.e. (1 and 1000 nanometers) in diameter and they remain uniformly dispersed all over the solution. The particles of materials remain scattered and they are not being settled at the base of the container so it is also called as colloidal dispersions. Particles are small enough to remain suspended indefinitely in the suspending medium due to Brownian motion, a random walk resulting from momentum imparted by collision with molecules of the suspending medium. A scattering of solid molecules in a liquid phase is termed a sol. In colloids, one substance is uniformly dispersed in another. The substance being scattered is called dispersed phase and the substance wherein it is scattered is called movable phase.

Solution is a mixture of at least two or more chemical substances. In solution, the substance that is used to dissolve other substances is the solvent (dispersion medium) and the substance which get dissolved is the solute (dispersed phase). The solution state may be solid, liquid or gaseous in which particles are in the form of atoms, ions, or molecules. Colloids or Colloidal solutions is an intermediate stage of a mixture between true solution and suspension [50]. Colloids are too a binary type heterogeneous arrangement consisting of the dispersed medium (continuous or external phase) and dispersion phase (discontinuous or internal phase). The colloidal state seems homogenous when observed with an ordinary microscope or even with naked eye due to uniform distribution of dispersed phase in the respective dispersion medium and invisibility of particles in the colloids. However it is a heterogeneous diffusion of two immiscible phases when observed under an electron-microscope, where colloidal particles reflect the light. Colloidal particles are not being

settled under gravity and colloidal dispersed particles cover large interfacial area due to their submicroscopic size. The large area-to-volume proportion figure outs characteristic properties and behavior of colloids. In other words, it seems that the number of dispersed particles in the colloids is very large and in turn their overall surface area is extremely large too , therefore the interactive force between two phases is significant. Large interfacial action between the two phases is the important factor to study the colloids with the surface phenomena. Adsorption processes taking place on the interface between the dispersed and continuous phases apply considerable effect on the colloid physical properties, chemical reactions in the system and its stability. Colloid properties modify when surface active substances are added to it. Colloidal solutions are classified into two types as lyophilic (solvent loving) and lyophobic colloids (solvent hating) on the basis of interactions between dispersed phase and the dispersion medium

Sol-Gel

The sol-gel process can be expressed as a formation of an oxide network through polycondensation reactions of a molecular precursor in a liquid. A sol is a colloidal or polymer solution in a solvent which is quite stable at room temperature. It contains amorphous or crystalline particles. A gel is made up of a three dimensional uninterrupted network, which includes a liquid phase and a solid medium. In a colloidal gel, the network is built from collection of colloidal particles. The sol–gel process is a wet chemical technique also known as a chemical solution deposition, and involves a sequence of steps which incorporates chemical and physical processes in the following chronological order: hydrolysis and polycondensation, gelation, aging, drying, densification, and crystallization.

Sol-gel synthesis includes a wide scope of organic, inorganic and organic-inorganic permeable materials which follows a common preparation procedure. Ordinarily, the sol-gel process associate the transformation of inorganic system via the development of a colloidal suspension known as sol and sol gelating to form a web in a constant liquid phase (gel). A free streaming sol is changed into a 3D solid network encasing the solvent medium in the process of gelation. At the point of gelation, sudden increase in viscosity and an elastic return to force can be examined. For preparation of aerogels, the gelation is most advantageously incited via pH adjustment of the reaction solution. Under controlled conditions, the pH

change decreases the electrostatic barrier to agglomeration and encourage inter-cluster crosslinking, prompting the development of the 3D network.

The sol-gel process consistently comprises in choosing the precursor of the required material, water and catalysts. Sol-Gel processing assigns a kind of solid materials synthesis procedure, acted in a fluid and at low temperature (commonly T < 100 °C). The solid is composed as a result of a polymerization procedure between the metallic element M of the precursor through bridge formation such as M-OH-M or M-O-M Such changes are what might be compared to the polymerization procedure notable to happen in organic chemistry and which comprises of the foundation of direct bonds between the carbon atoms of organic precursors. A sol is a scattering of suspended colloidal particles through Brownian movement inside a fluid. A mixture having suspended particles of linear dimensions in the range of about 1nm (10 A^o) and 1µm (10^4 A^o) are termed as colloids [51].

The stability of emulsions and suspensions contrary to coagulation is controlled by the interparticle forces. If the particles are forever free, dispersion is expected to be steady. Brownian motion is responsible for the frequent attacks between the particles when fine particles dispersed in a fluid. Such attacks may bring about everlasting connection or the particles remain free rely on the forces between them. The particles experience various kinds of forces between them as follows:-

a) Van der Waals forces: - Van der Waals attractive forces are ever present the particles of the same nature. Hamaker [52] determined equations for these attractive forces based on additivity of Vander Waals energies between pairs of atoms or molecules, and expecting these energies to be corresponding to the inverse sixth-power dependence on the separation.

b) Electrostatic forces:- Electrostatic forces are present because of the inter-attractive forces of the electrical twofold layers surrounding the particles. If particles are chemically similar and they have surface potentials and surface charges of a similar sign and magnitude then repulsion takes place between the particles because of electrostatic forces.

Monoliths, films, powders and fibers got from the gel phase mixed with microstructural and configurational control and depressed preparing temperature finds applications in different fields. Thin films as well as coatings find utilizations for electronic, optical, porous and protective thin films or else coatings. Furthermore, Monoliths find utilizations as transparent super protection, ultra-low enlargement glasses and optical parts. Powders, grains and spheres are utilized as ceramic precursors or cutting grains. Fibers drawn from viscous sols are utilized mainly for support or manufacture of refractory textiles. Gels can be utilized as molds for particle-fortified composites and as anchors for organic, ceramic or metallic

phases. Porous gels and membranes find application in filtration, separations, catalysis and chromatography.

Sol-gel method offers many advantages for synthesizing large materials with homogeneity due to mixing at the molecular level and great purity. This method is considered as versatile method due to better control of the structure, including porosity and particle size; possibility of incorporating nanoparticles and organic materials into sol-gel-derived oxides. It also provides extended composition ranges and allows the fabrication of any oxide composition but also some non-oxides as well as the production of new hybrid organic-inorganic materials, which do not exist naturally. It requires less energy consumption as there is no need to reach the melting temperature and the network structure can be achieved at relatively low temperatures. It has found a wide range of applications from coatings to preparation of thin films, monoliths, composites, porous membranes, powders and fibers. Also it does not require special or expensive equipments.

Chemical Bath Deposition

Chemical Bath Deposition technique includes controlled precipitation of a compound from the solution on an appropriate substrate.

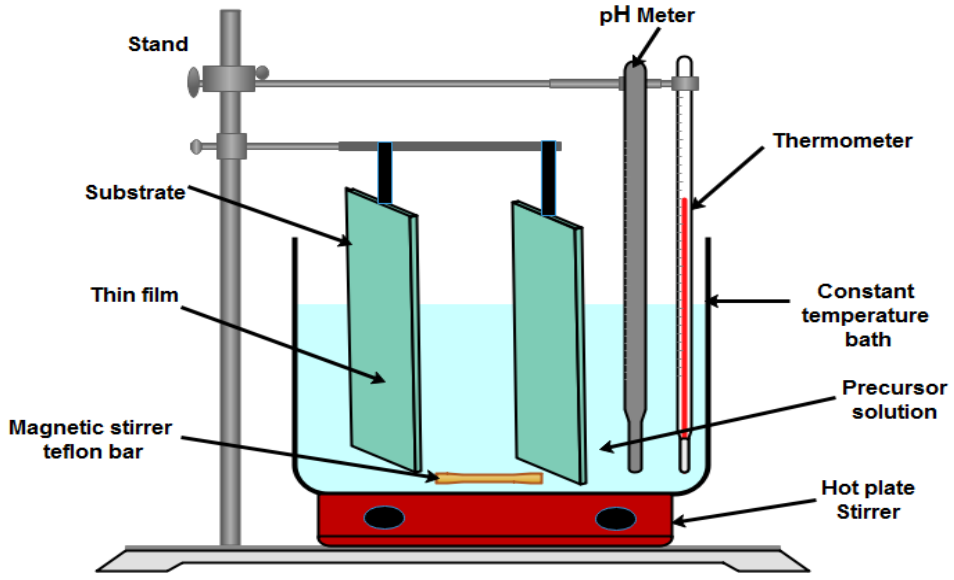

FIGURE 1.5 Set up of chemical bath deposition process

The chemical bath deposition (CBD) (Fig.1.5) technique has extraordinary commercial esteem when compared to the thermal vaporization, sputtering and other chemical methods,

and has pulled in much consideration by the scientist due to its reproducibility, large area scaling, simplicity, comfort, and industrial production [49]. The chemical bath deposition has a favorable position over different techniques since it is exceptionally simple, it does not require specific equipments, it utilizes low temperature and has low cost of deposition. The ability of this method to coat large areas in a reproducible and low cost process is the most appealing favorable stand. Elsewise, CBD method has important advantages over the other methods as follows.

- → CBD is the simplest method.
- → It makes possible to deposit multi compound chalcogenide thin films over a wide scope of stoichiometry.
- → In CBD, high vacuum is not required for chemicals and can be carried out even at room temperature.
- → Large area deposition can be obtained by taking some precautions, for example, lying down the substrate on a shallow tray containing the deposition bath.
- → Uniform well adherent and reproducible thin films for photovoltaic applications are the advantages of this method.
- → It is an economical method for large scale industrial usages.
- → The material is used in less amount with minimum loss.
- → The size of crystallites in the CBD prepared films is very small.

1.5 Application of ZnO thin films

The interest in studying ZnO thin films decreased more and more. Subsequently, the possibility to combine simultaneously the benefits of thin-film based synthesis technologies along with a high surface area and a permeable structure might represent an incredible solution to synthesize ZnO thin films with extraordinary physical and chemical characteristics that may find use in novel application fields. The outcomes of different research works brought out by various groups confirm that the structural, morphological, electrical, optical and optoelectronic properties of ZnO change broadly relying upon the method of development. Enormous variety of properties of pure and doped ZnO thin films has been accounted till date. In this chapter, significant utilizations of ZnO thin films have been talked about. ZnO is acceptable material whereupon to construct useful devices, because of their less hazardous nature, acceptable thermal stability, great oxidation

resistibility, great biocompatibility, huge specific surface area and high electron mobility [53].

ZnO is an alluring material for applications in electronics, photonics, sensing and acoustics. It is a critical component in different industrialized processes, for example, paints, cosmetics, drugs, plastics, batteries, electrical equipment, rubber, cleanser, textiles, floor coverings, and so on Development advances of ZnO single crystals, epitaxial layers, nanostructures, and nanoparticles are improving step by step.

ZnO nanoparticles have caused revolution in the advancement of improved sunscreens, paints and coatings to give some examples. Moreover, the radiation hardness of ZnO to high energy proton irradiation makes it an ideal possibility for space applications [54].

Zinc oxide likewise has antibiotic and oxygenating properties. Hence it is applied in clinical operations, for example, in baby powder and ointments to treat diaper rashes, other skin irritations and even dandruff. Because of its reflective properties it is also utilized in sunblocks and can regularly be seen on the nose and lips of lifeguards at the sea shore. ZnO as of now has a wide scope of utilizations, because of its novel properties which are being investigated and applied, recently. It very well may be anticipated that in future ZnO devices will become essential part of our everyday lives.

1.6 Significant contribution of the present work

In present work, zinc oxide (ZnO) multilayer thin films are grown on glass substrate using chemical bath deposition technique and the consequence of these multilayer films on optical, morphological and structural properties are explored. It is noticed that these multilayer thin films have considerable effect on the properties of ZnO. X-ray Diffraction (XRD) affirms the hexagonal wurtzite structure of ZnO. Scanning Electron Microscopy (SEM) demonstrates the scratch-free films which have evenly scattered crystalline structures and presence of particles of ZnO on thin films. The optical absorption spectra measured using UV–Vis. displayed the average transmittance in the visible region for all films which is favorable for solar spectra. The consummation of the multilayer just as transparent conducting material is preferable compared to the single layer of ZnO. TGA analysis of powder obtained by drying precursor solution determines the appropriate annealing temperature for the as grown films.

Zinc oxide thin films were developed on glass substrate using aqueous solution of $ZnCl_2$ and NH_3 through chemical bath deposition method (CBD). Films of various thicknesses, particle size and other useful analysis have been obtained by varying the concentration of $ZnCl_2$ from 0.1M, 0.2M, 0.3M, 0.4M and 0.5M. Optical properties of grown films and influence of precursor concentration on them are analyzed by the transmittance recorded in the range 200-1200 nm. Deposited films are also characterized by powder X-ray diffraction and SEM to understand the influence of variation in precursor concentration on structural and morphological properties of grown films. XRD patterns confirmed the hexagonal wurtzite structure of the deposited pure ZnO films.

The consequences of copper (Cu) doping on the properties of ZnO thin films grown on glass substrates by chemical bath deposition (CBD) and dip coating method are explored. Optical properties are explored through UV-VIS-NIR transmittance and reflectance spectroscopy. Photoluminescence spectra of the samples display prominent peaks reciprocal to blue emission, defect relevant green emission in the visible region at room temperature and their feasible mechanism have also been analyzed. Hall Effect Measurements, Resistivity, Raman and photoluminescence (PL) examinations of pure ZnO and copper (Cu), potassium (K) and sodium (Na) doped ZnO thin films on glass substrate through colloidal solution route have been executed. The affects of dopant content on carrier concentration, electrical resistivity, and hall mobility of the thin films were assessed from Hall Effect measurements. Temperature dependent electrical resistivity measurements are executed using two probe method and activation energy for the electrical conductivity of pure and doped ZnO are determined. The Raman scattering of the pure ZnO and Copper (Cu), Potassium (K) and Sodium (Na) doped ZnO displays the first and second orders of polar and non-polar forms. Photoluminescence (PL) at room temperature outcomes express the emission arises at close band lines and the outcomes are classified with a few constitutional imperfections in the doped ZnO thin films. Raman spectroscopy and photoluminescence affirm presence of zinc interstitials (Zni) as well as oxygen vacancies (V_o). The spectroscopy study to the samples concluded the significance of phonon-electron connections, expecting the vital role play in the semiconductor e.g. ZnO.

CHAPTER 2

Literature Review and Aim of the Work

2.1 Review of literature

2.1.1 ZnO structure

Zinc oxide (ZnO) is an inorganic compound. It typically shows up as a white powder, almost insoluble in polar solvents like water. In powder form, it is broadly utilized as an added substance into various materials and items including plastics, earthenware production, glass, cement, elastic (for example vehicle tyres), oils, paints, balms, cements, sealants, shades, nourishments (wellspring of Zn supplement), batteries, ferrites, fire retardants, etc.[55]. ZnO is available in the Earth crust as a zincite mineral; in spite, most ZnO utilized economically is formed artificially. In materials science, ZnO is frequently called a II-VI semiconductor since zinc and oxygen have a place in the second and sixth group of the modern periodic table, respectively. This semiconductor has a few positive properties: good transparency, high electron mobility, wide band gap, stable and high room temperature, incandescence, and so on. [56-57].

Zinc oxide usually takes shape in hexagonal wurtzite, cubic zinc blende, and infrequently noticed in cubic stone salt structure. The wurtzite structure is generally substantial and hence generally typical at ambient conditions.

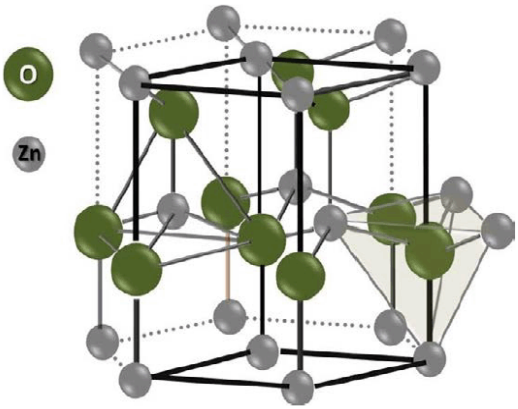

FIGURE 2.1 Wurtzite Hexagonal Crystal Structure of Zinc Oxide

The zinc blende structure can be balanced out by developing ZnO on substrates with the structure of cubic lattice. In the two cases, the zinc and oxide are tetrahedral. The hexagonal and zinc blende lattice have no reversal conformity ((reflection of a crystal moderately any given point doesn't change it into itself). All these lattice symmetry properties bring about piezoelectricity of the hexagonal and zinc blende ZnO, and in pyro-electricity of hexagonal ZnO. As in most II-VI substances, the bonding in ZnO is more ionic in nature, which supports its considerable piezoelectricity property. Because of this more ionic nature, zinc and oxygen planes carry electric charge (positive and negative, individually). In this aspect, to maintain electrical neutrality, those planes come about at atomic level in most corresponding materials, yet not in ZnO - its surfaces are molecularly even, balanced and show no reformation [58].

ZnO can develop on single crystal substrates. ZnO is non-poisonous and thermally steady; subsequently it is generally utilized in coatings of the substances. ZnO shows crystallization in two significant structures, hexagonal wurtzite [59] and cubic zinc blende. The wurtzite structure is generally steady at ambient conditions and hence most regularly found in ZnO. Preparation of ZnO on substrates with cubic lattice structure preserves the zinc blende structure. For both the cases, the Zn and O develop tetrahedrons with the most extraordinary geometry for Zn (II). ZnO to the rock salt pattern conversion occurs at moderately high pressures around 10 GPa [60]. Hexagonal and zinc blende polymorphs have irreversible symmetry. Piezoelectricity of the hexagonal and zinc blende ZnO is due to lattice symmetry properties. The lattice constants are a = 3.25 Å and c = 5.2 Å; their proportion c/a ~ 1.60 is near the ideal value for hexagonal cell c/a = 1.633 [61]. Structural properties of pure and doped ZnO thin films are shown in Table 2.1.

Table 2.1 Structural properties of ZnO (pure and doped) thin films.

Sr	Precursor materials Solvent Method of preparation Substrate	Thickness (nm)	Crystalline/ amorphous	Particle Size (nm)	Orientation of film	Crystal structure	Surface roughness (nm)	Ref.
ZnO-CBD								
1	Zinc acetate dihydrate Water	---	Crystalline	30-44	[100], [002], [101]	Hexagonal wurtzite	---	[62]
2	Zinc sulphate Water	---	Crystalline	64-187	[100], [002], [101]	Hexagonal wurtzite	---	[63]
3	Zinc sulphate Water Glass	2000–5000	Crystalline	---	[002]	Hexagonal wurtzite	---	[64]
4	Zinc sulphate Water Glass	200 to 700	Crystalline	10	[100], [002], [102]	Hexagonal wurtzite	---	[65]
5	zinc chloride Ammonia Glass	---	Crystalline	---	---	---	---	[66]
6	zinc chloride NaOH Glass	286 - 180	Crystalline	---	[100], [002], [101], [110], [002]	---	---	[67]
7	zinc chloride Water Silicon	---	Crystalline	57	---	---	---	[68]
8	Zinc sulphate Glass	1100-1700	Crystalline	---	---	---	---	[69]

ZnO-Sol gel								
9	Zinc acetate water	250-334	Crystalline	25.5-31.9	[100],[002],[101]	Hexagonal wurtzite	---	[70]
10	Zinc acetate dihydrate 2-methoxyethanol Glass	---	Crystalline	30, 70.5, 88.1	[100], [002], [101]	Hexagonal wurtzite	---	[71]
11	Zinc acetate dihydrate Ethanol Glass	370	Polycrystalline	---	[002]	Hexagonal wurtzite	---	[72]
12	Zinc acetate n-propanol and glycerol Si[100] and Quartz	180	Polycrystalline	45	[002], [101]	Hexagonal wurtzite	---	[73]
13	Zinc acetate Silicon	380	Polycrystalline	4.87	[100], [002], [101], [102], [110]	Hexagonal wurtzite	---	[74]
14	Zinc acetate dihydrate Ethanol Glass	---	---	32-104	---	---	---	[75]
15	Zinc acetate dihydrate Methanol	200	Polycrystalline	40	---	Hexagonal wurtzite	---	[76]
16	Zinc acetate dihydrate Ethanol		Crystalline	28, 54	[100], [002], [101]	Hexagonal wurtzite		[77]
17	Zinc acetate dihydrate 2-methoxyethanaol Glass	257-277	Crystalline	---	[002]	Hexagonal wurtzite	6 to19 nm	[78]
18	Zinc acetate dihydrate 2-methoxyethanol	---	Crystalline	1127	[100], [002], [101]	Hexagonal wurtzite	---	[79]
19	Zinc acetate dihydrate 2-methoxyethanol Silicon	100	Crystalline	---	[002]	Hexagonal wurtzite	---	[80]

Cu:ZnO- CBD								
20	Zinc salt Water	18.95-37.80	---	---	[100], [101]	---	---	[82]
21	Zinc acetate dehydrate Water	---	---	40-26	[101]	---	---	[83]
22	Zinc acetate	---	Crystalline	74.14- 86.09	[101]	Hexagonal wurtzite	---	[84]
Cu:ZnO- Spray pyrolysis								
23	Zinc nitrate Water Glass	1000	Nanocrystalline	10 - 22	[002]	Hexagonal wurtzite	---	[81]
24	Zinc chloride Water Glass	---	---	46.8- 52.2	[100], [101], [002]	Hexagonal wurtzite	---	[85]
25	Zinc acetate Water Glass	---	Nanocrystalline	36.7- 38.2	[101], [002]	Hexagonal wurtzite	---	[86]
26	Zinc acetate dehydrate Chloroform Glass	---	---	96.2-22.3	[100]	Hexagonal wurtzite	---	[87]
Cu:ZnO- Sol gel								
27	Zinc acetate dehydrate Water Glass	---	Polycrystalline	---	---	Hexagonal wurtzite	---	[88]
28	Zinc acetate dehydrate 2-methoxyethanol Glass	---	Polycrystalline	13.88-9.25	[101]	---	---	[89]

29	Zinc acetate dehydrate Glass	---	Polycrystalline	30-45	[100], [101], [002]	---	---	[90]
30	Zinc acetate Water Glass and Silicon	230-160	---	8-22	[002]	---	---	[91]
Na:ZnO- Sol gel								
31	Zinc acetate dehydrate Ethanol Glass	---	Crystalline	---	[002]	Hexagonal wurtzite	10.92	[92]
32	Zinc acetate ethylene glycol monomethyl ether Silicon	---	---	---	---	Hexagonal wurtzite	---	[93]
33	Zinc acetate dehydrate ethylene glycol monomethyl ether Silicon	365	Crystalline	---	---	Hexagonal wurtzite	44.4	[91]
34	Zinc acetate dihydrate 2-methoxyethanol Glass	300	Polycrystalline	42.97 - 56.17	[002]	Hexagonal wurtzite	16.2-53	[95]
35	Zinc acetate dihydrate Silicon	---	Polycrystalline		[002]	Hexagonal wurtzite	3.37-16.9	[96]
36	zinc acetate 2-methoxyethanol Glass	150	Crystalline	58.11 - 66.86	[002]	Hexagonal wurtzite	---	[97]
37	Zinc acetate dihydrate 2-methoxyethanol Glass	300	Crystalline	---	[002]	Hexagonal wurtzite	---	[98]
38	Zinc acetate dihydrate 2-methoxyethanol Silicon	---	Polycrystalline	38 - 49	[002]	Hexagonal wurtzite	---	[99]

39	Zinc acetate dehydrate 2-methoxyethanol Glass	---	Crystalline	20.4 - 21.6	[002]	Hexagonal wurtzite	2.49 - 3.23	[100]
40	Zinc acetate dihydrate 2-methoxyethanol Glass	1310-823	Crystalline	50	[002]	Hexagonal wurtzite	---	[101]
41	Zinc acetate dehydrate ethylene glycol monomethyl ether Glass	497	Polycrystalline	6.2 - 16.6	[002]	Hexagonal wurtzite	---	[102]
42	Zinc acetate dehydrate 2-methoxyethanol Glass	---	Crystalline	17.1 - 21.7	[002]	Hexagonal wurtzite	---	[103]
K:ZnO- CBD								
43	Zinc chloride Water Glass	1880-4180	Polycrystalline	6 - 11 nm	---	Hexagonal wurtzite	---	[104]
44	Zinc acetate Methanol	---	Crystalline	10-17 nm	[100], [002], [101]	Hexagonal wurtzite	---	[105]
45	Zinc chloride Water Glass	4.348-6.520 µm	Crystalline	77.39-82.55 nm	[002]	Hexagonal wurtzite	---	[106]
46	zinc nitrate Water Glass	---	Crystalline	11.26 nm	---	Hexagonal wurtzite	---	[107]
47	Zinc chloride Water Glass	570-905	Polycrystalline	---	[100], [002], [101]	Hexagonal wurtzite	---	[108]

K:ZnO- Sol gel								
48	Zinc acetate dehydrate 2-methoxyethanol Glass	450 nm	Polycrystalline	---	[002]	Hexagonal wurtzite	---	[109]
49	Zinc acetate dehydrate 2-methoxyethanol Glass	---	Crystalline	20.87-21.96	[002]	Hexagonal wurtzite	---	[110]
50	Zinc acetate dehydrate Isopropanol Glass and Silicon	230-440	Polycrystalline	33-25	[002]	Hexagonal wurtzite	---	[111]
51	Zinc acetate dehydrate 2-methoxyethanol Glass	---	Crystalline	30.24-32.48	---	Hexagonal wurtzite	9.79	[112]
52	Zinc acetate dehydrate Ethanol Glass	138-145	Crystalline	95	---	---	---	[113]
53	Zinc acetate Ethanol Glass	---	Crystalline	18	[002]	Hexagonal wurtzite	---	[114]

2.1.2 Electrical properties of ZnO

Lately, researchers have made fast and noticeable advances in the field of materials science, particularly in semiconductor material science. One of the main fields of current interest in materials science is the improvement of basic forms and uses of transparent conducting oxide thin films (TCO). The attributed properties of such coatings are low electrical resistivity and high transparency in the visible region. The ZnO thin films have appealed important consideration as a wide gap semiconductor because of their wide scope of electrical properties. The high chemical stability, melting point and enormous exciton binding energy of ZnO cause it to turn into a promising UV and blue optoelectronic material. ZnO has a generally wide direct band gap of ~3.3 eV at room temperature. A wide band gap put together higher breakdown voltages, capacity to support wide electric fields, lower electronic buzz, and high-temperature as well as high-power applications.

The free carriers' concentration can be readily controlled in this compound, for example, by getting "as grown" ZnO thin films with significantly decreased degree of electrically dynamic unexpected imperfections, which present donor levels under the conduction band and subsequently raise n-type conductivity. These imperfections can either be local (e.g., oxygen vacancies, zinc interstitials [115]) or fused ones, (for example, hydrogen atoms [116]).

Mostly ZnO shows n-type behavior even in the case of without doped material. Nonstoichiometric is normally the origin of n-type behavior [117]. For the hypothetical computations a constituent clarification proposed that unexpected substitutional hydrogen impurities are liable [118]. Predictable p-type doping of ZnO lasts unsettled and this complication initiates from low solubility of p-type dopants and their compensation by many n-type impurities.

Current drawbacks to p-doping restrict electronic and optoelectronic properties of ZnO, which generally depend on junctions of n-type and p-type material. Common p-type dopants are group-I elements Li, Na, K; group-V elements N, P and As; just as copper and silver. Be that as it may, many of these structure very intense acceptors and don't cause noteworthy p-type conduction at room temperature [115].

It is researched the impact of pure ZnO and doped ZnO on electrical properties of ZnO thin films with the intention to improve the film properties. The electrical properties were graded by two-probe analysis. Cu: ZnO, Na: ZnO and K: ZnO films have drawn in expanding

measures of consideration because of their auspicious feasible applications in semiconductor appliances. ZnO behaves as a n-type conductor, and efforts have been made for the different types of doping in ZnO to upgrade the electrical properties. This research explored the growth in electrical properties of Cu: ZnO, Na: ZnO and K: ZnO films and decided the dopant concentration at which the conductivity of doped thin films will change from n-type to p-type. The electrical resistivity, conductivity, ionization energy, versatility and carrier concentration are estimated for the thin films. Electrical properties of pure and doped ZnO thin films are shown in Table 2.2.

Table 2.2 Electrical properties of ZnO (pure and doped) thin films

Sr	Precursor materials Solvent Method of preparation Substrate	Resistivity (Ω-cm)	Conductivity (Ω^{-1} cm^{-1})	Mobility (cm^2/Vs)	Carrier type	Carrier concentration (cm^{-3})	Ref.
ZnO -CBD							
1	Zinc acetate dihydrate Water	---	---	---	n-type	---	[62]
2	Zinc sulphate Water	---	---	---	n-type	---	[63]
3	Zinc sulphate Water Glass	---	---	---	n-type	---	[64]
4	Zinc sulphate Water Glass	6.48×10^{-1}	---	1.1×10^{-2}	---	2.24×10^{19}	[65]
5	zinc chloride Ammonia Glass	---	---	---	---	---	[66]
6	zinc chloride NaOH Glass	---	---	---	---	---	[67]
7	zinc chloride Water Silicon	---	$1.28\ x10^{11}$	---	n-type	---	[68]
8	Zinc sulphate Glass	---	---	---	---	---	[69]
ZnO-Solgel							
9	Zinc acetate	---	---	---	---	---	[70]

	water						
10	Zinc acetate dihydrate 2-methoxyethanol Glass	2.5×10^{-3}	---	---	---	---	[71]
11	Zinc acetate dihydrate Ethanol Glass	5×10^{-2}	---	---	n-type	---	[72]
12	Zinc acetate n-propanol and glycerol Si[100] and Quartz	---	---	---	n-type	---	[73]
13	Zinc acetate Silicon	---	---	---		---	[74]
14	Zinc acetate dihydrate Ethanol Glass	---	---	---	n-type	---	[75]
15	Zinc acetate dihydrate Methanol	---	---	---	n-type	---	[76]
16	Zinc acetate dihydrate Ethanol	---	---	---		---	[77]
17	Zinc acetate dihydrate 2-methoxyethanaol Glass	---	---	---		---	[78]
18	Zinc acetate dihydrate 2-methoxyethanol	---	---	---	n-type	---	[79]
19	Zinc acetate dihydrate 2-methoxyethanol Silicon	---	---	---	n-type	---	[80]
Cu:ZnO-CBD							
20	Zinc salt Water	---	---	---	---	---	[82]
21	Zinc acetate dehydrate	---	---	---	---	---	[83]

	Water						
22	Zinc acetate	---	---	---	---	---	[84]
Cu:ZnO- Spray pyrolysis							
23	Zinc nitrate Water Glass	---	---	---	---	---	[81]
24	Zinc chloride Water Glass	0.36	---	---	---	---	[85]
25	Zinc acetate Water Glass	6.58 - 2.93	---	---	---	---	[86]
26	Zinc acetate dehydrate Chloroform Glass	---	---	---	---	---	[87]
Cu:ZnO- Solgel							
27	Zinc acetate dehydrate Water Glass	---	---	---	---	---	[88]
28	Zinc acetate dehydrate 2-methoxyethanol Glass	---	---	---	---	---	[89]
29	Zinc acetate dehydrate Glass	---	---	---	---	---	[90]
30	Zinc acetate Water Glass and Silicon	9.64 -214.56 x 10^{-4}	---	---	---	---	[91]
Na:ZnO - Solgel							

31	Zinc acetate dehydrate Ethanol Glass	1.89×10^{3} -2.35×10^{3}	---	p-type	$2.19\text{x } 10^{13}$ -$7.15\text{x } 0^{13}$	$1.50\text{x}10^{2}$ - $3.70\text{x}10^{1}$	[92]
32	Zinc acetate ethylene glycol monomethyl ether Silicon	75.7	---	p-type	$2.955 \text{ x } 10^{16}$	2.1	[93]
33	Zinc acetate dehydrate ethylene glycol monomethyl ether Silicon	---	---	---	---	---	[94]
34	Zinc acetate dihydrate 2-methoxyethanol Glass	---	---	---	---	---	[95]
35	Zinc acetate dihydrate Silicon	---	---	---	---	---	[96]
36	zinc acetate 2-methoxyethanol Glass	0.92	---	p-type	$5.17 \text{ x } 10^{18}$	1.3	[97]
37	Zinc acetate dihydrate 2-methoxyethanol Glass	---	---	---	---	---	[98]
38	Zinc acetate dihydrate 2-methoxyethanol Silicon	---	---	p-type	---	---	[99]
39	Zinc acetate dehydrate 2-methoxyethanol Gass	826.47 - 514.19	---	---	$4.9 \text{ x } 10^{16}$	0.15 - 10.66	[100]
40	Zinc acetate dihydrate 2-methoxyethanol Glass	---	---	---	---	---	[101]

41	Zinc acetate dehydrate ethylene glycol monomethyl ether Glass	---	---	---	---	---	[102]
42	Zinc acetate dehydrate 2-methoxyethanol Glass	---	---	---	---	---	[103]
K:ZnO-CBD							
43	Zinc chloride Water Glass	---	---	---	---	---	[104]
44	Zinc acetate Methanol	---	---	---	---	---	[105]
45	Zinc chloride Water Glass	---	---	---	---	---	[106]
46	zinc nitrate Water Glass	---	---	---	---	---	[107]
47	Zinc chloride Water Glass	---	---	p-type	---	---	[108]
K:ZnO -Solgel							
48	Zinc acetate dehydrate 2-methoxyethanol Glass	---	---	---	---	---	[109]
49	Zinc acetate dehydrate 2-methoxyethanol Glass	---	---	---	---	---	[110]
50	Zinc acetate dehydrate Isopropanol	---	---	p-type	4.0×10^{16}	39 - 85	[111]

	Glass and Silicon						
51	Zinc acetate dehydrate 2-methoxyethanol Glass	---	---	---	---	---	[112]
52	Zinc acetate dehydrate Ethanol Glass	---	---	---	---	---	[113]
53	Zinc acetate Ethanol Glass	---	---	n-type	---	---	[114]

2.1.3 Optical properties of ZnO

Semiconductor are classified as intrinsic and extrinsic on the basis of their optical properties. Intrinsic transitions arise between the electrons and holes present in the conduction band and valence band respectively. Dopants or deficiencies commonly make different electronic states in the band gap which helps in identification of extrinsic transitions. So by contemplating the optical properties one can discover the crystalline quality, band gap of the material as well as the position of the deficiency levels in the semiconductor. An exact information on the optical properties of ZnO is significant for the design and investigation of different optical and optoelectronic devices. There are a variety of experimental methods accessible for the investigation of optical transitions in ZnO, for example, optical absorption, transmission, photoluminescence (PL), cathodoluminescence, photo-reflection, and spectroscopic ellipsometiy and so forth among which the initial three properties relevant to the aim of the current thesis work would be discussed in brief. Optical constants values of ZnO, for example, refractive index (n) and extinction coefficient (k) respectively are reported to be 1.60 and 0.022 at the wavelength 550 nm. [119].

However, the optical constants also shift contingent upon the development strategy. PL spectrum of ZnO is typically made out of a near band edge (NBE) UV-emission band which is associated with the excitonic transition and a green emission band (- 510 nm) [120-121]. In wurtzite ZnO, the conduction band emerges from the Zn^{2+} 4s state, though the upper valence band from the O2' 2p state with an admixture of Zn^{2+} 3d levels. Because of the impact of hexagonal crystal-field and spin-orbit interactions, the valance band cleave into three bands [122].

Origin of the green emission has been a subject of incredible discussion [123]. Various hypotheses have been proposed to clarify the green emission, for example, transition between singly ionized oxygen vacancy and photoexcited hole [124], transition between electron near the conduction band and a deeply trapped hole at V_{0t}^{+} [125], surface deficiencies [126], and so on. If there should arise an occurrence of Cu doped ZnO, this green luminescence band occurs with a characteristic of fine structures. Zn vacancy is also recommended as a reason for this green luminescence [127-128], Theoretically, it is discovered that transition level between the - 1 and - 2 charge states happens at 0.9 eV over the valance band maximum [129] and subsequently a transition between the conduction band (or a shallow donor) and the V_{Zn} acceptor level would offer ascent to luminescence around

2.5 eV which is in acceptable concurrence with noticed green luminescence. Optical properties of pure and doped ZnO thin films are shown in Table 2.3.

Table 2.3 Optical properties of ZnO (pure and doped) thin films

Sr	Precursor materials Solvent Method of preparation Substrate	Bang gap (eV)	Transmittance	Reflectance	Refractive index	Dielectric constant-Real part	Dielectric constant-Imaginary part	Extinction coefficient	Ref.
ZnO-CBD									
1	Zinc acetate dihydrate Water	3.23 - 3.20	---	---	---	---	---	---	[62]
2	Zinc sulphate Water	3.27-3.30	---	---	---	---	---	---	[63]
3	Zinc sulphate Water Glass	3.37	---	---	---	---	---	---	[64]
4	Zinc sulphate Water Glass	3.3	60-80%	---	---	---	---	---	[65]
5	zinc chloride Ammonia Glass	2.72 - 2.60	---	---	---	---	---	---	[66]
6	zinc chloride NaOH Glass	2.59 - 3.57	---	---	---	---	---	0.2-0.3	[67]
7	zinc chloride Water Silicon	---	---	---	---	---	---	---	[68]
8	Zinc sulphate Glass	3.3 - 3.95	90%	---	---	---	---	---	[69]
ZnO-Solgel									
9	Zinc acetate water	3.28-3.29	92%	---	---	---	---	---	[70]

10	Zinc acetate dihydrate 2-methoxyethanol Glass	3.3	---	---	---	---	---	---	[71]
11	Zinc acetate dihydrate Ethanol Glass	3.3	80-90%	---	---	---	---	---	[72]
12	Zinc acetate n-propanol and glycerol Si[100] and Quartz	3.271	---	---	---	---	---	---	[73]
13	Zinc acetate Silicon	3.37	---	---	---	---	---	---	[74]
14	Zinc acetate dihydrate Ethanol Glass	3.16 -3.41	80%	---	---	---	---	---	[75]
15	Zinc acetate dihydrate Methanol	3.34 - 3.21	---	---	---	---	---	---	[76]
16	Zinc acetate dihydrate Ethanol	2.276 - 2.279	---	---	---	---	---	---	[77]
17	Zinc acetate dihydrate 2-methoxyethanaol Glass	3.23- 3.30	80%	---	---	1.87 to 2.11	---	0.014-0.143	[78]
18	Zinc acetate dihydrate 2-methoxyethanol	3.24–3.28	---	80-90%	---	---	---	---	[79]
19	Zinc acetate dihydrate 2-methoxyethanol Silicon	3.2	---	90%	---	---	---	3.9	[80]
Cu:ZnO- CBD									
20	Zinc salt Water	3.13 - 2.94	---	---	---	---	---	---	[82]
21	Zinc acetate dehydrate Water	3.1 - 2.88	---	---	---	---	---	---	[83]
22	Zinc acetate	3.42 - 3.54	---	---	---	---	---	---	[84]

Cu:ZnO- Spray pyrolysis									
23	Zinc nitrate Water Glass	3.28 - 3.17	60- 80%	---	---	---	---	---	[81]
24	Zinc chloride Water Glass	3.3 -3.42	---	---	---	---	---	---	[85]
25	Zinc acetate Water Glass	3.27 -3.24	70 -80%	---	---	---	---	---	[86]
26	Zinc acetate dehydrate Chloroform Glass	---	---	---	---	---	---	---	[87]
Cu:ZnO - Solgel									
27	Zinc acetate dehydrate Water Glass	3.294 - 3.342	89%	---	---	---	---	---	[88]
28	Zinc acetate dehydrate 2-methoxyethanol Glass	3.358- 3.278	86 -80%	---	---	---	---	---	[89]
29	Zinc acetate dehydrate Glass	3.17 - 3.36	90 -100 %	---	---	---	---	---	[90]
30	Zinc acetate Water Glass and Silicon	3.20 - 3	76 -93%	---	---	---	---	---	[91]
Na:ZnO - Solgel									
31	Zinc acetate dehydrate Ethanol Glass	3.28	78%	---	---	---	---	---	[92]
32	Zinc acetate	---	---	---	---	---	---	---	[93]

	ethylene glycol monomethyl ether Silicon								
33	Zinc acetate dehydrate ethylene glycol monomethyl ether Silicon	3.12	70%	---	---	---	---	---	[94]
34	Zinc acetate dihydrate 2-methoxyethanol Glass	3.293 - 3.25	62%	---	---	---	---	0.15	[95]
35	Zinc acetate dihydrate Silicon	---	---	---	---	---	---	---	[96]
36	zinc acetate 2-methoxyethanol Glass	3.217	80-90%	---	---	---	---	---	[97]
37	Zinc acetate dihydrate 2-methoxyethanol Glass	3.20- 3.24	---	---	---	---	---	---	[98]
38	Zinc acetate dihydrate 2-methoxyethanol Silicon	---	---	---	---	---	---	---	[99]
39	Zinc acetate dehydrate 2-methoxyethanol Gass	3.25 - 3.89	78%	---	---	---	---	---	[100]
40	Zinc acetate dihydrate 2-methoxyethanol Glass	3.25	80%	---	---	---	---	---	[101]
41	Zinc acetate dehydrate ethylene glycol monomethyl ether Glass	3.26 - 3.27	---	---	---	---	---	---	[102]
42	Zinc acetate dehydrate 2-methoxyethanol Glass	3.213 - 3.29	---	---	---	---	---	---	[103]

K:ZnO- CBD									
43	Zinc chloride Water Glass	3.86- 3.94	40-50%	---	---	3.5-11	0.055-0.085	0.088-0.0135	[104]
44	Zinc acetate Methanol	3.23-3.31	---	---	---	---	---	---	[105]
45	Zinc chloride Water Glass	3.59-3.06	45%	---	---	---	---	0.0070- 0.0110	[106]
46	zinc nitrate Water Glass	3.22	---	---	---	---	---	---	[107]
47	Zinc chloride Water Glass	3.89-4.04	27-32%	---	---	---	---	---	[108]
K:ZnO-Solgel									
48	Zinc acetate dehydrate 2-methoxyethanol Glass	3.28-3.30	85%	---	---	---	---	---	[109]
49	Zinc acetate dehydrate 2-methoxyethanol Glass		80-90%	---	---	---	---	---	[110]
50	Zinc acetate dehydrate Isopropanol Glass and Silicon	3.28-3.14	10-90%	---	---	---	---	---	[111]
51	Zinc acetate dehydrate 2-methoxyethanol Glass	3.28-3.30	85%	---	---	2 to 3	0.04-0.07	0.02-0.03	[112]
52	Zinc acetate dehydrate Ethanol Glass	3.30-3.39	90%	---	---	---	---	---	[113]

53	Zinc acetate Ethanol Glass	---	---	---	---	---	---	---	[114]

2.1.4 Effect of doping ZnO with impurity

The perfect measure of doping with intentional impurities assumes significant role in semiconductor devices that invigorates the properties of the host material and have promising applications in the semiconductor innovation. Impurities can alter electronic, optical, structural and magnetic properties of material [130]. Dopant can also actively impact optical behaviour of the material. The doped semiconductor with metal ions can facilitate to control of the band gap and Fermi energy.

To acknowledge utilizations of ZnO in different fields, the first step is to get high characterized n-type and p-type ZnO materials. It is notable that ZnO is commonly a n-type semiconductor because of its constitutional deficiencies, for example, oxygen vacancies (VO) and zinc interstitials (Zni). Its electron concentration could be additionally advanced by donor impurity doping, for example, Cu. Na and K.

To enhance and alter the constitutional and optical properties of ZnO thin film to meet the constantly expanding mechanical requirements, various methodologies have been implemented. Among all, suitable element doping which can emphasize significant diversities in physical properties. As the doping material Cu, Na and K has a place with Group I and is an appropriate acceptor with generally high hole concentration [131].

The higher Cu doping concentration increases the resultant energy, and that higher doping concentration decimates the system stability. The addition of copper degenerates the impurity band and valence band of the ZnO system, and shift to the low energy direction is observed in the conduction band. Consecutive to doping, the forbidden band width lower down, with the goal that the energy needed to the electrons for the transition from the valence band to the conduction band decreases, and the light absorption passes through a red shift phenomenon [131].

Examining factors, for example, the electron shell and ionic size, sodium is noticed as a acceptable dopant for ZnO film for alteration of its structure, surface morphology, luminescence, and different properties. Na doping appealed more consideration because of feasible shallow acceptor production by substituting ZnO and Na is tested being a acceptable element for the production of different p-n junction devices [132]. Na also described for decreasing oxygen vacancy density which is additionally a significant advance for accomplishing stable p-type conduction. Other than acquainting p-type properties with ZnO, it's demonstrated that Na substitution ZnO lattice improved transformation efficiency in dye-

sensitized solar cells (DSSCs) when ZnO based nanostructures are utilized as photo-anode [133].

Sodium (Na) can replace the Zn site to act as a shallow acceptor and has been noticed as a wonderful element for p-type doping into ZnO. These properties make them reasonable for optoelectronic devices, light emitting diodes, photodetectors, sensors, solar cells, optical switches, photocatalysis, waveguides and piezoelectric materials [134-135]. Despite the fact that the trustworthy and high aspect p-type Na doped ZnO for efficient application has not been carried out, some helpful and significant outcomes were obtained from the earlier works. As revealed by Park et al., Na interstitials (Nai) were the main executioner deficiency which would hinder p-type doping in the Na-doped ZnO [136].

Alkali (soluble base) elements are acknowledged materials for tuning ZnO optical and electrical characteristics. Alkali doped ZnO films have been comprehensively researched in ongoing many years. Kim et al. revealed that, when K doped ZnO thin films were developed, the optical properties were improved.

2.2 Aims and objectives of the present work

Preparedness and characterization of thin films of pure ZnO and doped ZnO through various methods have drawn significant consideration because of their wide application possibilities. Consideration of simplicity, economy and input energy recommend that thin films of these materials be deposited by a low temperature and easier chemical route. The aim of the work consequently incorporates investigating the possibility of utilizing chemical route to improve ZnO thin film with certain metals (Cu, Na and K). The primary goal of the current work was to utilize a generally new and less used chemical bath deposition and sol-gel technique to develop pure ZnO, Cu: ZnO, Na: ZnO and K:Zno thin films from change in zinc concentration and change in no. of coats and their characterization. The method provides a wide spectrum of deposition criterions to control the factors such as appropriate precursors, concentration and pH of the responding precursors etc. Optimum synthesis condition that gives normal development for each specific dopant needs be determined.

Very few reports are available for Na and K doping in ZnO thin films by chemical bath deposition. The objective of the work was to prepare such doped films from various cationic precursors utilizing the adaptability of technique and the influence exerted by the metal dopants on the physical properties (structural and morphological properties, optical band gap, electrical properties etc.) of pure and doped ZnO thin films.

2.3 Summary

Zinc oxide (ZnO) is a versatile and inexpensive semiconductor with a wide direct band gap that has applicability in several scientific and technological fields. Zinc oxide thin films have attracted much attention in the recent years as alternative transparent conducting oxide because of their lower cost and comparable properties to those of conventional ITO films. ZnO possess novel properties such as wide band gap, good conductivity, high transparency, in addition to low deposition temperature, low cost and nontoxicity. At ambient conditions, ZnO exhibits a hexagonal wurtzite structure with a tetrahedral coordination typical of sp^3 covalent bonding, but has considerable ionic character. The unit cell is composed of two interpenetrating hexagonal-closed-packed (HCP) sublattices, where each Zn atom is surrounded by four O atoms in a tetrahedral coordination, and vice versa. There is a deviation from the ideal wurtzite crystal due to lattice expansions and ionicity. Lattice expansions are attributed to free charges, point defects, and threading dislocations. Thus, undoped ZnO is typically non-stoichiometric and shows n-type conductivity. ZnO exhibits a direct and large bandgap, which allows it to sustain large electric fields and higher breakdown voltages. In addition, lower noise generating, high temperature, high power devices can be fabricated. ZnO has not yet shown its full potential because some challenges remain unsolved. It is seen particularly in the failure to fabricate a stable, competent and reproducible p-type doped material. The various properties of ZnO thin films are shown below in Table 2.4.

Table 2.4 The various properties of ZnO

Sr.	Property	Value	Reference
1	Molecular formula	ZnO	
2	Molecular mass	81.408 g/mole	
3	Appearance	White solid	
4	Odor	Odorless	
5	Specific gravity	5.6	
6	Stable crystal structure	Wurtzite	[139]
7	Refractive Index	2.008	[141]
8	Dielectric constant	8.656	[140]
9	Band gap energy	3.370 eV (Direct)	[138,142]

10	Melting point	1975 °C	[145]
11	Boiling point	2360 °C	[145]
12	Solubility in water	0.16 mg per 100 ml at 30 °C	[138]
13	Density	5.606 g/cm^3	[138]
14	Lattice parameters	a=b=3.2458 Å, c= 5.2006 Å	[137-139]
15	Exciton binding energy	60 meV	[144]
16	Electron effective mass	0.24	[139]
17	Hole effective mass	0.59	[139]
18	Hole mobility (300 K)	5-50 cm^2/Vs	[144]
19	Electron mobility (300 K)	100-200 cm^2/Vs	[144]
20	Intrinsic carrier concentration	<10^6 cm^{-3} (max n-type doping >10^{20} cm^{-3} electrons; max p-type doping < 10^{17} cm^{-3} holes)	[145]

CHAPTER 3

Instrumental Techniques and Theoretical Considerations

3.1 Instrumental techniques

Distinctive experimental procedures which have been utilized to characterize the pure and doped ZnO thin films are covered in this section. A short discussion about X-ray diffraction (XRD), Scanning electron microscope (SEM), Ultraviolet-visible (UV-VIS) spectroscopy, Photoluminescence (PL), Raman spectroscopy, Thermo gravimetric analysis (TGA), Hall effect and resistivity measurement (from room temperature to 200°C) has been incorporated here.

3.1.1 X-ray Diffraction (XRD) Analysis

X-rays are electromagnetic radiation of wavelength about 1 Å, which is about the similar in size to an atom. They appear between gamma-rays and the ultraviolet part of the electromagnetic spectrum. X-ray diffraction is a versatile interpretive strategy to exceptionally recognize the crystalline phases present and to examine the constitutional properties. A given substance consistently delivers a characteristic diffraction arrangement, disregarding of whether the substance is present in the pure state or as a one constituent of a blend of substances. This reality is the reason for the diffraction technique of investigation. The X-ray discovery in 1895 empowered researchers to test crystalline structure at the nuclear level. At the point when X-rays associate with a crystalline substance which is a phase, one gets a diffraction arrangement. Around 95% of every solid substances can be depicted as crystalline. Every crystalline solid has its remarkable characteristic X-ray diffraction arrangement which might be utilized as a "unique finger impression" for its

recognizable proof. Figure 1 shows the reflection of x-rays from two planes of particles in a solid.

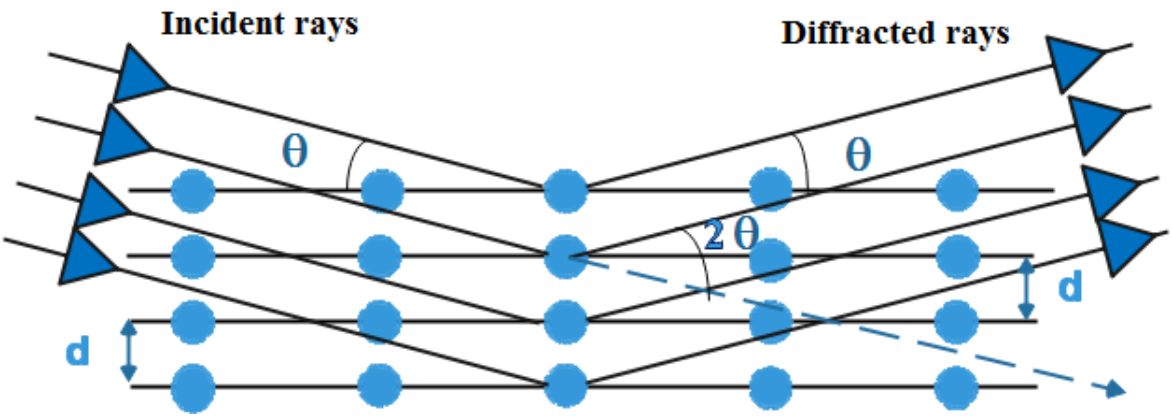

FIGURE 3.1 X-ray diffraction

A crystal lattice is a definitive three-dimensional appropriation of particles in space. These are ordered with the goal that they structure a progression of parallel planes isolated from each other by a separation d, which changes as indicated by the nature of the material. For any crystal, planes exist in various directions in which each having its own particular d-spacing. At the point when a monochromatic X-ray beam having wavelength lambda is anticipated onto a crystalline material at an edge theta, diffraction happens just when the distance covered by the rays reflected from progressive planes varies by a total number n of wavelengths, which prompts well known Bragg's Law [146]:

$$\mathbf{n\lambda = 2dsin\theta} \tag{3.1}$$

Where n is a positive integer 1, 2, 3….. (usually equal to 1), λ is wavelength in angstroms i.e. for copper 1.54 Å, d is interatomic spacing in angstroms, and θ is the diffraction edge in degrees. By changing the edge theta, the Bragg's Law conditions are fulfilled by various d-spacing in polycrystalline substances. Plotting the angular positions and extents of the consequence diffracted apexes of radiation produces a design, which is one of the sample's attributes. Where a blend of various phases is available, the resultant diffractogram is developed by expansion of the individual designs. On the basis of the X-ray diffraction principle, an abundance of auxiliary, physical and chemical data about the material examined can be gathered. The diffracted beam is recognized in a counter (gas or solid counter) which travels through the angular field of reflections and intensity of diffracted beam is recorded on a collectively propelling outline. Contrasting this information and the standard Joint Committee of Powder Diffraction Standards (JCPDS) information document, one can

distinguish the structure of the material, the lattice parameters as well as the planes present there. The crystallite size or moleculer size (D) can be found applying the Scherer's formula on the basis of X-ray diffraction designs [2].

$$\mathbf{D = \frac{k\lambda}{\beta cos\theta}} \tag{3.2}$$

Where k is a constant dictated by the geometry of the crystallites and ball-shaped particles have about 0.94, β is the full width at half maximum intensity or FWHM of the detected diffraction apex and θ is the dispersed edge. The widening considered in Scherrer equation is because of molecule size only. The angular width at a point where the intensity has tumbled to half of its greatest value (FWHM) is a proportion of widening of x-ray apex [147]. XRD has been being used in two primary fields, for the unique finger impression nature of crystalline materials and the verification of their structures. When the material has been recognized, X-ray crystallography might be utilized to decide its structure, for example how the particles well-adjusted with each other in the crystalline structure and what the interatomic separation and angle are and so on. The diffraction of x-rays decide most effectively the size and the geometry of the unit cell for any compound. The X-ray diffraction (XRD) designs explore the crystal structure and orientation of the pure ZnO and doped ZnO films. The XRD designs were recorded with D_2 phaser Bruker advanced X-ray diffractometer utilizing a Cu - Kα radiation source (λ = 1.547 Å). Diffraction peaks were compared with those of the standard compounds reported in the JCPDS files (36-1451 card) and the Miller indices were indexed to the peaks.

3.1.2 Scanning Electron Microscopes (SEM)

Scanning electron microscopy is used to assess the morphology or grain size and layer thickness. For SEM analysis, the samples are coated with a thin layer of platinum to avoid sample charging.

The scanning electron microscope utilizes a directed beam of high-energy electrons to produce an assortment of signals on the outer layer of solid samples. The signals that get from electron-sample interactions uncover data about the sample including outside morphology (surface), chemical composition, and crystalline structure.

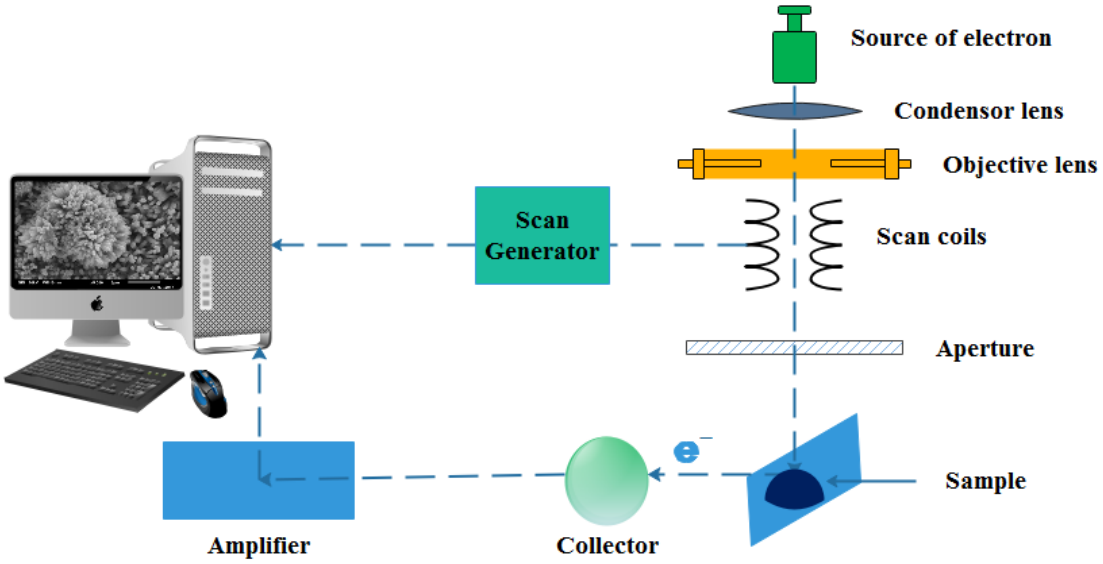

FIGURE 3.2 Schematic diagram of scanning electron microscope (SEM)

SEM creates images by scanning the sample with a beam of electrons [148-149]. In many applications, information are gathered over a selected zone of the surface of the sample, and a 2D image is created which shows spatial alterations in these properties. Zones extending from around 1 cm to 5 microns in width can be seen in a scanning mode utilizing ordinary SEM techniques (amplification ranging from 20 times to roughly 30,000 times, spatial resolution of 50 to 100 nm). Accelerated electrons in a SEM carry meaningful amounts of kinetic energy, and this energy is dissolved as an assortment of signals created by electron-sample interactions when the incident electrons are slow down in the solid sample Secondary electrons, backscattered electrons, diffracted backscattered electrons, photons, visible light, cathodoluminescence, and heat are the part of these signals. Secondary electrons and backscattered electrons are commonly utilized for observing sample: secondary electrons are utmost beneficial for displaying morphology and topography of sample and backscattered electrons are utmost beneficial for depicting contrasts in composition in multiphase sample i.e. for rapid phase discrimination. X-ray generation is produced by inelastic collisions of the incident electrons with electrons in discrete energy levels (shells) of atoms in the sample. As the energized electrons come back to lower energy levels, they yield X-rays that are of a fixed wavelength (that is identified with the distinction in energy levels of electrons in various shells for a given component). Hence, distinctive X-rays are created for every component in a mineral that is "energized" by the electron beam. SEM analysis is viewed as "non-destructive"; means x-rays produced by electron interactions do not prompt volume loss of the sample, therefore it is conceivable to analyze the similar

materials over and again. SEM was used for morphological characterization of sample. The surface morphology of the pure and doped ZnO thin films were determined by scanning electron microscope (SEM) JSM-6010LA.

3.1.3 Ultraviolet – Visible (UV-Vis) spectroscopy

UV-VIS spectroscopy is considered as the most significant spectrophotometric procedure that is most broadly utilized for the examination of different types of compounds. Ultraviolet-visible spectroscopy is one of the most familiar investigative method since it is very flexible and ready to identify almost each molecule. With UV-Vis spectroscopy, the

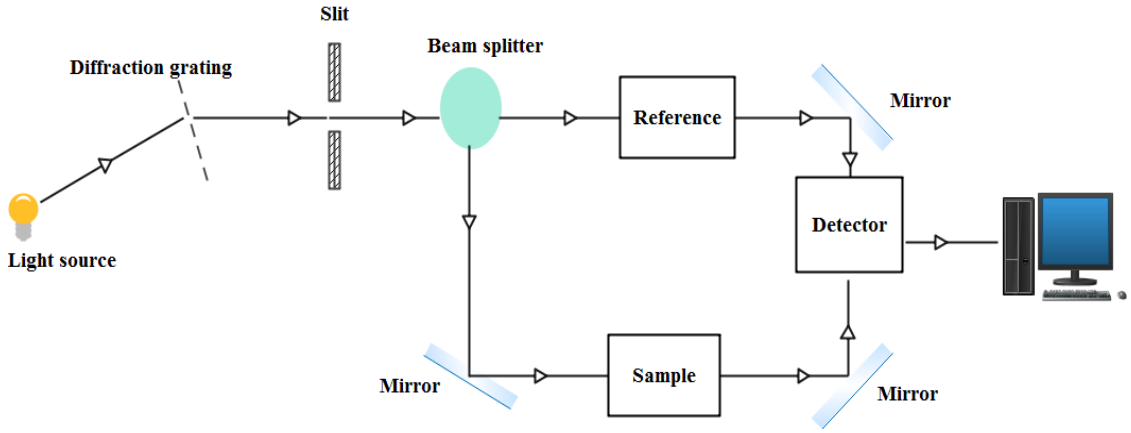

FIGURE 3.3 Schematic for a UV-Vis spectrophotometer

UV-Vis light is travelled through a specimen and the transmitted light by a specimen is estimated. The transmittance (T) can be determined from the correlation [150]

$$\mathbf{A} = \mathbf{log}\left(\frac{\mathbf{1}}{\mathbf{T}}\right) \tag{3.3}$$

Where A is the absorbance and T is given by [150]:

$$\mathbf{T} = \frac{\mathbf{1}}{\mathbf{10^{A}}} \tag{3.4}$$

The reflectance (R) is determined from the interrelation [150]:

$$\mathbf{A + R + T = 1 \ \ Or} \tag{3.5}$$

$$\mathbf{R = 1 - (A + T)} \tag{3.6}$$

An absorbance spectrum is attained which shows the absorbance of a compound at various wavelengths. The measure of absorbance at any wavelength is because of the chemical

structure of the molecule. The bandgap of materials is a significant parameter that decides the utilization of the films. It is assessed utilizing the equation [150].

$$\alpha = \left(\frac{A}{h\nu}\right)\left(h\nu - E_g\right)^n \tag{3.7}$$

At the point when a light beam attack on a thin film semiconducting material, a portion of the beam will be reflected, another portion will be transmitted through the film, and the remained portion of the beam will be absorbed. Absorption of photons leads to shift of the electrons from valance band to conduction band.

Optical examinations give a decent method of analyzing the properties of semiconductors. Especially estimating the absorption coefficient for different energies provides data about the band gaps of the material. The optical data is achieved using spectrophotometer. The absorption coefficient is realized by the following relationship.

$$\alpha = \frac{2.303\ A}{t} \tag{3.8}$$

Where t is the thickness of the deposited film, A is the absorbance. UV-Vis can be utilized in a qualitative way, to recognize functional groups or verify the identity of a compound by coordinating the absorbance spectrum. UV-Vis measurements are commonly taken using a spectrophotometer. UV-Vis is additionally an exceptionally well known identifier for other analytical methods, for example, chromatography, since it can identify numerous compounds.

3.1.4 Photoluminescence (PL)

Photoluminescence which investigates optical property of luminescent semiconductor materials is a strong and nondestructive invention. As per analytic information of photoluminescence, we can know the type of impurities, bandgap, and impurity activation energy etc. from the spectra. We can approximate the structure of the compound from the apex intensity of PL spectra.

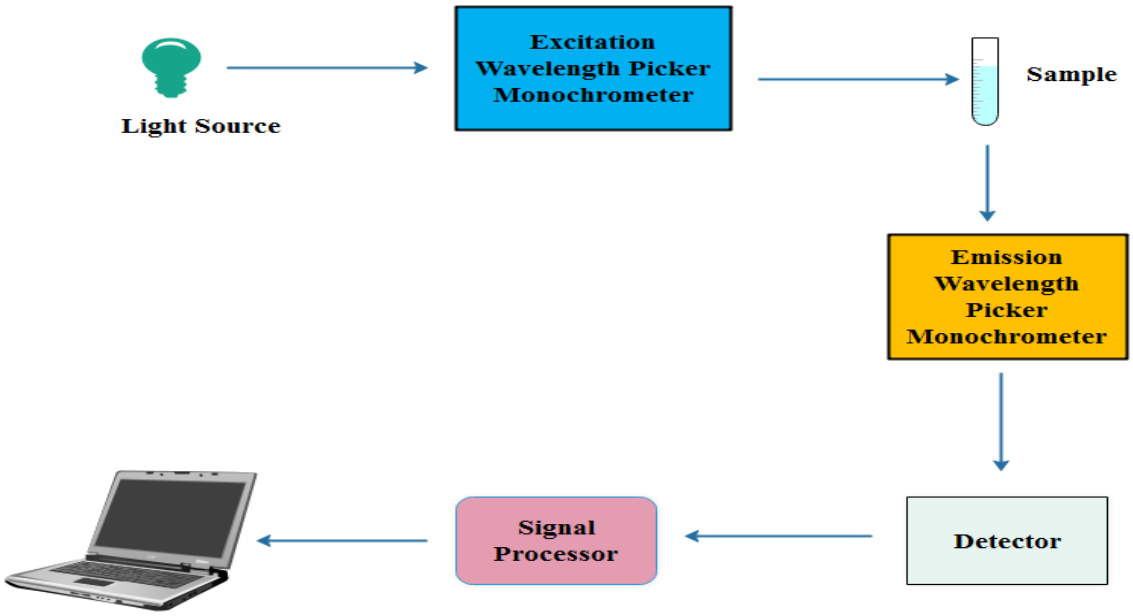

FIGURE 3.4 Diagram of PL experiment set-up

Utilizing photoluminescence, the internal interface of hetero-structure can be investigated which common physical or electronic measurements cannot measure. Luminescence process comprises of three procedures:

(1) Excitement

(2) Heat balance

(3) Recombination

Incident light produces electron-hole pairs and recombines to produce photons after heat stabilization. Contaminations and imperfections in structure form different energy levels in the bandgap and their relating energy will create radiation by radiation recombination process or produce absorption by nonradiative recombination process.

In PL, a material gets energy by absorbing photon at some wavelength by advancing an electron from a lower to a higher energy level. This might be depicted as making a shift from ground state to an energized state of an atom or a molecule or from the valance band to conduction band of a semiconductor crystal. The system at that point experiences a no irradiative internal relaxation including interaction with crystalline or molecular vibration modes. After a characteristic life time in the energized state, electron will come back to the ground states.

In the luminescence material the energy discharged during the final shift is as light, for this condition the relaxation is known to be radiative. It ought to be noticed that relying upon the

characteristic life time of emission, quick PL with life time of sub-micro seconds is known as fluorescence, whereas slower one are pointed out as phosphorescence.

PL spectrum of all the samples were obtained at room temperature through shimadzu RF-5301 PC spectro-fluoro-photometer under the condition that the excitation wavelength λ is 325 nm and the emission spectra was recorded at the wavelength range of 350 – 550 nm. Also Ozone free Xenon-quartz light of 150 W was applied for excitation

3.1.5 Raman spectroscopy

Raman spectroscopy is the measurement of the wavelength and intensity of inelastically dispersed light from particles. The Raman dispersed light results at wavelengths which are moved from the incident light by the energies of molecular vibrations.

Raman spectroscopy is utilized to decide the molecular motions, particularly the vibrations. A mechanism of Raman spectrometer is that when a substance is irradiated with a monochromatic light of well-defined frequency, the light dispersed at right edge to the incident light contains light of (1) Incident frequency and (2) lower frequency. Once in a while lines of higher frequency are too gained that of the incident beam will be dispersed. It is termed as Raman scattering. The line with lower frequency are termed as Stoke's lines. The line with higher frequency are termed as Antistoke's lines. The line with the similar frequency as that of the incident light is termed as Rayleigh line. Raman frequencies for a specific substances are attributes of that substances.

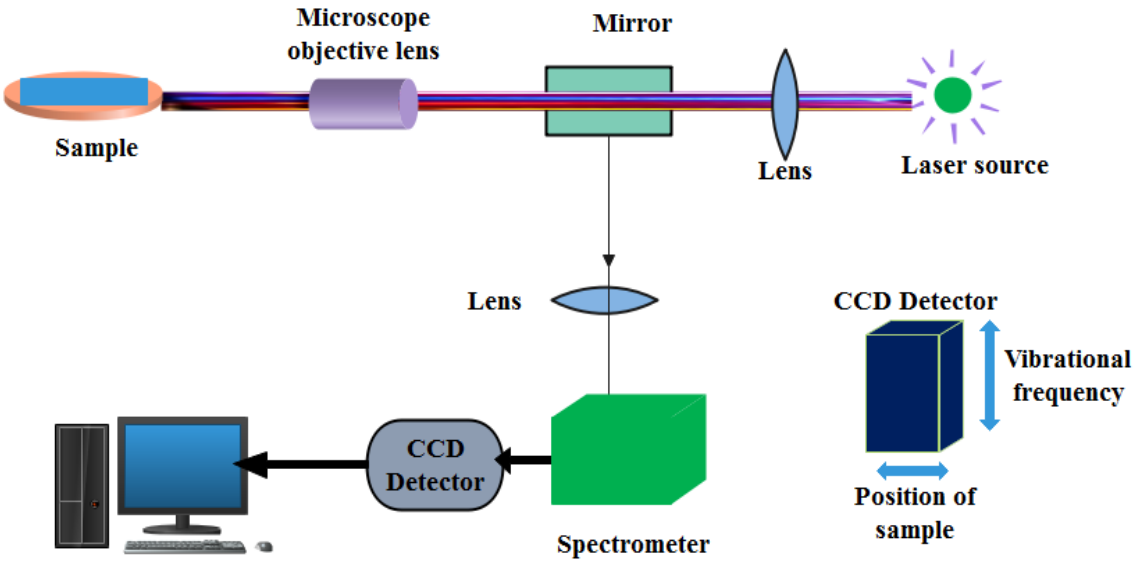

FIGURE 3.5 Schematic of Raman spectrometer

Raman spectroscopy works as a versatile technique to establish the resemblance of defects generated due to dopant and deficiency in lattice of source crystal particularly regarded to material isolate on or second level states in material. The vibrational properties of all the four films are investigated using Raman spectra. ZnO thin films with hexagonal wurtzite structure fit into the $P6_3mc$ position group. The optical phonons at Γ point of the Brillouin zone for the perfect ZnO crystal lattice is added in top Raman scattering. According to the group hypothesis, wurtzite ZnO have to be with optical modes and can be explained by the following equation.

$$\boldsymbol{\Gamma_{opt} = 1A_1 + 2B_1 + 1E_1 + 2E_2} \tag{3.9}$$

Here, two polar branches A_1 and E_1 modes split into longitudinal optical (LO) and transversal optical (TO) segments with varying frequencies, as macroscopic electric fields are associated with the LO type phonons. A_1, E_1 and E_2 modes are taken into account as a first order Raman-active modes.

Raman scattering spectra reported with the help of Renishaw in Via Raman Microscope with a laser excitation source (λ = 514 nm) at room temperature. So vibrational properties analysed for pure and doped thin films to check the influence of dopant materials such as Cu, Na and K on pure ZnO

3.1.6 Thermo gravimetric analysis (TGA)

Thermograviometric Analysis or TGA is a kind of testing which is performed on specimens to decide changes in weight corresponding to change in temperature. Such examination depends on a high level of accuracy in three estimations: weight, temperature, and temperature change. As many weight loss curves appear to be comparative, the weight loss curve may require change before results might be interpreted. A subsidiary weight loss curve can be utilized to tell where weight reduction is most probable. Once more, interpretation is restricted moving along without any more alterations and deconvolution of the overlapping apexes might be required.

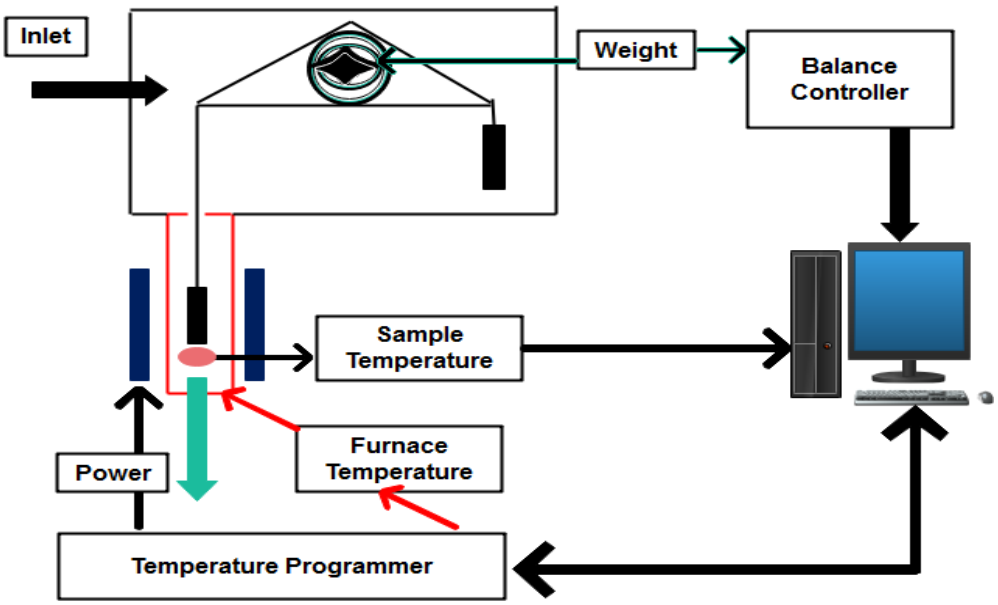

FIGURE 3.6 Block diagram of Thermo gravimetric analysis (TGA)

TGA is usually utilized in research and testing to decide qualities of materials such as polymers, to decide degradation temperatures, absorbed moisture content of materials, the degree of inorganic and organic components in materials, deterioration purpose of explosives, and solvent residues. It is additionally frequently utilized to evaluate the erosion kinetics in high temperature oxidation. The analyzer ordinarily comprises of a high-accuracy balance with a sheet (generally platinum) loaded with the specimen. The sheet is put in a small electrically heated oven with a thermocouple to precisely measure the temperature. The climate might be cleaned with an ideal gas to avoid oxidation or other undesired responses. A computer is utilized to control the instrument. A technique known as hi-res TGA is frequently utilized to get more prominent accuracy in regions where the derivative curve apex appear. In this technique, temperature rise slows as weight reduction increases. This is done with the goal that the specific temperature at which an apex obtained can be more precisely recognized. thermo gravimetric analyzer (TGA, METTLER TOLEDO, Model: DSC3) was utilized to study the thermal stability of ZnO.

3.1.7 Hall Effect

The Hall Effect was determined by Edwin Hall in 1879 [151] and it attributes to the potential difference that appears over an electrical conductor on employing a magnetic field perpendicular to the electrical current flow. Hall Measurements were obtained by the van

der Pauw method [152-153]. Specimens were mounted on a board and appended at 4 contacts by graphite paste.

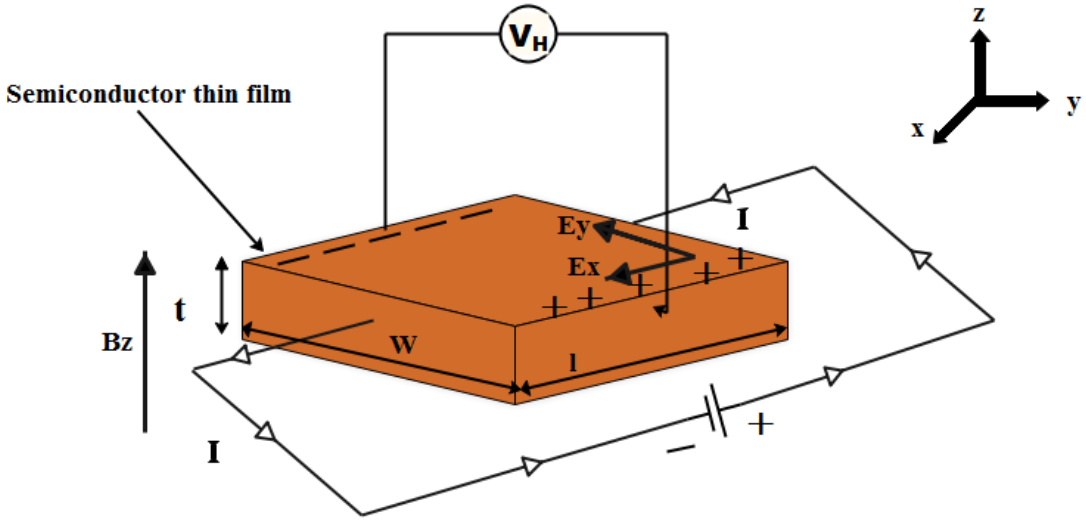

FIGURE 3.7 Hall Effect measurement setup

The electric field, or Hall field, is a consequence of the force that the magnetic field applies on the moving positive or negative particles that comprise the electric flow. Regardless of whether the flow is a movement of positive particles, negative particles the other way, or a mixture of the two, a perpendicular magnetic field displaces the moving electric charges a similar way sideways at right edges to both the magnetic field and the direction of current flow. The aggregation of charge on one side of the conductor leaves the opposite side oppositely charged and creates a difference of potential. A proper meter may recognize this difference as a positive or negative voltage. The induction of this Hall voltage decides if positive or negative charges are conveying the current. The Hall Effect can be utilized additionally to measure the thickness of current carriers, their freedom of movement, or mobility, just as to identify the presence of a current on a magnetic field. The Hall coefficient is represented as,

$$\mathbf{R_H} = \frac{\mathbf{V_H} \cdot \mathbf{t}}{\mathbf{I_x} \cdot \mathbf{B}} \tag{3.10}$$

Where R_H is hall coefficient, V_H is Hall voltage, t is the thickness of the film, I is the current moving through the conductor and B is the magnetic field.

Hall-effect measurements were done in the van der Pauw setup (DNE 21A) at room temperature for the assurance of kind of conduction mechanism, Hall mobility and carrier concentration.

3.1.8 Two probe resistivity measurement

The measuring procedures generally known to decide electrical properties of materials are the two-probe technique and the four-probe technique wherein the former is the most ordinarily utilized one since it is simple and reasonable compared to the four-probe technique. The beneficial thing in two-probe technique is easy to set-up and singular apparatus could be available. The two-probe and four-probe techniques have been utilized to characterize approximately all semiconductor products present in the world today. These procedures have made development easier in discovering semiconductor materials other than the materials found in the periodic table of elements. Different models and techniques have been proposed to quantify the electrical resistance. Factors affecting the suitability of different techniques and accuracy attainable cover contact resistance and fashion of the specimen for example regardless of whether it is as single crystal, thin film, powder pellet or small crystallite. Among the techniques to be talked about is two probes can be utilized for estimation of resistivity. In this technique, voltage drop V across the specimen and current through the specimen I are estimated. At that point the resistivity is given as,

$$\boldsymbol{\rho = \frac{V \times a \times h}{I \times s}} \tag{3.11}$$

Where ρ is the specimen resistivity, V is the potential distinction measured between the two voltage studies, I is the uniform current being moved through the specimen, a is the specimen width, h is the specimen height, and s is the distance between two contacts.

The Electrical conductivity and activation energy of charge bearers in Pure ZnO , Copper doped ZnO (Cu:ZnO), Sodium doped ZnO (Na:ZnO) and potassium doped ZnO (K:ZnO) thin films was evaluated by examining the variation of resistivity ρ with temperature (from room temperature to ~200°C) through two probe methods. A plot of log ρ against 1/T will yield a straight line with a slope giving activation energy.

3.1.9 Thermoelectric power measurements

Thermoelectric power generation process is based on the Seebeck effect which states that loop of dissimilar metals will develop an emf if the two junctions are kept at different temperatures. This principle is already being used in thermocouples for measurement of temperature. The efficiency of the thermoelectric material can be calculated by knowing the electrical conductivity and the Seebeck coefficient.

The thermoelectric effect is the direct conversion of temperature differences to electric voltage and vice versa via a thermocouple. Thermoelectric device (Figure 3.8) create a voltage when there is a different temperature on each side. Conversely, when a voltage is applied to it, heat is transferred from one side to the other, creating a temperature difference. At the atomic scale, an applied temperature gradient causes charge carriers in the material to diffuse from the hot side to the cold side. This effect can be used to generate electricity, measure temperature or change the temperature of objects. Because the direction of heating and cooling is determined by the polarity of the applied voltage, thermoelectric devices can be used as temperature controllers. The term "thermoelectric effect" encompasses the separately identified effects: the Seebeck effect and Peltier effect. The thermoelectric effect is the direct conversion of temperature differences to electric voltage and vice versa via a thermocouple. Thermoelectric devices create a voltage when there is a different temperature on each side. Conversely, when a voltage is applied to it, heat is transferred from one side to the other, creating a temperature difference. The Seebeck coefficient S, which describes the magnitude of induced TE voltage (ΔV) in response to a temperature difference (ΔT) in the material. A setup based on dynamic method was developed for Seebeck coefficient measurement from room temperature to 473 K. As shown in figure 1 two heaters (H_1 and H_2) with maximum 250 W power were symmetrically embedded in the ceramic base. In the measurement, channels 1 and 2 (CH_1 and CH_2) were set to accept temperature signals (T_1 and T_2). Channel 3 (CH_3) was set to accept the Seebeck voltage (ΔV) signal. These data was recorded.

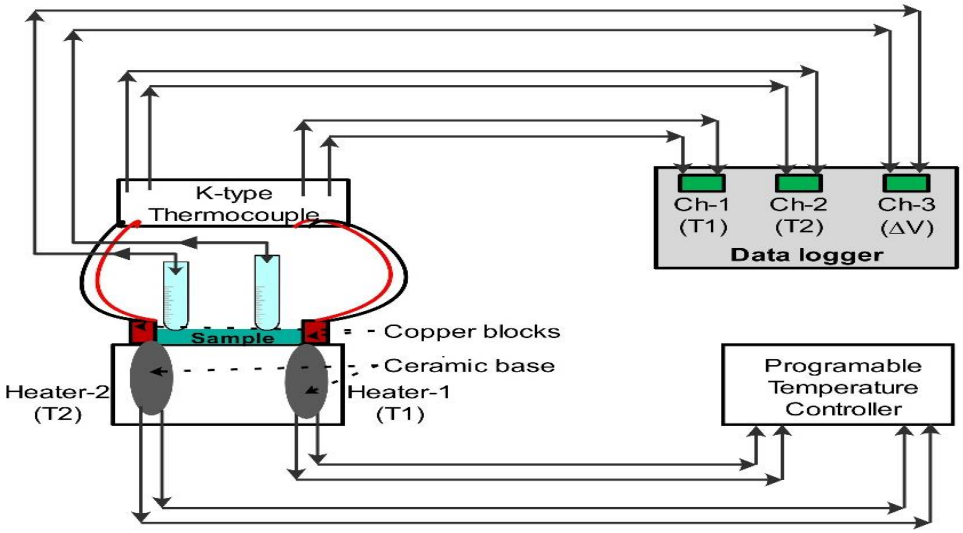

FIGURE 3.8 Set up for the measurement of thermoelectric power

At the atomic scale, an applied temperature gradient causes charge carriers in the material to diffuse from the hot side to the cold side. For a nondegenerate n- type and p-type semiconductor with spherical constant energy surface under thermal equilibrium the thermoelectric power is given by [154],

$$\mathbf{S} = \frac{-\mathbf{k_B}}{\mathbf{e}}\left(\frac{\mathbf{E_c} - \mathbf{E_F}}{\mathbf{k_B\,T}} + \mathbf{A}\right) \textbf{(For n} - \textbf{type)} \tag{3.12}$$

$$\mathbf{S} = \frac{\mathbf{k_B}}{\mathbf{e}}\left(\frac{\mathbf{E_F} - \mathbf{E_V}}{\mathbf{k_B\,T}} + \mathbf{A}\right) \textbf{(For p} - \textbf{type)} \tag{3.13}$$

Where k_B is the Boltzmann constant and E_c is the energy of the conduction band edge; A is a constant that depends on the nature of the scattering process which is runs between 0 and 4. E_F is the energy of Fermi level.

$$\mathbf{E_C} - \mathbf{E_F} = \mathbf{E_0} - \boldsymbol{\gamma}\mathbf{T} \tag{3.14}$$

Where E_0 is the low-temperature limit of E_c - E_F and corresponds to the activation energy equivalent to the band gap, and γ is the temperature coefficient. Putting equation 3.14 into equation 3.12 and 3.13 we get,

$$\mathbf{S} = \frac{-\mathbf{E_0}}{\mathbf{eT}} + \left(\frac{\boldsymbol{\gamma}}{\mathbf{e}} - \frac{\mathbf{Ak_B}}{\mathbf{e}}\right) \textbf{(For n} - \textbf{type)} \tag{3.15}$$

$$\mathbf{S} = \frac{\mathbf{E_0}}{\mathbf{eT}} + \left(-\frac{\boldsymbol{\gamma}}{\mathbf{e}} + \frac{\mathbf{Ak_B}}{\mathbf{e}}\right) \textbf{(For p} - \textbf{type)} \tag{3.16}$$

Comparing equation 3.15 and 3.16 with y = mx + c, we get y = S, x = 1/T. By plotting a graph of S versus 1/T, we get the slope m = - $\frac{E_c - E_F}{e}$ (For n-type) and slope m = $\frac{E_F - E_V}{e}$ (For p-type). It means $E_C - E_F$ = -me (For n-type), E_F-E_V = me (For p-type) and $A = \frac{ec}{k_B}$.

3.1.9.1 Peltier coefficient

The Peltier coefficient is given by,

$$\boldsymbol{\pi} = \mathbf{ST} \tag{3.17}$$

By putting equation 3.15 and 3.16 in to equation 3.17 we get,

$$\boldsymbol{\pi} = \frac{-\mathbf{E_0}}{\mathbf{e}} + \left(\frac{\boldsymbol{\gamma}}{\mathbf{e}} - \frac{\mathbf{Ak_B}}{\mathbf{e}}\right)\boldsymbol{T} \textbf{(For n} - \textbf{type)} \tag{3.18}$$

$$\boldsymbol{\pi} = \frac{\mathbf{E_0}}{\mathbf{e}} + \left(-\frac{\boldsymbol{\gamma}}{\mathbf{e}} + \frac{\mathbf{Ak_B}}{\mathbf{e}}\right)\boldsymbol{T} \textbf{(For p} - \textbf{type)} \tag{3.19}$$

Comparing equation 3.18 and 3.19 with equation y = mx + c we get $y = \pi$ and $x = T$. Also we get $= \frac{\gamma - Ak_B}{e}$; $c = \frac{-E_0}{e}$ for n-type and $m = \frac{Ak_B - \gamma}{e}$, $c = \frac{E_0}{e}$ for p-type. The value of γ can be obtained from the slope of the graph π versus T.

3.1.9.2 Thermoelectric power factor

The power factor is important parameter characterizing the TE properties. In thermoelectricity, a material with high power factor is more important than having a high ZT because most of the waste heat sources are free and unlimited. So, effective strategies to achieve a high-power factor have fundamental importance. Power factor (PF) determine the performance of thermoelectric energy converter. It is calculated by the values of Seebeck coefficient and electrical conductivity as [155],

$$\textbf{Power factor} = \boldsymbol{\sigma S^2} \tag{3.20}$$

Where S is Seebeck coefficient, σ is electrical conductivity. The product is usually named as "thermoelectric power factor" or simply "power factor" which characterizes the electrical transport properties and is widely used in literatures. The power factor (PF) can be used as an index for thermoelectricity. Well-established approaches say traditional ones; the aim is to increase the power factor.

3.1.9.3 Jonker Analysis

Jonker [156] developed an analysis for semiconductors that involve plotting Seebeck coefficient versus logarithm of conductivity (known as a ''Jonker plot'') as a useful means to obtain important electrical properties. The two primary thermoelectric effects are the Seebeck effect and the Peltier effect, which when combined with the laws of thermodynamics, can be used to derive all other thermoelectric effects [157].

$$\mathbf{S} = \pm \frac{\mathbf{k_B}}{\mathbf{e}} [\mathbf{ln}(\boldsymbol{\sigma}) - \mathbf{ln}(\boldsymbol{\sigma_0})] \tag{3.21}$$

Where ''+'' is for the n-type case and '-' is for the p-type case. Thus, in what is referred to as the ''extrinsic'' nondegenerate regime, a Jonker plot of Seebeck coefficient versus logarithm of conductivity should be a line with a slope of $\pm$ k_B/e = $\pm$86:15 mV/K with a positive slope for n-type semiconductors and a negative slope for p-type semiconductors.

CHAPTER 4

Preparation of ZnO Thin Films by CBD and Their Characterizations

4.1 Introduction

Oxide thin films of zinc oxide (ZnO) have attracted great attention from both academic and industrial communities due to their enhanced characteristics for potential applications. ZnO thin films have been deposited onto the glass substrates by the chemical bath deposition method. In this work we have studied the various properties of ZnO thin films prepared by chemical bath deposition method. Zinc chloride was used as the precursor material. Many investigations are still carried out to improve the characteristics of ZnO materials. In the present proposed work, thin films of zinc oxides in pure form was prepared using chemical bath deposition method and to study the various properties of ZnO thin films.

4.2 Preparation of ZnO thin films

The ZnO thin films were prepared through chemical bath deposition method using aqueous solution of $ZnCl_2$ anhydrous as a precursor. Commercial quality glass microscope slides having dimensions 25 mm x 75 mm x 1 mm are taken as a substrate. Before performing deposition, concentrated HCl was used to soak these glass slides minimum for 24 hours. After that to get the proper degreased and clean substrate surface all the glass slides were washed thoroughly in cold detergent solution and rinsed using distilled water. Also these are ultra-sonicated in methanol solution for 15 minutes and dried at 50 °C in oven. The reagents used in this experiment were anhydrous zinc chloride (Mol. Wt.136.29 g/mol) and aqueous

ammonia (~25% pure). Solution of 0.1 molar zinc chloride prepared in aqueous medium and from that solution 80 ml was taken for the experiment in which drop wise aqueous ammonia with continuous stirring added to get the pH of the solution 9.6. When ammonium hydroxide in excess amount is added to zinc chloride solution, firstly the white gelatinous $Zn(OH)_2$ is formed which then dissolves in excess NH_4OH to form coordinated complex compound of zinc as shown in the following reactions:

$$\mathbf{ZnCl_{2(aq)} + 2NH_4OH_{(aq)} \rightarrow Zn(OH)_{2(s)} + 2NH_4Cl_{(aq)}}$$

$$\mathbf{Zn(OH)_{2(s)} + 2NH_4Cl_{(aq)} + 2NH_4OH_{(aq)} \rightarrow [Zn(NH_3)_4]Cl_2 + 4H_2O_{(l)}}$$

$$\mathbf{ZnCl_{2(aq)} + 4NH_4OH_{(aq)} \rightarrow [Zn(NH_3)_4]Cl_2 + 4H_2O_{(l)}}$$

After that the solution was shifted to a 100 ml beaker and the substrate was immersed vertically. The beaker was kept in a constant temperature water bath maintaining 80 °C of temperature. Turbidity was observed slowly in this clear solution which supports the initialization of thin film deposition. Substrate was removed from the bath after 120 minutes, washed with distilled water and dried at 50 °C in oven. The turbid solution remained after the deposition was converted into powder by keeping at 50 °C in the oven. This dry powder was then analyzed by DTA to determine the temperature at which the film deposited on the substrate converts in to ZnO. Dried thin films were annealed at 500 °C for 2 hours to confirm their conversion into ZnO.

Using same experimental method ZnO thin films were also prepared for other concentrations 0.2M, 0.3M, 0.4M and 0.5M respectively.

Also total 5 multilayer thin films were made by depositing ZnO thin films (using 0.1 M precursor solution) one by one and marked as 1C, 2C, 3C, 4C and 5C for Single coat, Double Coat, Triple Coat, Quadruple coat and Quintuple coat ZnO thin films respectively

4.3 Thermogravimetric analysis

Thermal behavior of dried powder of precursor complex was analyzed by thermo-gravimetric analysis and differential thermal analysis as shown in Fig. 4.1 TGA curve shows the weight loss occurring in two steps and even actually reaching to 62.58% of starting weight at 516 °C firmly matches with the ratio of molecular weight of ZnO to the combined molecular weight of precursor mixture. DTA curve exhibits an endothermic peak above 100°C may be attribute to the evaporation of moisture and another endothermic peak between 350-400°C may be attributed to evaporation of other volatile compounds. The

endothermic reaction observed between 400-500°C may correspond to the reaction between components of the precursor materials after which the resultant weight loss matches firmly with ratio of molecular weight of ZnO to the combined molecular weight of precursor mixture. This confirms the annealing temperature required for the as grown thins films to be ~500°C.

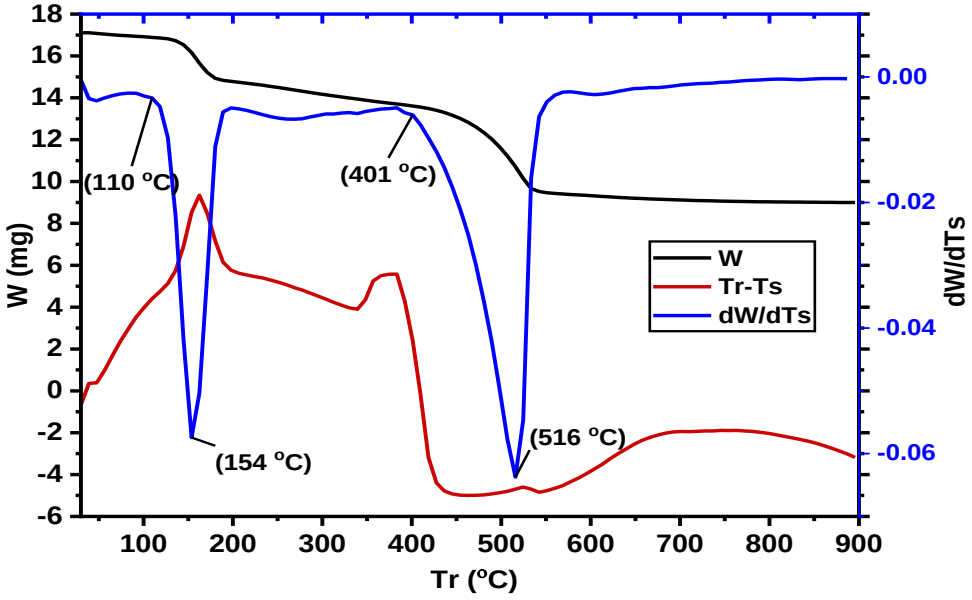

FIGURE. 4.1 TGA-DTA curve of dried precursor complex.

4.4 Variation in precursor concentration

ZnO nanostructure's growth, applications and characteristics depend on influencing parameters like precursor concentration [158]. Effect of precursor concentration on the characteristics of ZnO thin films has been experimented in this study. Generally, the Zn^{+2} cation from precursor solution acts as source for nanostructure formation. This implies a change in growth rate with changes in the precursor concentration. In an experiment it has been observed that the thickness of the film increased with increase in the precursor concentration. [159]. There is a high dependency between the precursor concentration and density of particles. Increasing precursor concentration results in high nucleation sites which in turn increases the formation of dense ZnO growth. This morphological change has a great influence on the performance of sensors. This study reports the importance of the effect of variation in precursor concentrations on the structural, morphological and optical properties of the ZnO thin films using the colloidal solution route.

In the present work, we report properties of ZnO thin films deposited by bath consisted of equal volumes of zinc chloride ($ZnCl_2$) solutions having precursor concentrations varying from 0.1 M to 0.5 M.

Thin films were characterized for structure, morphology and optical properties. Structural parameters of thin films are analyzed using powder XRD by patterns recorded with D_2 phaser Bruker advanced X-ray diffractometer using a Cu - Kα radiation source (λ = 1.547 Å). Diffraction peaks were compared with those of the standard compounds reported in the JCPDS files. Surface morphologies of thin films were studied by scanning electron microscope (SEM) JSM-6010LA. UV-Vis-NIR absorption spectra of thin films were recorded in the wave length range of 200-1200 nm using a Shimadzu UV-3600 UV-Vis-NIR spectrometer.

4.4.1 Structural characterization by XRD

X-ray diffraction (XRD) patterns of ZnO thin films deposited on glass substrate for different solution concentrations from 0.1 M to 0.5 M are shown in Fig. 4.2.

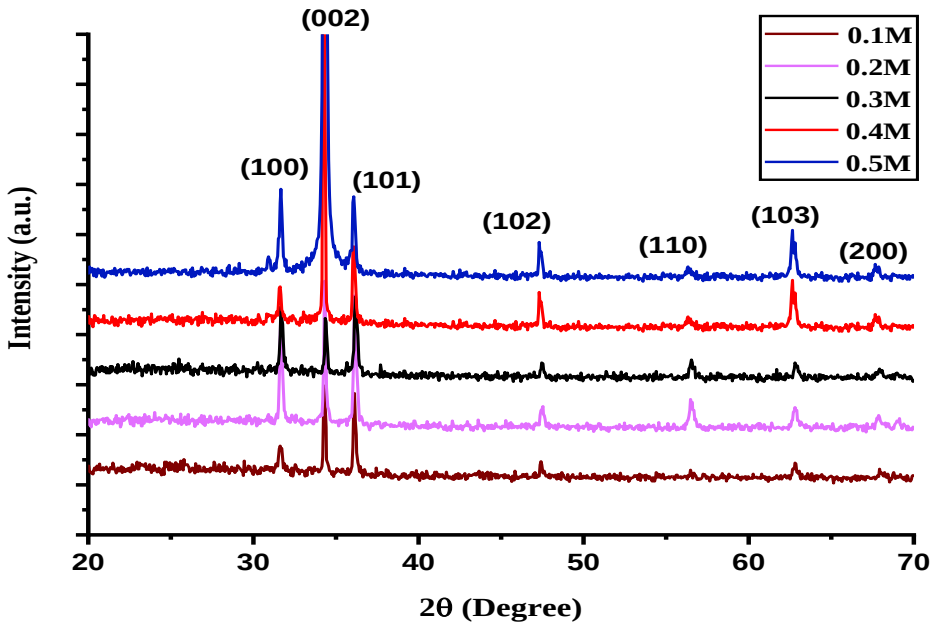

FIGURE 4.2 Powder XRD patterns for ZnO thin films prepared with different precursor concentrations.

Matching of observed and standard ‘d’ values of ZnO using JCPDS card No. 36-1451 confirms that deposited films fit well with hexagonal wurtzite structure. XRD patterns exhibit strong peaks (100), (002), (101), (102), (110), (103) and (200) planes assigned to hexagonal wurtzite structure. As shown in Fig. 4. 2 the relative intensity of the (0 0 2) peak

increases as the concentration of precursor increases, which indicates that the growth is enhanced along the c axis. All of the peaks are well matched with the bulk ZnO, which could be indexed as the hexagonal wurtzite structure of ZnO [160].

It can be seen from the XRD (Fig. 4.2) data that all samples are of single phase ZnO wurtzite structure (JCPDS, 36-1451), and the crystallinity of the films becomes better with increasing concentration. Diffraction peaks corresponding to the impurity were not found in the XRD patterns, confirming the high purity of the synthesized products. The crystallite size of the ZnO nanoparticles was calculated by the X-ray line broadening method using the Scherrer's equation [161].

$$\mathbf{D} = \frac{\mathbf{K\lambda}}{\boldsymbol{\beta} \cos \boldsymbol{\theta}} \tag{4.1}$$

Where D is the crystallite size, λ is the Cu -Kα radiation of wavelength (1.547A˚), K the shape factor 0.94, β_{hkl} is the full width at half maximum (FWHM) in radian and θ is the scattering angle. The dislocation density (δ), defined as the length of dislocation lines per unit volume. The dislocation density was calculated by the relation [162].

$$\boldsymbol{\delta} = \frac{\mathbf{1}}{\mathbf{D^2}} \tag{4.2}$$

Where D is the grain size. The micro strain of the thin films is estimated using the equation [163].

$$\boldsymbol{\varepsilon} = \frac{\boldsymbol{\beta} \cos \boldsymbol{\theta}}{\mathbf{4}} \tag{4.3}$$

Where, A is absorbance and t is the thickness. The grain size is found to be 233 nm, 238 nm, 228 nm, 218 nm and 184 nm for the variation in precursor concentration i.e. 0.1m, 0.2m, 0.3m, 0.4m and 0.5m respectively. The average value of grain size and dislocation density (δ) are presented in Table 4.1.

4.4.2 Morphological analysis

Morphologies of deposited films were examined using scanning electron microscopy. All the films were deposited under the optimized conditions and were smooth and uniformly covering the substrate with good adherence. Fig. 4.3(a) to 4.3(e) shows the surface morphology of ZnO thin films grown with different concentrations i.e. 0.1 mol/L, 0.2 mol/L, 0.3 mol/L, 0.4 mol/L and 0.5 mol/L respectively. Overall surface structure is seen to have grains of hexagonal shape, uniformly covering the substrate, without any cracks or pores.

From the Fig. 4.3, it can be seen that the specific surface area was gradually increased with the increasing of the concentration of reactants. Therefore, it can be concluded that the sizes of ZnO hexagonal pillars depend on the concentration of reactants, which can lead to the products with different length and diameters. It can be seen from the Fig. 4.3, the concentration had a great influence on the morphology of the ZnO thin films.

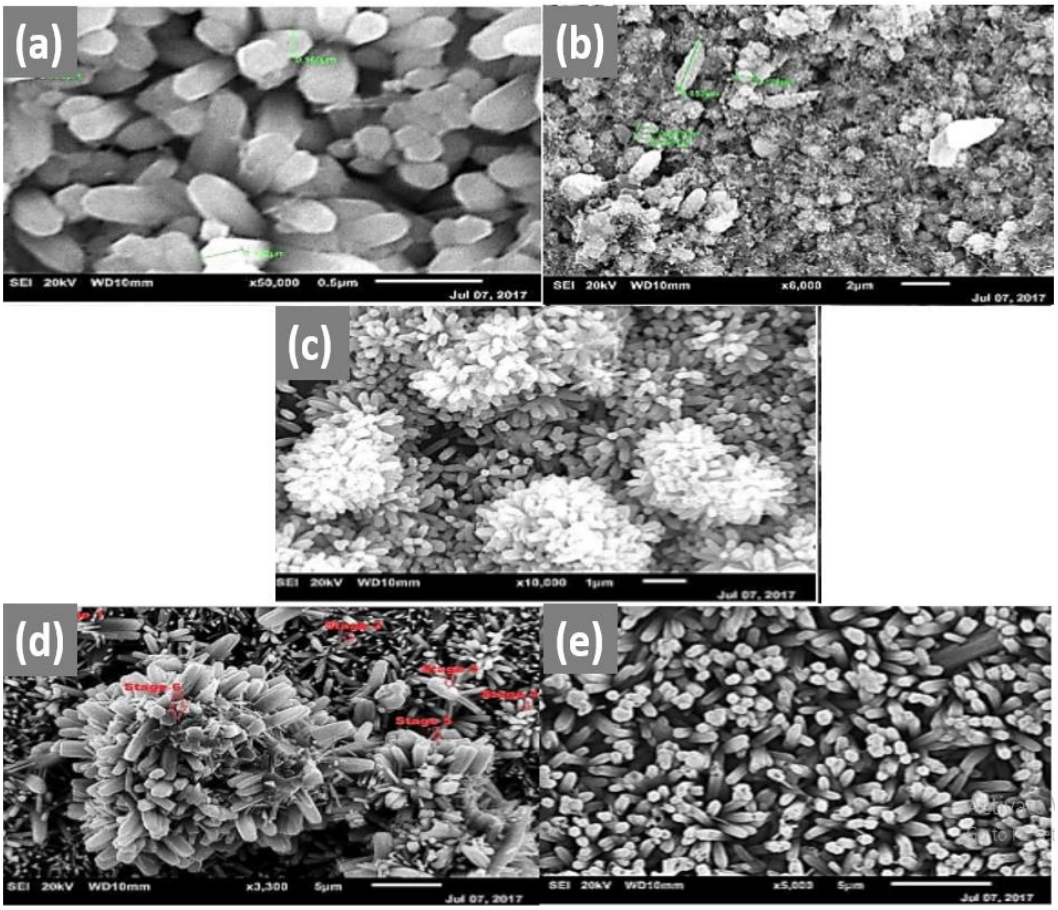

FIGURE 4.3(a) to 4.3(f) SEM micrographs of ZnO thin films prepared with precursor concentrations (a) 0.1M, (b) 0.2M, (c) 0.3 M, (d) 0.4 M and (e) 0.5M.

Figure 4.3(a)-(f) as a whole also explains the growth habit of ZnO thin films. For 0.1 M concentration of precursor, uniform hexagonal pillar structure is observed. As the concentration of precursor increases the growth rate increases which results in agglomeration of these pillars and formation of new nucleation over the ZnO surface (0.2 M; Figure 4.2(b)), followed by growth of nucleation (0.3 M; Figure 4.3(c) and 0.4 M; Figure 4.3(d)). Finally a continuous film having hexagonal pillar structure is prepared for 0.5 M concentration as shown in Figure 4.3(e).

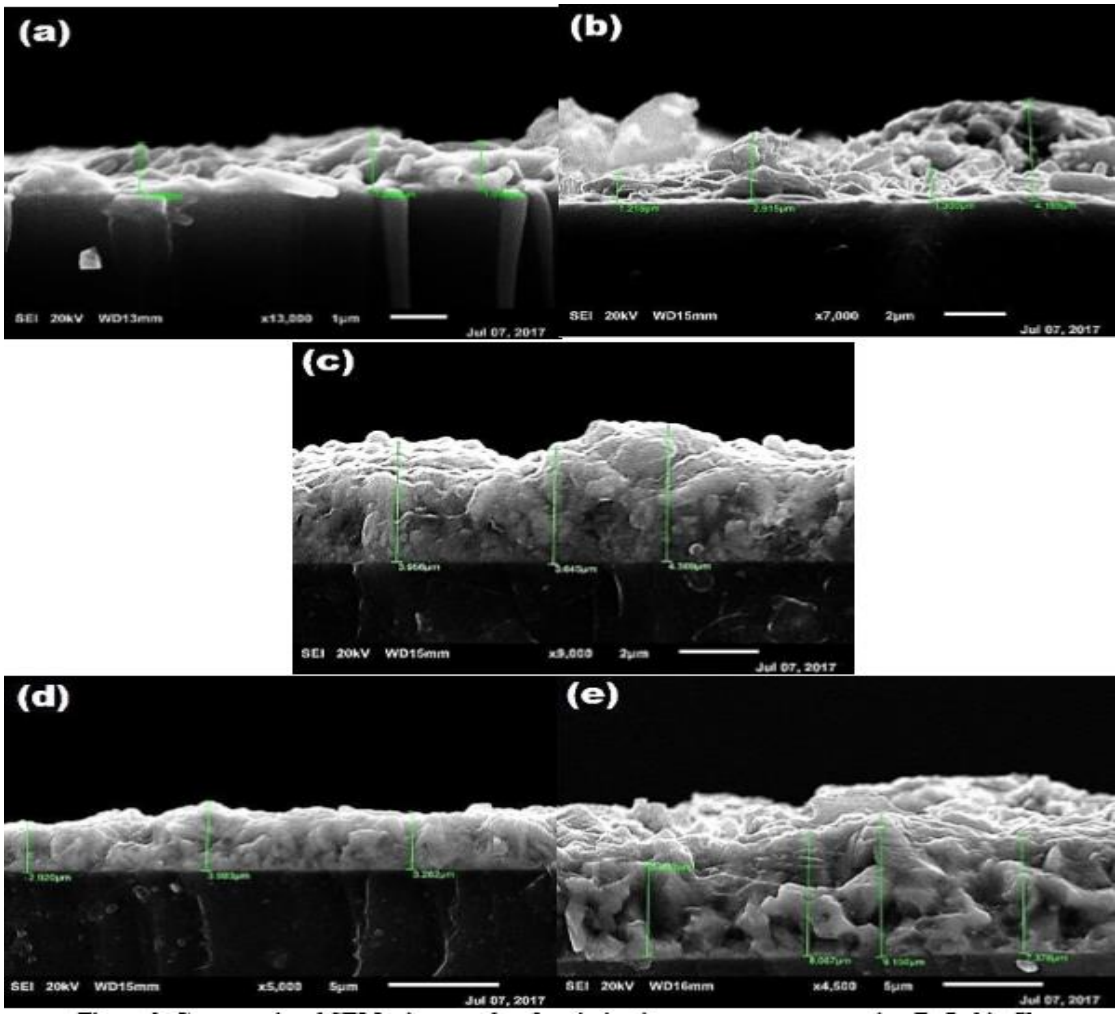

FIGURE 4.4 Cross-sectional SEM micrographs of ZnO thin films prepared with precursor concentrations (a) 0.1M, (b) 0.2M, (c) 0.3 M, (d) 0.4 M and (e) 0.5M.

Thickness of the ZnO thin films measured with the help of cross section SEM micrographs is shown in Fig. 4.4. Thickness of the films found 1.14 µm, 1.81µm, 3.99 µm, 4.67 µm and 10.2 µm for the variation in precursor concentration from 0.1M to 0.5M respectively. It reveals that thickness of the film increases with increase in precursor concentration. The results of thickness show influence of variation in precursor concentration on the thickness of the film.

4.4.3 UV-VIS-NIR Spectroscopy

Optical properties of ZnO thin films with increasing precursor concentration from 0.1M to 0.5M were studied using UV–VIS measurements in the 200–1200 nm wavelength range.

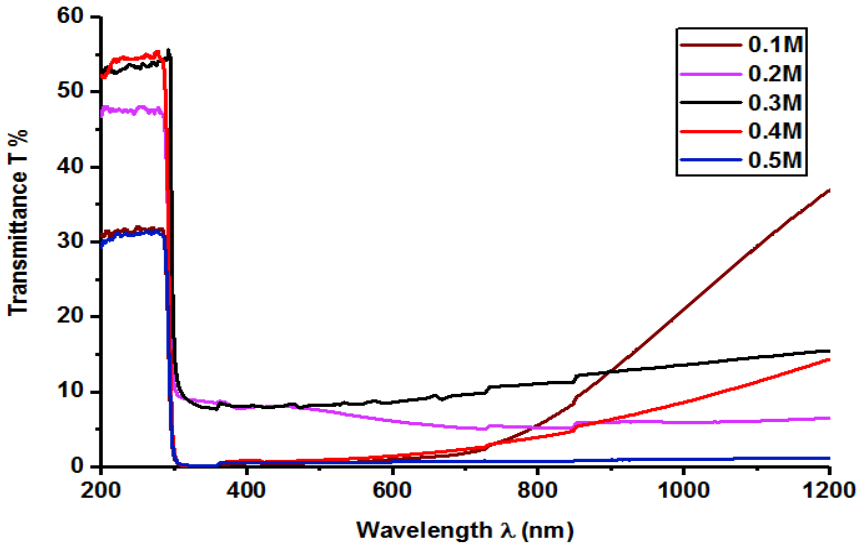

FIGURE 4.5 Transmittance spectra of ZnO thin films prepared with different precursor concentrations.

Figure 4.5 shows the optical transmittance (T) versus wavelength (λ) curves of variation in precursor concentration ZnO thin films from 0.1M to 0.5M. Optical transmission spectrum shows that transmission increases with increase in the concentration up to 0.3 M and the maximum transmission in visible region is about 10% for ZnO films prepared with 0·3M. After that transmittance for 0.4M and 0.5M decreases with precursor concentration.

Absorbance was calculated from the Pankove relationship [164] as below.

$$\mathbf{A} = \log\left(\frac{\mathbf{1}}{\mathbf{T}}\right) \tag{4.4}$$

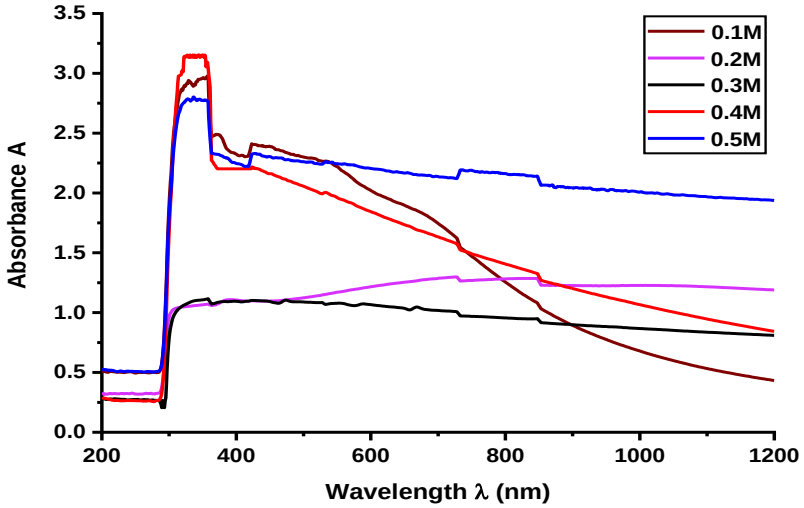

FIGURE 4.6 Absorbance spectra of ZnO thin films prepared with different precursor concentrations.

The absorbance versus wavelength curve for ZnO thin films with different concentrations is shown in Fig. 4.6. The absorbance near 350 nm is sharp and the bend near absorption edge confirms the polycrystalline structure of ZnO thin films [165]. Absorbance of thin films are found to increase with increase concentration because of increase in thickness as well as increase in height of hexagonal pillars which forces incident radiation to suffer multiple reflections between their vertical surfaces. It is observed in Fig.4.6 that the absorbance is very high up to ~350 nm and falls rapidly with desreasing wavelength indicating the absorption edge in this region for all thin films. The absorption coefficient is obtained from the relation [166].

$$\alpha = \frac{2.303\ A}{T} \tag{4.5}$$

Where t is the thickness of thin films obtained from cross-sectional SEM. Optical band gap of thin films were determined by plotting $(\alpha h\nu)^2$ as a function of hν, and extrapolating the linear portion of absorption edge up to $(\alpha h\nu)^2 = 0$. The band gap of thin films is evaluated from Tauc equation [166]. The Tauc equation for a direct band gap material is narrated as,

$$\alpha h\nu = A\left(h\nu - E_g\right)^n \tag{4.6}$$

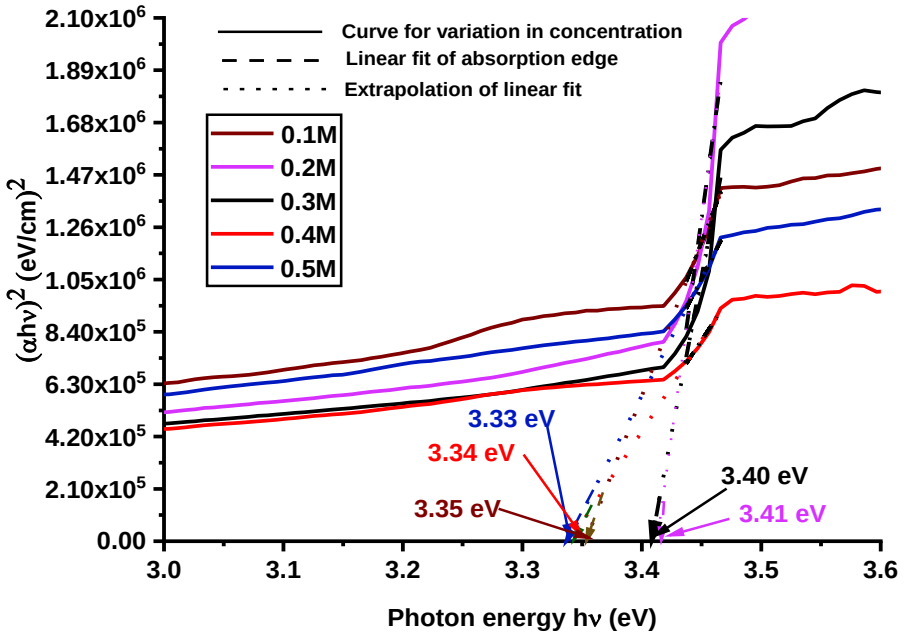

FIGURE 4.7 Plot of $(\alpha h\nu)^2$ vs. photon energy hν (in eV) of ZnO thin films prepared with different precursor concentrations.

Figure 4.7 shows the plot of $(\alpha h\nu)^2$ vs photon energy hν. The obtained values of optical bandgaps are 3.35 eV, 3.41 eV, 3.40 eV, 3.34 eV and 3.33 eV for ZnO films produced using 0.1M, 0.2M, 0.3M, 0.4M and 0.5M precursor concentrations respectively. Here, the bandgap of ZnO films decreases with increasing precursor concentration from 0.2M to 0.5M. The decrease in bandgap can be attributed to the variation of strain. Strain changes the inter-atomic spacing of semiconductors which affects the energy gap. The decrease in Eg may be attributed to increase in film thickness [167].

Refractive indices of all thin films are calculated using the relation reported by Islam and podder [168].

$$\mathbf{n} = \left(\frac{\mathbf{1}+\mathbf{R}}{\mathbf{1}-\mathbf{R}}\right) \tag{4.7}$$

Where n is the refractive index and R is the optical reflectance.

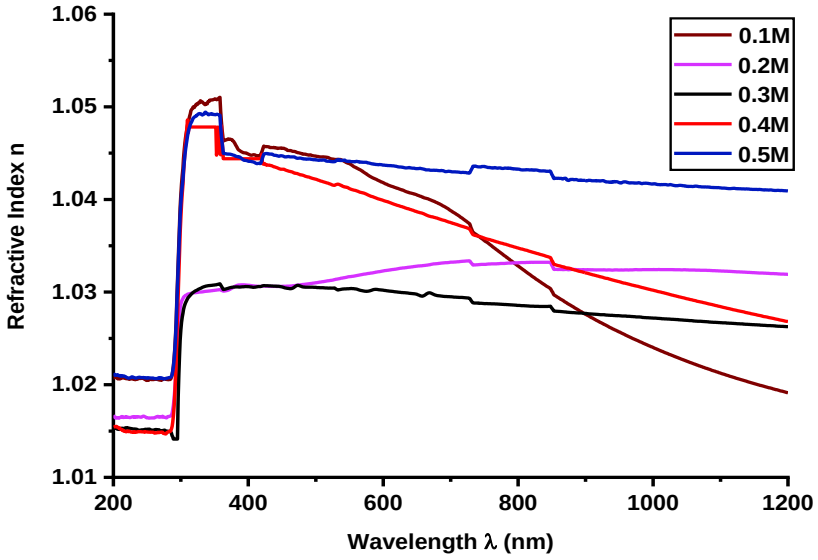

FIGURE 4.8 Refractive index vs wavelength of ZnO thin films prepared with different precursor concentrations.

The refractive index is an important parameter for optical materials and their applications [169]. Therefore, it is important to determine the refractive index of the films. The refractive index and extinction coefficient of these films were determined using transmittance and reflectance measurements. The refractive index of pure ZnO thin films was found to exhibit values ranging between 1.01 and 1.02 as the wavelength increases from 200 to 300 nm, but from 300 nm to 1200 nm wavelength its value increase and ranging between 1.03 and 1.05 for different precursor concentration. The refractive index values for all samples are lower, as compared to theoretical refractive index of ZnO film in the visible region n = 2.

Shakti (2010) notes that the absorption coefficient α and the extinction coefficient k are related by the given formula [170].

$$\mathbf{k} = \frac{\boldsymbol{\alpha\lambda}}{\mathbf{4\pi}} \tag{4.8}$$

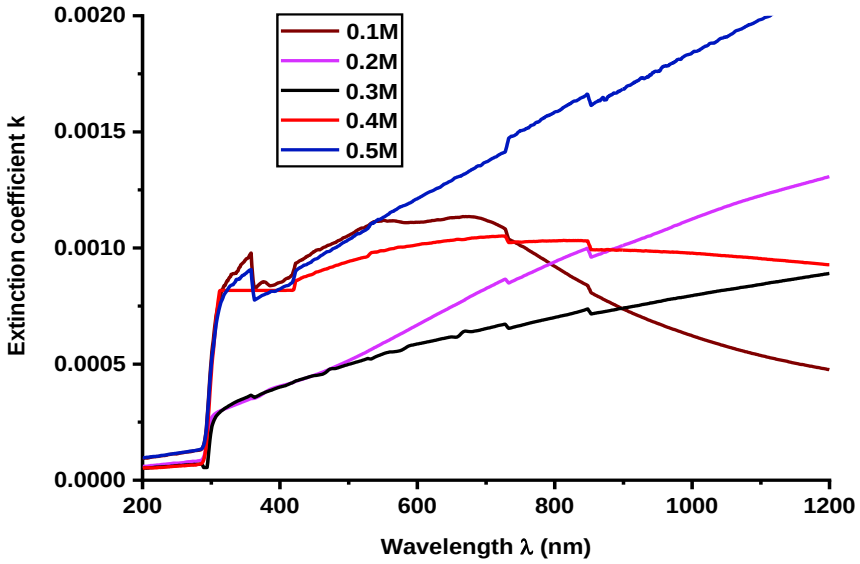

FIGURE 4.9 Extinction coefficient vs wavelength of ZnO thin films prepared with different precursor concentrations.

Fig. 4.9 shows extinction coefficient k as a function of incident photon wavelength (200 to 1200 nm) of 0.2M to 0.5M concentration of ZnO thin films are increases with increase in the wavelength. The extinction coefficient value is considerably low. This indicates that the ZnO film has the low dielectric losing.

The complex dielectric constant ε (ω) = ε_i (ω) - iε_r (ω) characterizes the optical properties of the solid material. The real εr and imaginary εi parts of the dielectric constant for ZnO thin films are determined by [171]:

$$\boldsymbol{\varepsilon_r} = \mathbf{n^2}\ (\boldsymbol{\lambda}) - \mathbf{k^2}\ (\boldsymbol{\lambda}) \tag{4.9}$$

$$\boldsymbol{\varepsilon_i} = \mathbf{2n}\ (\boldsymbol{\lambda})\ \mathbf{k}\ (\boldsymbol{\lambda}) \tag{4.10}$$

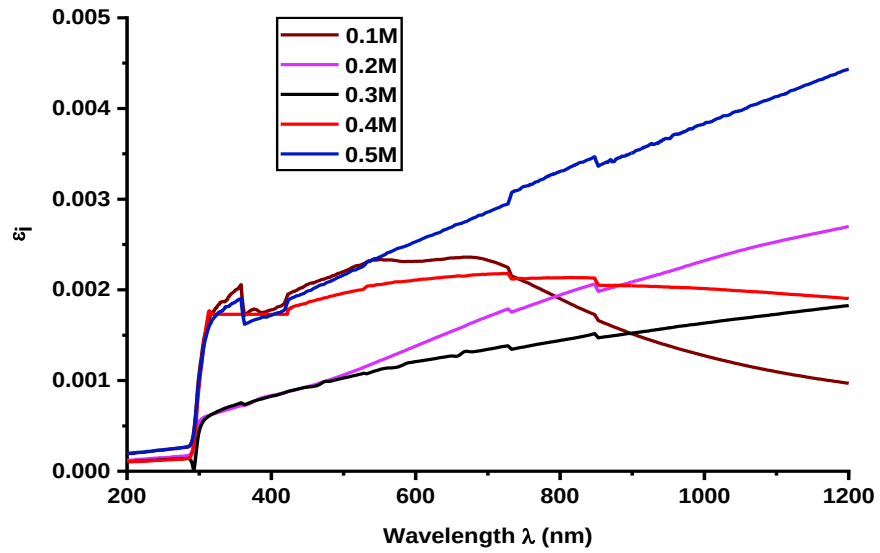

FIGURE 4.10 Imaginary part of dielectric constant vs wavelength of ZnO thin films prepared with different precursor concentrations.

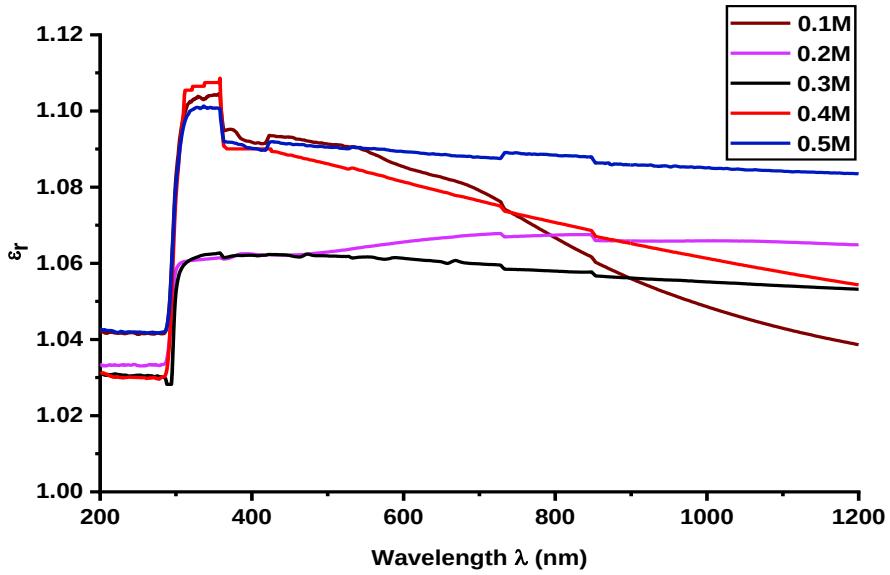

FIGURE 4.11 Real part of dielectric constant vs wavelength of ZnO thin films prepared with different precursor concentrations.

The variation of ε_i and ε_r with the variation in precursor concentration of the films is illustrated in Fig. 4.10 and 4.11 respectively. These figures reveal that the values of the real part are higher than the imaginary one, which confirms the good transparency of these thin films.

Table 4.1 Structural, morphological and optical parameters for ZnO thin films prepared with different precursor concentrations.

Variation in concentration	Crystallite size D (nm)	Average value of ε	Thickness of film (μm)	Band gap Eg (ev)	Refractive indices at 550 nm	Extinction coefficients at 550 nm	Average of δ value (lines/m^2)
0.1M	233	$5.00X10^{-3}$	1.14	3.35	1.04	$1.12 X 10^{-4}$	18.42
0.2M	238	$4.43X10^{-3}$	1.81	3.41	1.03	$5.90 X 10^{-3}$	17.65
0.3M	228	$5.17X10^{-3}$	3.99	3.40	1.03	$5.44 X 10^{-3}$	19.23
0.4M	218	$5.40X10^{-3}$	4.67	3.34	1.04	$9.88 X 10^{-3}$	21.04
0.5M	184	$6.02X10^{-3}$	10.2	3.33	1.04	$11.3 X 10^{-4}$	29.53

4.5 Variation in number of coat

4.5.1 Structural characterization by XRD

The X-ray diffraction (XRD) spectra of ZnO thin films from 1 coat to 5 coat are presented in Fig. 4.12. Crystallographic structures of grown thin films were studied by X-ray diffraction.

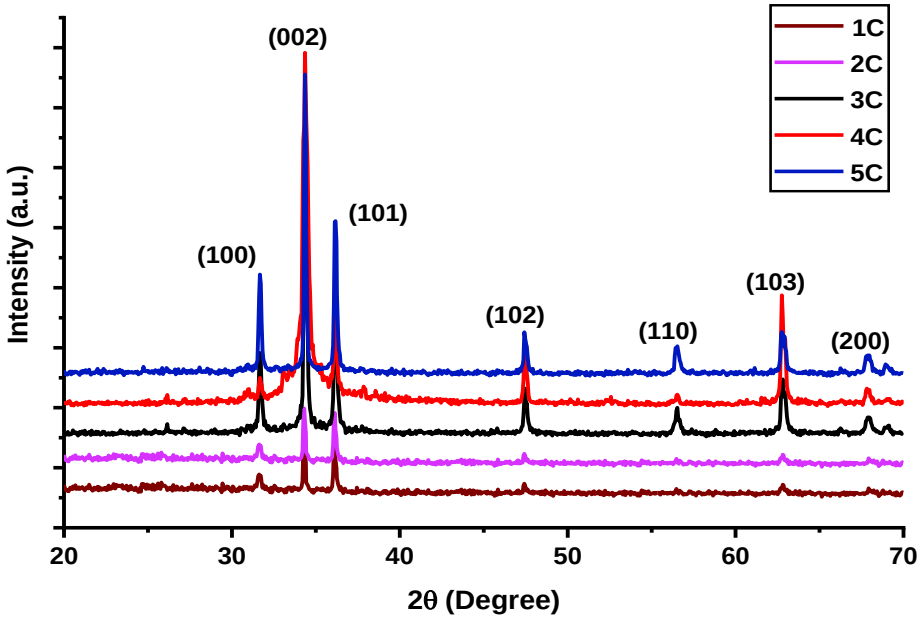

FIGURE 4.12 Powder XRD patterns of ZnO multilayer thin films.

Powder XRD patterns exhibit strong peaks (100), (002), (101), (102), (110), (103) and (200) planes assigned to hexagonal wurtzite structure as shown in Fig. 4.12. Experimental pattern

show very fine peaks indicating good crystallinity of thin films. Powder XRD patterns of all the thin films are found to have single phase ZnO wurtzite hexagonal structure in good accordance with JCPDS card no. 36-1451, and the crystallinity of the films seems to be increasing with number of coat.

XRD spectrum of ZnO film indicates that the diffraction peak corresponding to (002) orientation is more intense and sharp which is due to the highest density of Zn atoms in this plane. Due to the minimal surface energy, heterogeneous nucleation readily happens at the interface of film and substrate. The preferential orientation of the film grows along c-axis i.e. (002) plane, which is perpendicular to the substrate. Fig. 4.12 also shows some other small peaks which may be due to non-decomposed organic compounds or impurities in the solution used for deposition of the film.

The crystallite size of the ZnO nanoparticles was calculated by the X-ray line broadening method using the Scherrer's equation (4.4). Average crystallite size of the ZnO nanoparticles was found in the range from 38 nm to 44 nm and lattice strain gradually decrease as shown in Table 4.2.

4.5.2 Morphological analysis

Fig. 4.13 and 4.14 show SEM micrographs of top surface and the cross section of Zno multilayer thin films respectively.

ZnO thin films are developed in the form of randomly oriented hexagonal pillars which have micrometer sized diameter. Figure 4.13(a) to 4.13(e) represent single coat to quintuple coats of ZnO thin films. As figures show that size of hexagonal pillars are directly proportional to the number of coats. Also agglomeration occurs in these surface structures with increase in number of coats.

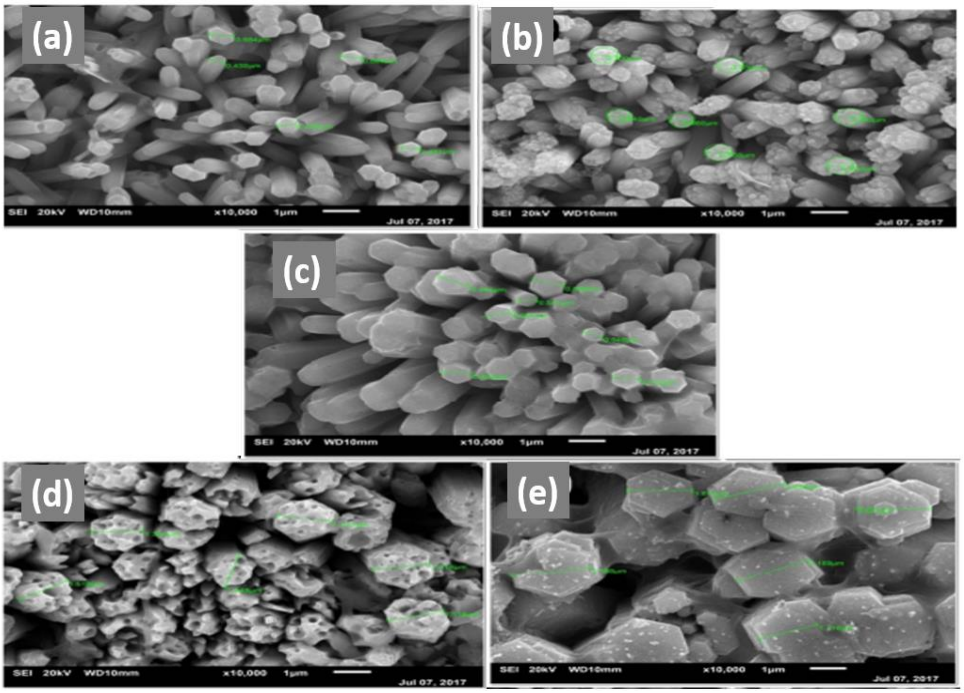

FIGURE 4.13(a) to 4.13(e) SEM micrographs of ZnO multilayer thin films of ZnO thin films prepared with variation in number of coat (a) 1C, (b) 2C, (c) 3C, (d) 4C and (e) 5C.

Fig.4.14 shows cross-sectional SEM micrographs which conclude that as number of coats increases, thickness of ZnO thin film also increases. Table 4.2 contains the average size of hexagonal surface structures and thickness of ZnO multilayer thin films.

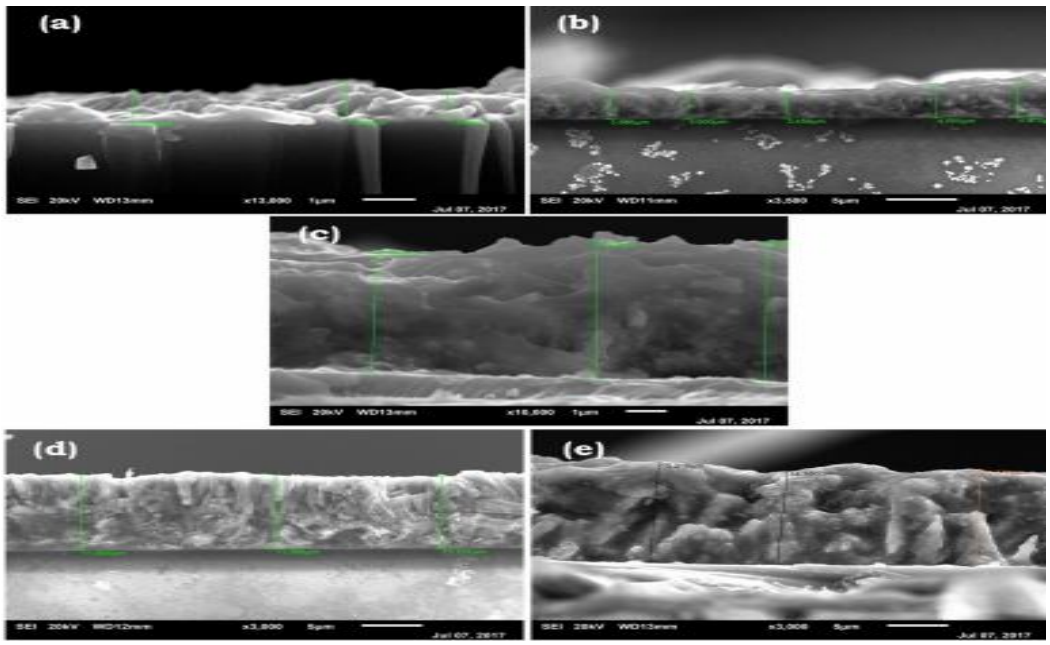

FIGURE 4.14(a) to 4.13(e) Cross-sectional SEM micrographs of ZnO multilayer thin films of ZnO thin films prepared with variation in number of coat (a) 1C, (b) 2C, (c) 3C, (d) 4C and (e) 5C.

4.5.3 UV-VIS-NIR Spectroscopy

The optical properties of multilayer thin films were studied using UV–VIS measurements in the 200–1200 nm wavelength region.

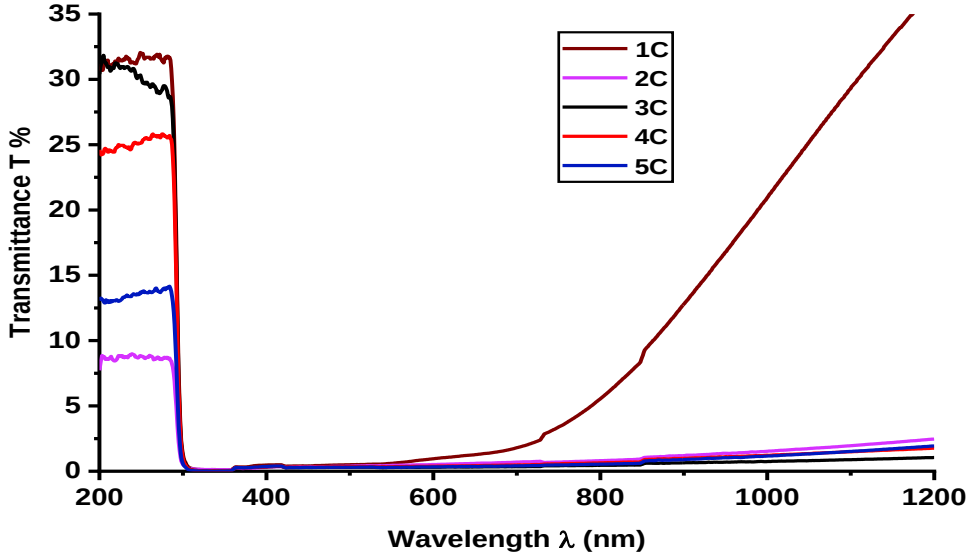

FIGURE 4.15 Transmittance spectra of ZnO multilayer thin films.

Figure 4.15 shows the transmittance spectrum for a wavelength range of 200-1200 nm of the variation in the number of coat from single coat i.e.1C to quintuple coat i.e. 5C of the ZnO thin films.

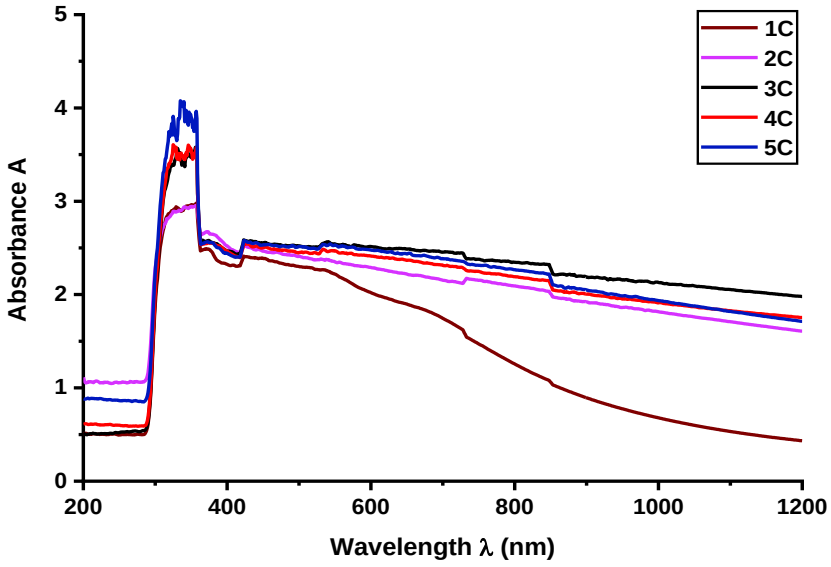

FIGURE 4.16 Absorbance spectra of ZnO multilayer thin films.

The optical absorbance spectra of the films are shown in Fig. 4.16. From the absorbance spectra, it is apparent that all the films have a low absorption in the ultra-violet range and a

high absorption in the visible range. It can be seen that increase of coat makes slightly shifts of absorption edge to higher wavelengths. In addition, the nearly flat spectra are shown in the higher wavelength area. It is evident from absorption spectra that the absorption increases with increasing number of coat of the films.

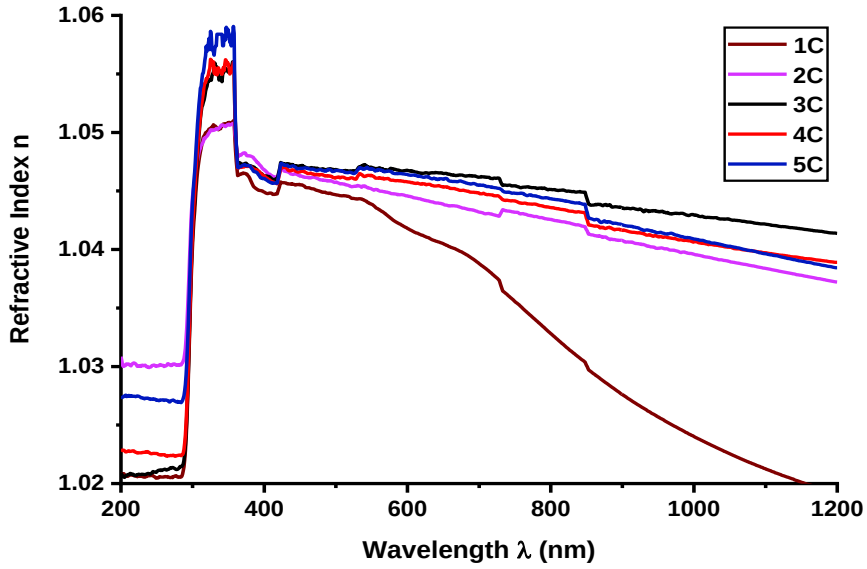

FIGURE 4.17 Refractive index vs wavelength of ZnO multilayer thin films.

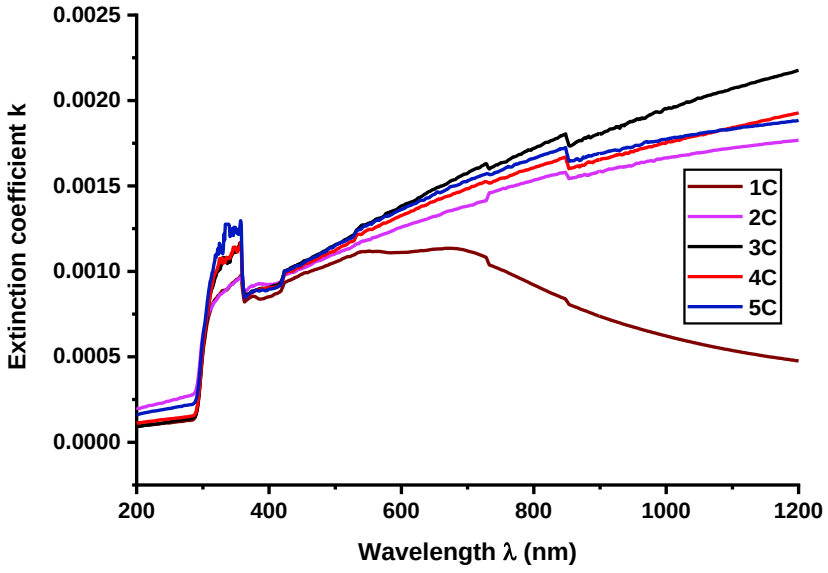

FIGURE 4.18 Extinction coefficient vs wavelength of ZnO multilayer thin films.

Refractive index of the films were calculated using (4.10). The variation in refractive index with wavelength were shown in Fig. 4.17.

As shown in Fig. 4.17 as the number of coat of ZnO thin film from single coat i.e.1C to quintuple i.e.5C increases refractive index is also increases. The value of refractive index are lies between 1.02 and 1.03 for the wavelength below 300 nm, but as wavelength increases refractive index increases up to 1.06.

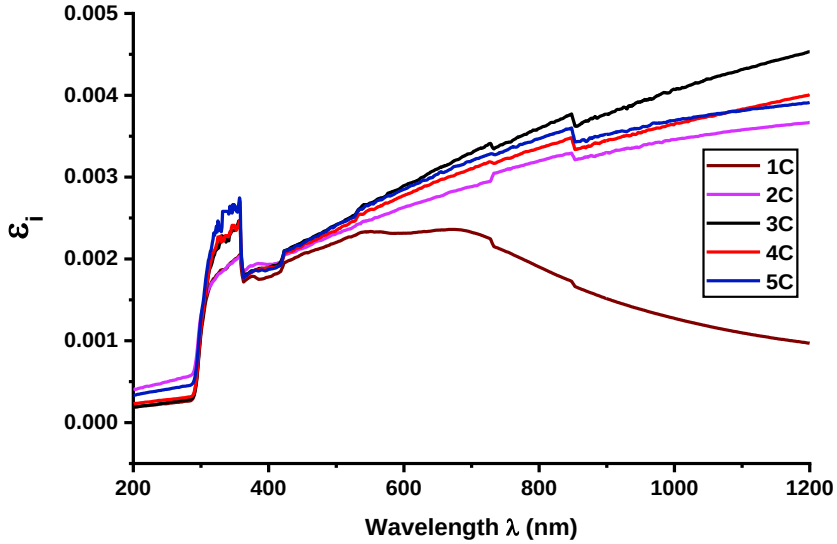

FIGURE 4.19 Imaginary dielectric constant ε_i vs wavelength for ZnO multilayer thin films.

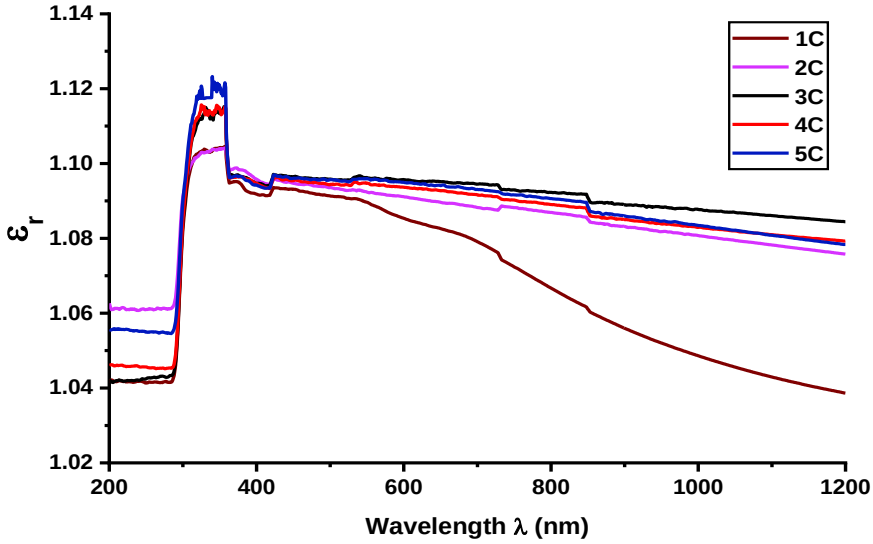

FIGURE 4.20 Real dielectric constant ε_r vs wavelength for ZnO multilayer thin films.

Extinction coefficient was calculated from (4.8). Figure 4.18 shows the variation of extinction coefficient as a function of wave length for ZnO multilayer thin films. It is observed from this figure that the extinction coefficient increase as increase in the wavelength. Also, it is observed from this figure that the extinction coefficient at wavelength 300 nm increases with the wavelength, opposite to the variation of the refractive index. But

the less values of extinction coefficient at 200 nm are due to the improvement of the structure.

Figure 4.19 and 4.20 shows the variation of real (ε_r) and imaginary (ε_i) dielectric constants for ZnO thin films. One can observed that the variation of εr is similar trend to that of the refractive index because of the smaller value of k^2 in comparison with n^2, while the variation of εi mainly depends on the k value, which are related to the variation of absorption coefficient. ε_i represent the absorption of radiation by free carriers. It is observed from the figures that the real and imaginary dielectric constants increase with the increase of the wavelength of the incident radiation and this behavior is due to the change of reflectance and absorbance. Small extinction coefficient k values were obtained over the entire visible region, indicating the high transparency nature of the prepared films.

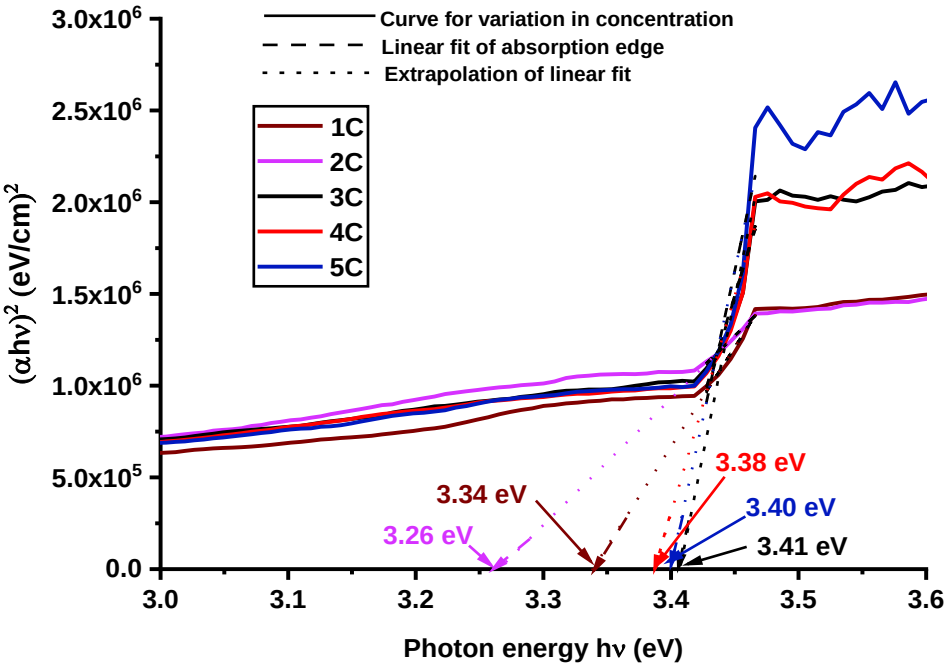

FIGURE 4.21 Plot of $(\alpha h\nu)^2$ vs. photon energy (in eV) of ZnO multilayer thin films

Theory of optical absorption gives the relationship between the absorption coefficients α and the photon energy hν for direct allowed transition (4.9). Band gap estimation of ZnO thin films of different coat of using Tauc's method, the value of band gap was calculated by extrapolating the linear part of the spectra of $(\alpha h\nu)^2$ versus hν plot. An examination of the optical transmission spectra showed that the energy band gap of the multilayer ZnO thin films ranges from 3.26 eV to 3.41 eV.

Table 4.2 Structural, morphological and optical parameters for the multilayer ZnO thin films.

Number of coat	Crystallite size D (nm)	Average value of E	Thickness of film (μm)	Band gap Eg (ev)	Refractive indices at 550 nm	Extinction coefficients at 550 nm
1C	233	5.00×10^{-3}	1.14	3.34	1.04	1.12×10^{-3}
2C	238	7.62×10^{-3}	3.91	3.26	1.05	1.18×10^{-3}
3C	228	5.70×10^{-3}	6.07	3.41	1.05	1.28×10^{-3}
4C	218	6.74×10^{-3}	11.38	3.38	1.05	1.24×10^{-3}
5C	184	5.08×10^{-3}	14.3	3.40	1.05	1.28×10^{-3}

4.6 Discussion of results of ZnO thin films

- Pure ZnO thin films have been successfully synthesized from zinc chloride as source of Zn by chemical bath deposition method on glass substrate.
- ZnO thin films were successfully synthesized by a low cost method which does not require high technology. Also it is a simple and one step method. It doesn't require catalyst or buffer layer on substrate before the reaction. In this method product is obtained with high quality. The films had good adherence to the substrate.
- Structural, optical and morphological studies were carried out. XRD spectra revealed that the films are crystalline with hexagonal wurtzite structure. XRD data confirmed that the ZnO thin films were highly oriented along (002) direction. The sharp peaks show good crystallinity, resulting in high quality films.
- Particle size evaluated using x-ray line broadening analysis shows a constantly increasing trend with increasing precursor concentration from 0.1M to 0.5M as well as increasing number of coats from single coat to quintuple coats.
- The undoped ZnO film is crystalline with strong preferred c-axis orientation. ZnO thin films with average crystallite size of 184-233 nm were successfully synthesized via aqueous chemical route. As the concentration of the precursor increases, thickness of the film increases and lattice strain is also increasing gradually.
- The band gap energies from Eg = 3.36 eV to 3.47 eV with intensive ultraviolet (UV) emission was concluded with increasing concentration from 0.1M to 0.5M.
- The bath temperature was found to influence the growth of ZnO crystallites: at temperatures at 80 °C, good crystalline film was produced. The pH 9.6 was found to be the most suitable for CBD growth of ZnO thin films.

- ZnO multilayer thin films were successfully prepared by growing new layers on other layers of ZnO by CBD route. Annealing temperature required for the conversion of precursor complexes in to ZnO is determined. The XRD results of thin films indicate purity and existence of single hexagonal wurtzite phase.
- Effect of multi-layering of ZnO thin films on morphology and optical properties were studied. Lattice strain, band gap, refractive index and extinction coefficient are found to be firmly unaffected by multiple layering of ZnO thin films, while surface morphology, crystallite size, transmittance and absorbance changes with number of coat.

CHAPTER 5

Preparation of pure and Cu doped ZnO Thin Films by Dip Coating, Powder Sample and Their Characterization

5.1 Introduction

Physical properties of ZnO greatly depend on the method and condition of depositing films. ZnO films has been prepared by various methods such as electrochemical deposition [172], chemical bath deposition (CBD) [173], molecular beam epitaxy [174], pulsed laser deposition [175], magnetron sputtering [176], MOCVD [177] and spray pyrolysis [178]. Sol-gel dip-coating method for depositing ZnO thin film seems more attractive because of its simple procedure; and it require no costly vacuum systems. It has broad advantage of large area deposition with uniform thickness. [179-180]. Dip coating is a simple and effective technique which is commonly used in manufacturing across a wide range of different products in industries. Within research and development, it has become an important coating method for the fabrication of thin films using a purpose-built dip coater. When the process is optimized, dip coating can be used to produce highly uniform films. Importantly, key factors such as film thickness can be easily controlled. One advantage of dip coating over other processing techniques is the simplicity of its design.

In studies designed to compare with the other methods it is noticed that sol–gel method is the extensively used due to its high versatility, simplicity, cost effective equipments, the its systematically and carefully controlled stoichiometry over the molecular level mixing, large area of covering, high homogeneity or uniformity and fairly low process temperature [181-

183]. In this research ZnO thin film is fabricated by sol-gel dip-coating route and a detailed investigation is given by analyzing its structural and optical characterization of the film.

Raman scattering is one of the effective techniques to investigate the crystallization, structure, and defects in the thin films. Upon Cu doping, the overall shape of the Raman spectrum changes, due to the loss of symmetry conservation leading to the appearance of "silent" and mixed Raman modes from points of the center of the Brillouin zone. The wurtzite ZnO belongs to the point group C_{6v} with two formula units in the primitive cell. Each primitive cell of ZnO has four atoms, each occupying C_{3v} sites, leading to 12 phonon branches, nine optical modes, and three acoustic modes [184]. The Brillouine zone (Γ point) group theory concludes that lattice optical phonons have the following irreducible representation [185].

$$\Gamma = \mathbf{1}\boldsymbol{A_1} + \mathbf{2}\boldsymbol{B_1} + \mathbf{1}\boldsymbol{E_1} + \mathbf{2}\boldsymbol{E_2} \quad (5.1)$$

Where A_1 and E_1 modes are infrared and Raman active and polar, whereas E_2 modes are only Raman active and non-polar. E_2 modes contain two types wave numbers, i.e. E_2 (high) and E_2 (low) correlated with the motion of oxygen and Zn sub lattice, respectively [184]. Strong E_2 (high) mode is unique for the wurtzite lattice and point outs good crystallinity. Unit cell shows polarization of the vibrations of A_1 and E_1 modes which forms a long range electrostatic field separation of polar modes into longitudinal optical (LO) and transverse optical (TO) component. Furthermore, A_1 and E_1 modes are infrared active so that they break down into longitudinal and transverse optical component (LO and TO). The mode assignment at present conditions is acknowledged in the literature [186]. The E_1 (LO) mode is related with the existence of oxygen vacancies, interstitial Zn or their complexes. The B_1 modes are Raman and infrared dormant (silent modes).

5.2 Growth of pure and Cu doped ZnO thin films using sol-gel dip coating technique and their powder samples

Pure ZnO thin film are developed onto glass substrates using sol–gel method via dip coating. 0.1M 120 mL clear and homogeneous solution of zinc chloride was prepared in methanol. Then the product was divided into two equal parts and in one part 20mL 0.1M cuprous chloride solution prepared in methanol was added. Final solutions were kept at room temperature. Thus two precursor solutions were prepared to make thin films of pure and copper doped ZnO thin films onto a glass substrate. Before immersing substrate into

precursor sols for deposition, glass substrates were thoroughly washed using HCl, detergent and distilled water as mentioned in previous deposition method. Also substrates were ultrasonicated in methanol for 15min and dried at 50°C in oven to confirm degreasing and removal all contaminated particles which could affect thin-film properties. Film depositions were performed via the dip-coating method onto glass substrates with 30 sec of dipping time. After coating, samples were kept in an oven at 70°C for 15min to dry by evaporating the solvent as well as to remove unwanted organic residues. Also samples were kept in horizontal position to avoid draining of the transferred sol which may lead to coatings. Grown films were annealed at 500°C for an hour in an oven and cooled down to room temperature.

In pure ZnO powder preparation, first of all 60 mL 0.1 molar zinc chloride solution in aqueous medium was prepared. After that drop wise aqueous ammonia added and stirred the solution continuously to get 9.6 pH. In order to prepare copper doped ZnO powder, 20mL 0.1 molar solution of cuprous chloride was supplemented in the prepared solution. Final solutions were kept at room temperature for the slow evaporation process to convert the solution into powder form. Powders prepared in this way were annealed at 500°C for an hour in oven and cooled down to room temperature.

5.3 Structural characterization by XRD

X-ray diffraction (XRD) patterns of pure and Cu doped ZnO thin films deposited on glass substrate and their powder samples are shown in Figure 5.1.

XRD technique was used for identification of crystal structure and for finding various lattice parameters. The XRD spectra of pure and copper-doped ZnO thin films and their powder samples are shown in Fig. 5.1. From the sharp and highly diffracted intensity of X-rays for pure ZnO, it is clear that all the particles exhibit good crystalline nature. The XRD patterns for Cu-doped samples were found to be exactly the same as that for pure ZnO. This information was easily indexed to hexagonal wurtzite phase with $P6_3mc$ group and JCPDS card (36-1451). Different characteristics peaks were observed at an angle 2θ i.e., at 31.80°, 34.47°, 36.29°, 47.59°, 56.64° and 62.94° which respond to the miller indices (1 0 0), (0 0 2), (1 0 1), (1 0 2), (1 1 0) and (1 0 3) respectively. All these peaks and Miller Indices are related

to the standard hexagonal wurtzite crystal structure of ZnO indexed and compared with JCPDS card (36-1451).

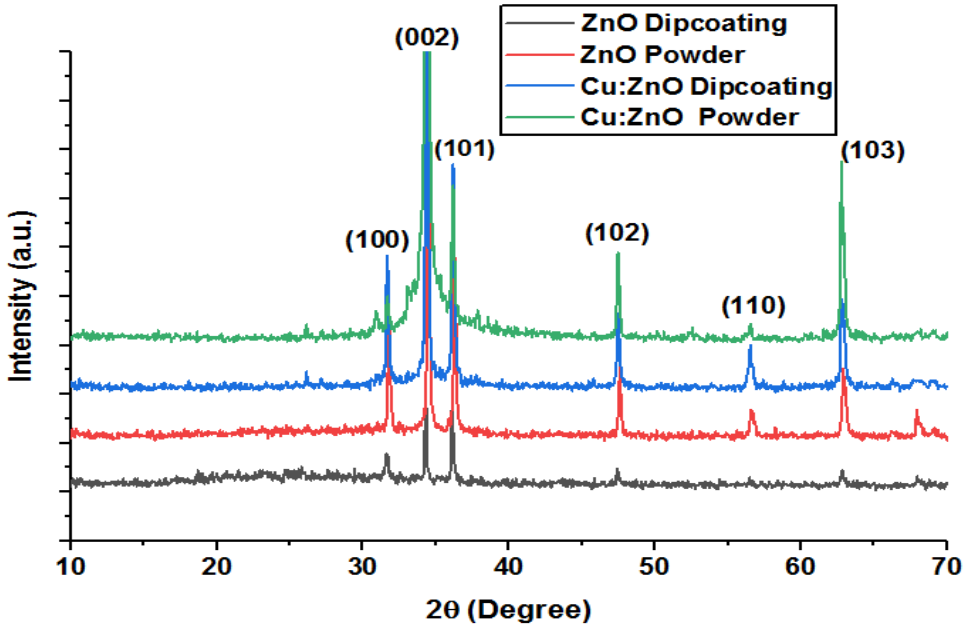

FIGURE 5.1 Powder XRD patterns for variation in number of coat of ZnO thin films.

The average grain size of all the samples was determined by using Scherer formula. Various parameters from XRD analysis of pure and Cu doped ZnO thin films and their powder samples are shown in Table 5.1. The reduction in the crystalline size by doping ZnO with Cu^{+2} is mainly due to the alteration in the host ZnO lattice, which decreases the nucleation and subsequent growth rate by the addition of Cu. The presence of Cu doped concentrations causes more defects and deformed lattice structures.

Table 5.1 Various parameters from XRD analysis of pure and Cu doped ZnO thin films and their powder samples.

Sample	Miller Indices (h k l)	2θ	FWHM β_{hkl}	d - spacing	Micro strain Ɛ X 10^{-2}	Crystallite size D (nm)	Average Crystallite size D (nm)	Dislocation density
ZnO Dip coating	100	31.80	0.1993	2.8135	0.3052	43.32	39.10	0.000533
	002	34.47	0.1928	2.6016	0.2290	43.14		0.000537
	101	36.29	0.2005	2.4750	0.2669	43.58		0.000526
	102	47.59	0.2165	1.9108	0.2143	41.92		0.000569
	110	56.64	0.3011	1.6249	0.2438	31.33		0.001019

	103	62.94	0.3110	1.4766	0.2217	31.30		0.001020
Cu: ZnO Dip coating	100	31.69	0.2151	2.8236	0.3307	40.13	35.68	0.000621
	002	34.36	0.2170	2.6099	0.2074	38.33		0.000681
	101	36.18	0.2319	2.4828	0.3098	37.67		0.000705
	102	47.48	0.2328	1.9147	0.2309	38.97		0.000658
	110	56.52	0.3176	1.6280	0.2578	29.68		0.001135
	103	62.84	0.3323	1.4787	0.2373	29.29		0.001166
ZnO Powder	100	26.55	0.1693	3.3575	0.3131	50.40	37.75	0.000394
	002	34.31	0.1928	2.6133	0.2725	45.07		0.000492
	101	36.14	0.2405	2.4852	0.3216	36.32		0.000758
	102	47.47	0.2665	1.9151	0.2645	34.04		0.000863
	110	56.48	0.3011	1.6290	0.2446	31.30		0.001020
	103	62.78	0.3313	1.4799	0.2369	29.36		0.001160
Cu: ZnO Powder	100	31.67	0.2134	2.8248	0.3283	40.45	36.72	0.000611
	002	34.35	0.2215	2.6103	0.3127	39.24		0.000649
	101	36.16	0.3119	2.4835	0.4168	28.01		0.001275
	102	47.47	0.2022	1.9151	0.2006	44.86		0.000497
	110	56.53	0.2654	1.6278	0.2154	35.52		0.000792
	103	62.81	0.3019	1.4792	0.2157	32.23		0.000963

5.4 Study of optical properties

UV–VIS spectroscopic measurements at room temperature carried out to find the band gap of ZnO thin films. The wavelength range used to record optical reflectance and transmittance spectra was 200–1200 nm. Fig. 5.2 and 5.3 shows the optical transmittance for powder samples as well as thin film samples of pure and Cu doped ZnO thin films grown by dip coating method.

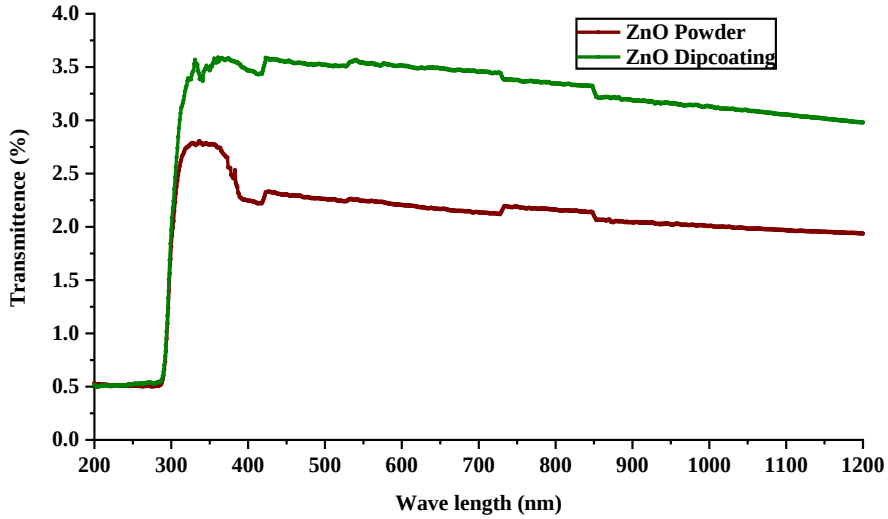

FIGURE 5. 2 Transmittance spectra of pure ZnO thin film and ZnO powder.

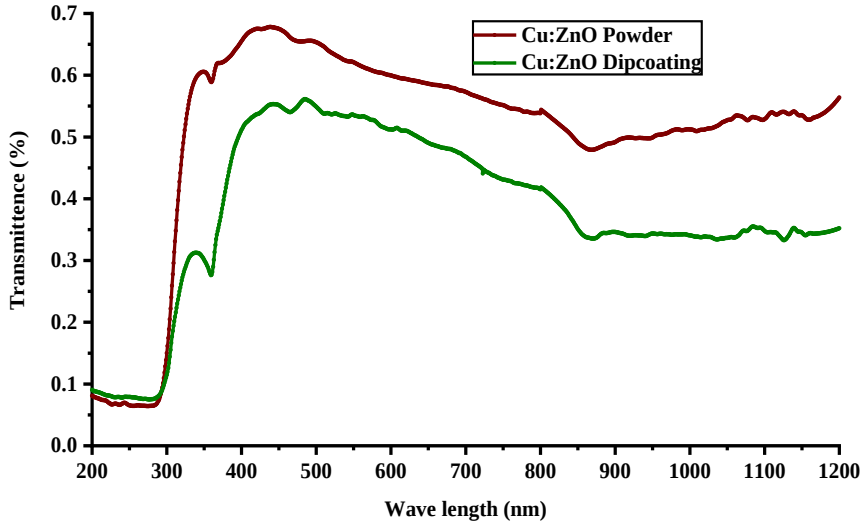

FIGURE 5.3 Transmittance spectra of Cu doped ZnO thin film and powder.

In Fig. 5.2 and Fig 5.3, optical transmittance spectrums show that transmittance becomes maximum in visible region for all the samples.

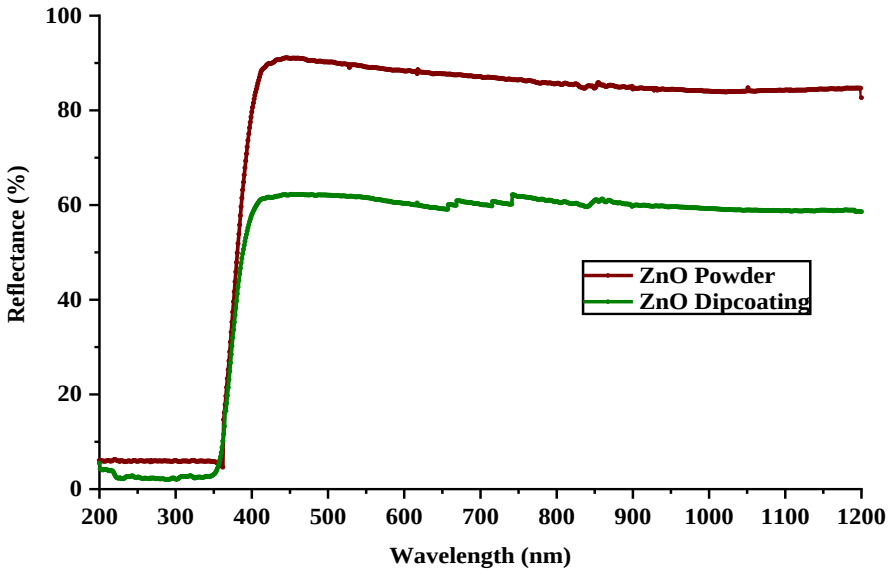

FIGURE 5. 4 Reflectance spectra of pure ZnO thin film and ZnO powder.

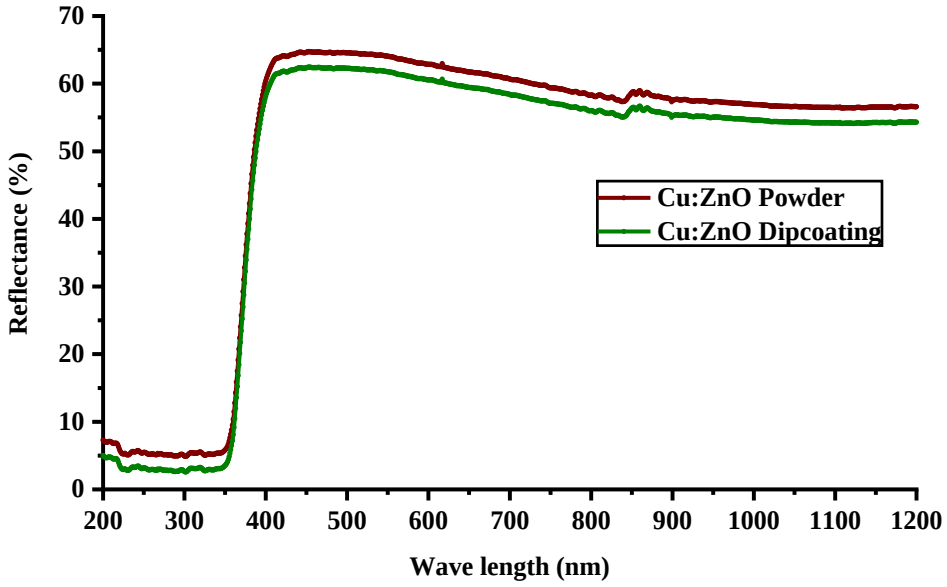

FIGURE 5. 5 Reflectance spectra of pure ZnO thin film and ZnO powder.

Reflectance spectra of the samples shown in Fig. 5.4 and Fig. 5.5 disclosed that the wavelength near 350 nm is suitable for characteristic absorption edge. Compared to pure ZnO thin film grown by dip coating method, Undoped ZnO powder shows very-high reflectance, i.e., 91% whereas absorption edge is observed approximately same in Cu doped ZnO powder but reflectance is reduced i.e. 65%. Flat reflectance of all samples is seen in visible region.

Optical absorbance shown in Fig. 5.6 and Fig. 5.7, is evaluated from transmittance using the relation [187] as below.

$$A = \log\left(\frac{1}{T}\right) \tag{5.2}$$

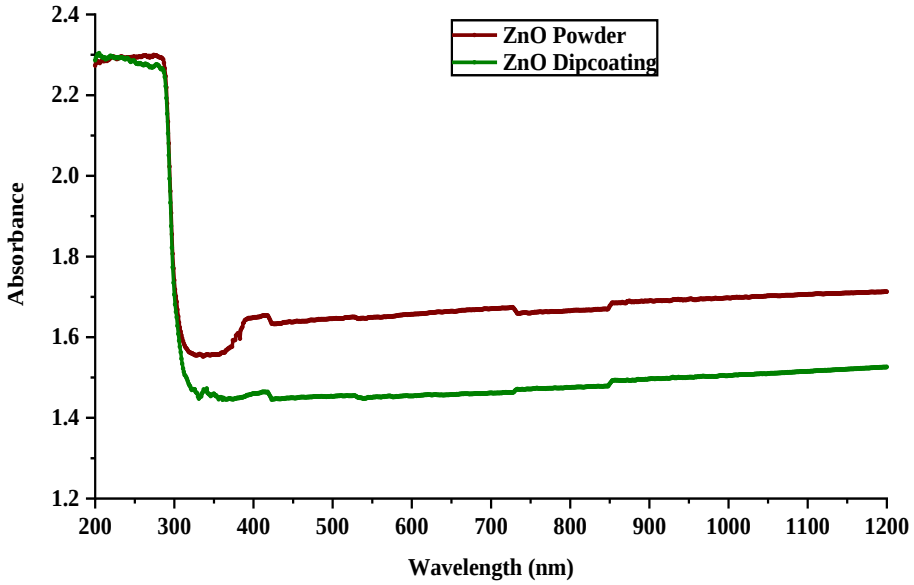

FIGURE 5. 6 Absorbance spectra of pure ZnO thin film and ZnO powder.

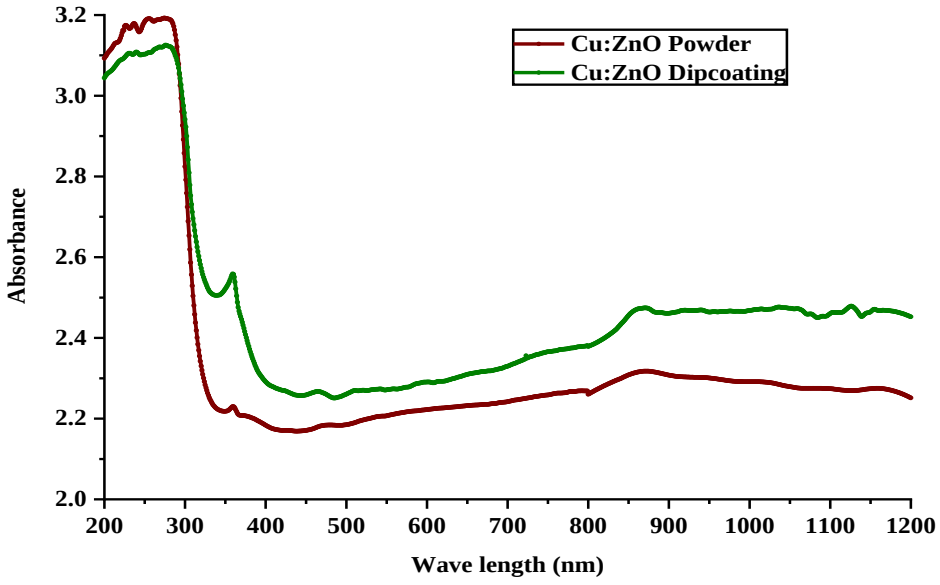

FIGURE 5.7 Absorbance spectra of Cu doped ZnO thin film and powder.

The absorbance is low in the visible/near infrared (NIR) region from ~300 nm to 800 nm in all the type of samples.

Refractive indices of all thin films are calculated using the relation reported by Islam and podder [189].

$$\mathbf{n} = \left(\frac{\mathbf{1+R}}{\mathbf{1-R}}\right) \tag{5.3}$$

Where n is the refractive index and R is the optical reflectance.

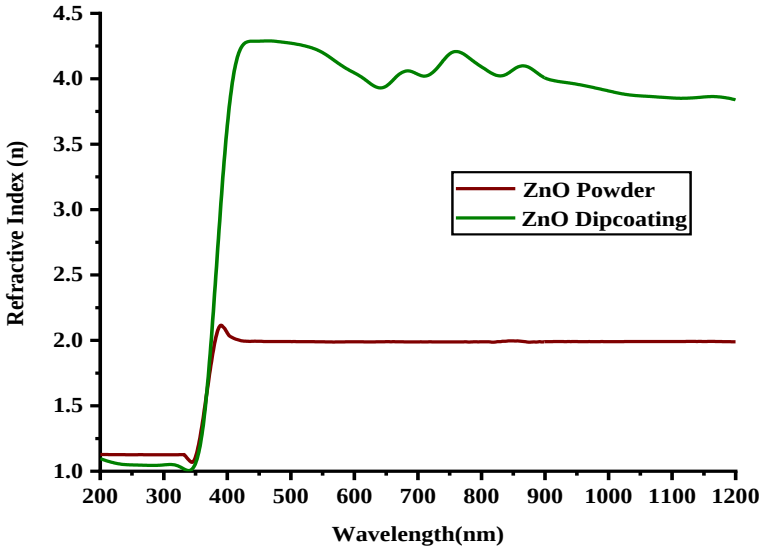

FIGURE 5.8 Refractive index of pure ZnO thin film and ZnO powder.

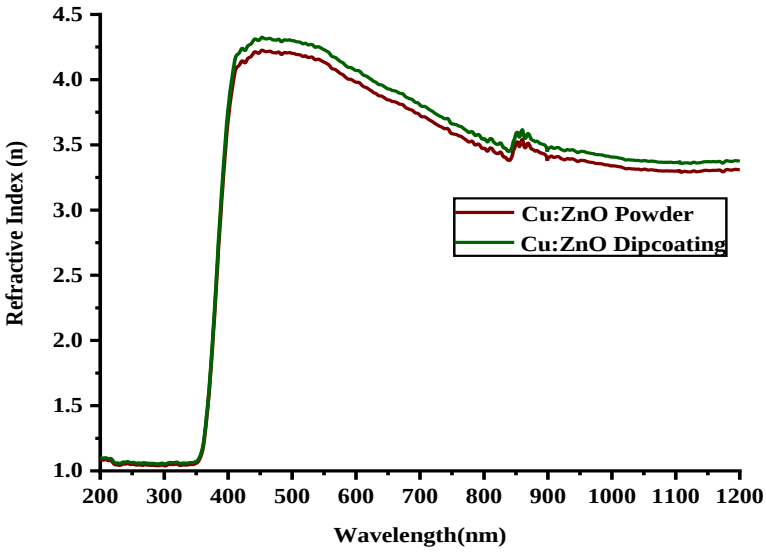

FIGURE 5. 9 Refractive index of Cu doped ZnO thin film and powder.

Fig. 5.8 shows the values of refractive index n for ZnO powder and pure ZnO thin as a function of wavelength. The vlaue of refractive index of pure ZnO thin films grown by dip coating method is found nearly 4.2 but in case of ZnO it is near to 2.1. From Fig. 5.9 it is

revealed that for Cu doped ZnO samples refractive index is inversely proportional to the wavelength of incident photon.

Extinction coefficient (k) for powder sample and pure ZnO thin film were computed using the following expression [190].

$$\mathbf{k} = \frac{\boldsymbol{\alpha\lambda}}{\mathbf{4\pi}} \tag{5.4}$$

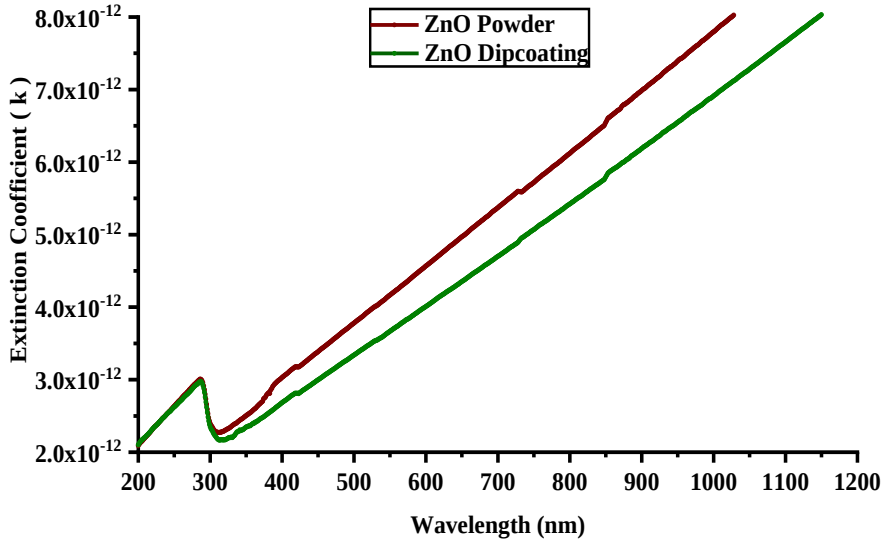

FIGURE 5. 10 Extinction coefficient of pure ZnO thin film and ZnO powder.

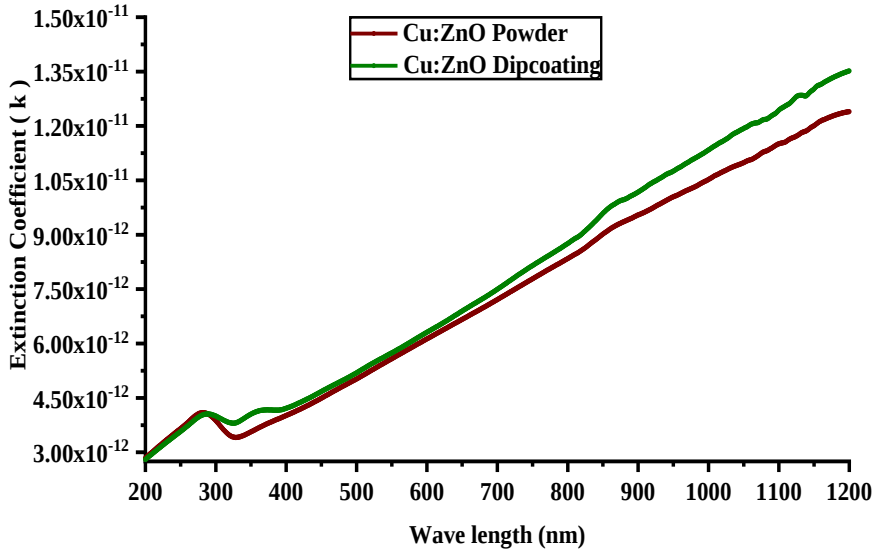

FIGURE 5.11 Extinction coefficient of pure ZnO thin film and ZnO powder

Figure 5.10 and Fig. 5.11 display the extinction coefficient k for powder samples and thin film samples of pure and Cu doped ZnO thin film as a function of wavelength. Values of

extinction coefficient k and wavelength of incident photon are directly proportional to each other. In addition, intrinsic absorption for higher energy gap is responsible to high values of k in the fundamental absorption region (for k<400 nm). In visible region, it is concluded that these layers are transparent as shown in the transmission spectra with respect to the low values of k. refractive index exhibits a normal dispersion in the wavelength range of 400–800nm and very low extinction coefficient k value is obtained. Low extinction coefficient value is recommended for the better quality of the film. Also the smoothness of the thin films is also depend on lower values of extinction coefficient. The calculated values of these parameters at wavelength of 400 nm are listed Table 5.2.

The real εr (λ) and the imaginary εi (λ) parts of complex dielectric function are related to refractive index n(λ) and extinction coefficient k(λ) via following relations [191].

$$\boldsymbol{\varepsilon_r = n^2\,(\lambda) - k^2\,(\lambda)} \tag{5.5}$$

$$\boldsymbol{\varepsilon_i = 2n\,(\lambda)\,k\,(\lambda)} \tag{5.6}$$

The calculated values of these constants at wavelength of 400nm are listed in Table 5.2.

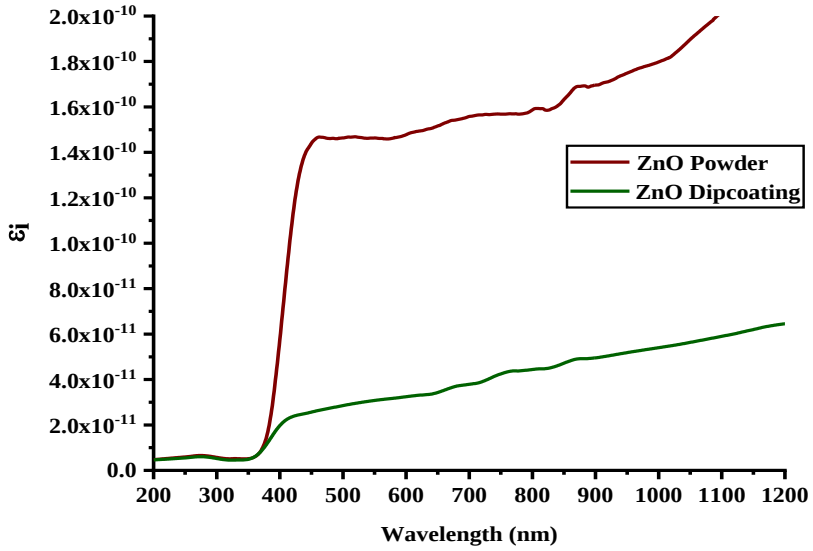

FIGURE 5.12 Imaginary part of dielectric constant vs wavelength of pure ZnO thin film and ZnO powder.

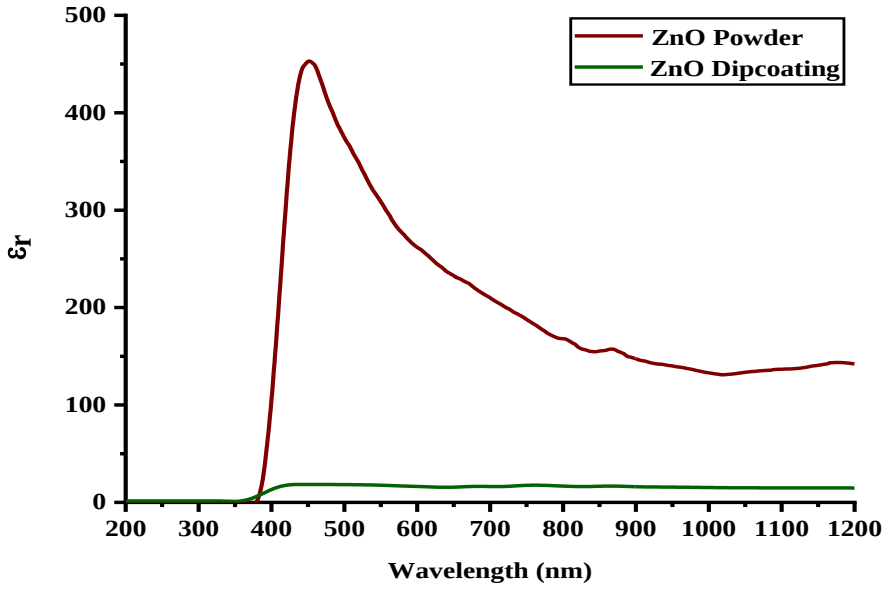

FIGURE 5.13 Real part of dielectric constant vs wavelength of pure ZnO thin film and ZnO powder.

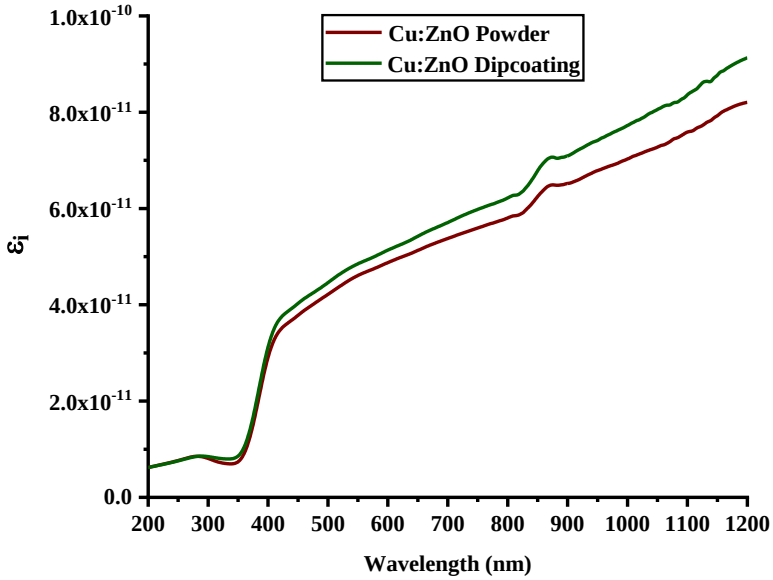

FIGURE 5.14 Imaginary part of dielectric constant vs wavelength of Cu doped ZnO thin film and powder

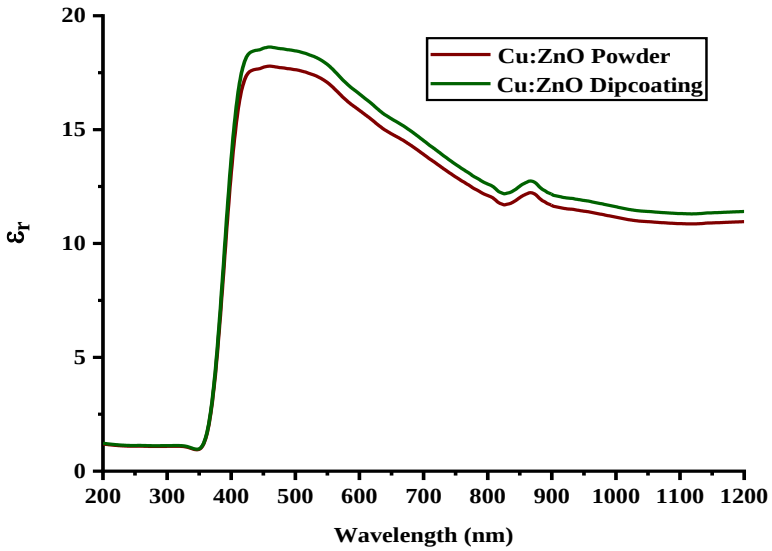

FIGURE 5.15 Real part of dielectric constant vs wavelength of Cu doped ZnO thin film and powder.

The real and imaginary part of dielectric constant (ε_r and ε_i) for pure and Cu doped ZnO thin films and powder samples have been calculated from Equation 5.5 and 5.6. The variation of real and imaginary parts of dielectric constants of the samples with wavelengths is shown in Fig.5.12 to 5.15. It is concluded that the variation of ε_r mainly depends on (n^2) because of small values of (k^2), while ε_i mainly depends on the (k) values which are related to the variation of absorption coefficients. The values of the real dielectric constant are high with respect to the imaginary dielectric constant.

Table 5.2. Various optical constants of pure and copper doped ZnO samples calculated 400 nm.

Physical Quantity	Dip Coating		Powder Samples	
	Pure ZnO	Cu Doped ZnO	Pure ZnO	Cu Doped ZnO
$k= \alpha\lambda/4\pi$	2.66×10^{-12}	4.20×10^{-12}	3.09×10^{-12}	4.05×10^{-12}
$n= (R+1)/(1-R)$	4.02	4.01	2.05	4.01
$E_r= n^2-k^2$	17.5	18.40	450	17.58
$E_i= 2nk$	2.30×10^{-11}	3.77×10^{-11}	1.47×10^{-10}	3.48×10^{-11}

The band gap energy of the samples were determined by plotting $(\alpha h\nu)^2$ as a function of $h\nu$, and extrapolating the linear portion of the curve. The band gap of the thin films is evaluated from the Tauc's plot method [188]. ZnO has a direct band gap and absorption coefficient of ZnO thin films is given by,

$$\alpha h\nu = A\left(h\nu - E_g\right)^n \quad (5.7)$$

Where α = absorption coefficient, A = constant, h = Planck's constant, ν = frequency of light radiation, Eg = band gap energy, and n = 2 (direct allowed transition).

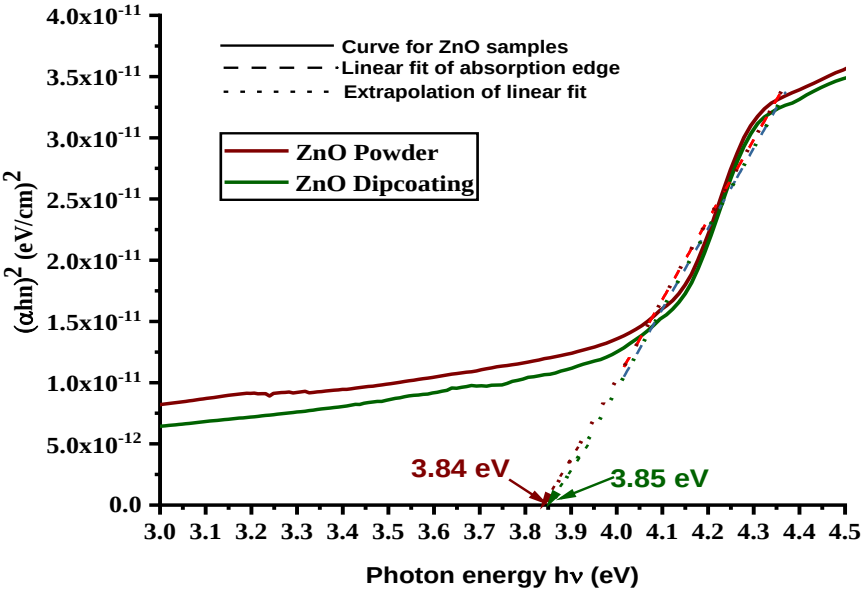

FIGURE 5.16 The plots $(\alpha h\nu)^2$ vs photon energy hν of the pure ZnO thin film grown using sol-gel dip coating technique and ZnO powder sample.

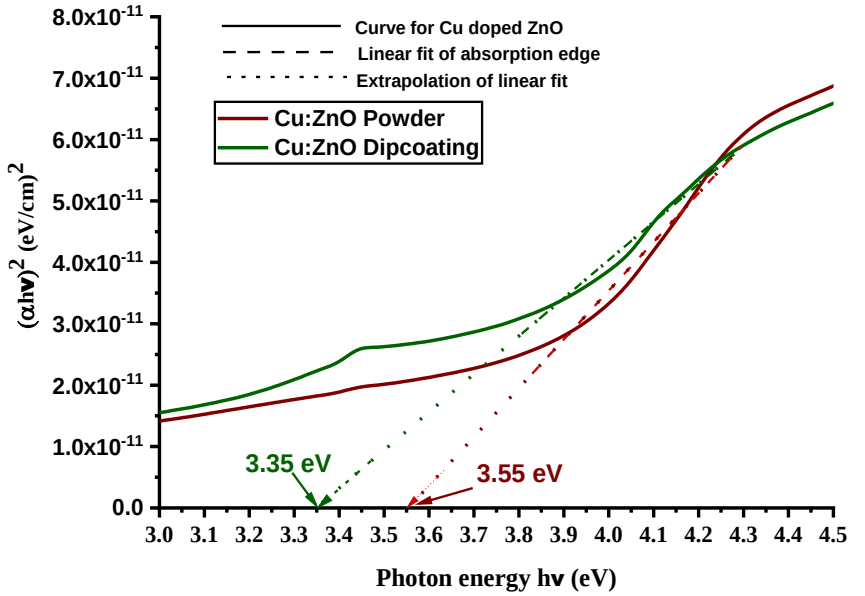

FIGURE 5.17 The plots $(ahν)^2$ vs photon energy hν of the Cu doped ZnO thin film grown using sol-gel dipcoating technique and powder sample.

The straight line part of the absorption edge, when extrapolated, its intercept to the energy axis gives the optical band gap. The optical band gap was found to be decreased from 3.84

to 3.55 eV and 3.85 to 3.35 eV with the doping for powder samples and thin films grown using dip coating method respectively. The reduction of optical band gap in Cu doped ZnO thin films at room temperature may be accredited to the sp-d exchange interaction between the band electrons and the localized d-electron of the Cu^{+2} ion substituting Zn^{+2} ions [192, 193]. The s-d and p-d exchange give rise to negative and positive corrections to the conduction band and the valence band, respectively, leading to the band gap narrowing generation of electron hole pair become efficient, assuming all incident photons with energy equal or greater than energy gap will be absorbed generating e-h pairs.

5.5 Photoluminescence studies

The optical properties of the ZnO thin films were investigated using photoluminescence (PL). Photoluminescence is a common technique used to characterize the optoelectronic properties of semiconductors and other materials. Its principle is simple: electrons are excited from the valence to the conductance band of the material by a laser with an energy larger than the bandgap. Luminescence is the process of emission of light by atoms or molecules excited. A molecule in the ground state is raised to the excited state due to the absorption of photons that have enough energy. The excited molecules undergo a vibrational relaxation of the level of energy toward the lowest excited state by nonradiative processes and then return to ground state by emitting photons. The phenomena of fluorescence and phosphorescence fall within this definition, and therefore, the two phenomena are often referred by the general term photoluminescence. PL spectroscopy technique involves measuring the energy distribution of emitted photons after the optical excitation. Particularly, the sol-gel method can be an appropriated route to maximize the luminescent properties of the ZnO films. Typical room temperature luminescence emission spectra of pure and Cu doped ZnO thin film synthesized by sol-gel method and powder sample are shown in Figure 5.18 and 5.19 respectively.

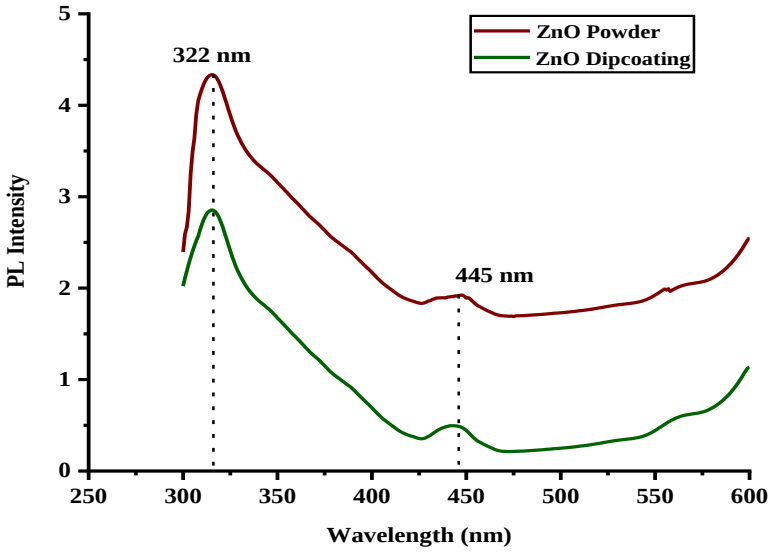

FIGURE 5.18 Photoluminescence spectra of pure ZnO thin film and ZnO powder.

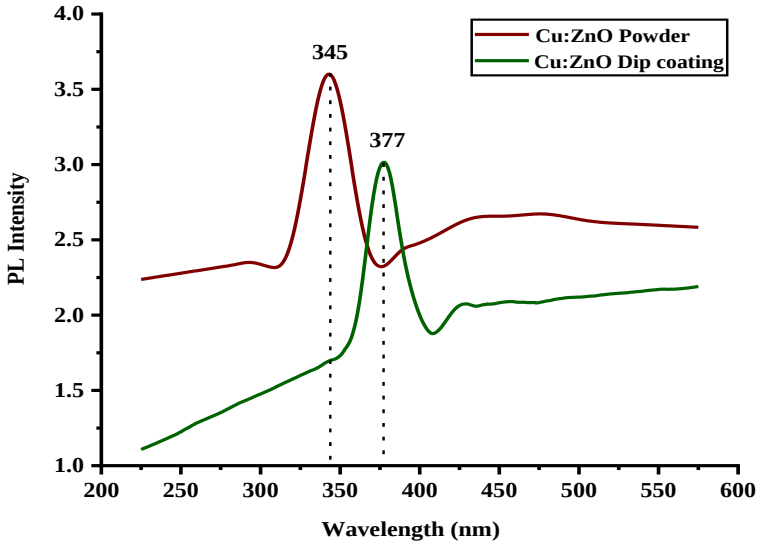

FIGURE 5.19 Photoluminescence spectra of Cu doped ZnO thin film and powder.

The PL spectra of the ZnO films and powder sample exhibited two peak: UV emission peak around 322 nm and blue luminescence at 445 nm. The first peak due to UV emissions is attributed to band-to-band transitions and excitonic emissions. The blue band at around 445 nm is due to the emissions in blue region, which is attributed to oxygen vacancies, zinc interstitials or zinc vacancies [194]. The spectrum shows a strong dominant broad peak at 322 nm in the UV region because of free exciton emission in PL spectrum near band edge (NBE), it relates to the amount of non-stoichiometric intrinsic defects. Similarly PL spectra of Cu doped ZnO powder and thin film sample as shown in Fig.5.19 exhibited UV emission

peak at 345 nm and 377 nm respectively. An idea of optical band gap can also be taken from PL spectrum shown in Fig. 5.18 and Fig. 5.19 by using the formula:

$$E_g(eV) = \frac{1240}{\lambda\,(nm)} \tag{5.8}$$

The estimated value of band gap from PL spectrum (Fig. 5.18) corresponding to wavelength 322 nm for ZnO thin film grown using dip coating and ZnO powder sample are observed to be 3.85 eV.

The estimated value of band gap from PL spectrum (Fig. 5.19) corresponding to wavelength 345 nm and 377 nm for Cu doped ZnO thin film grown using dip coating and Cu doped ZnO powder sample are observed to be 3.59 eV and 3.29 eV respectively. Band gap comparison of pure and Cu doped ZnO thin films grown using dip coating method and their powder samples are shown in Table 5.3.

Table 5.3. Band gap comparison of all the samples.

Physical Quantity	Dip Coating		Powder Samples	
	Pure ZnO	Cu Doped ZnO	Pure ZnO	Cu Doped ZnO
Band gap (Eg) from UVVIS	3.85	3.35	3.84	3.55
Band gap (Eg) from PL	3.85	3.29	3.85	3.59

5.6 Raman spectroscopy studies

Raman spectroscopy was used as the leading method for the estimation of the crystal and the crystallites symmetry. The peaks characteristic for the hexagonal structure were observed in bulk crystals, as well as in thin films. The Raman vibrations in different scattering geometries were determined using polarized Raman spectra. The Raman patterns of pure and Cu doped ZnO thin films grown through sol-gel dip coating method and powder samples were analysed in the range 40-600 cm^{-1}. Raman scattering was observed at room temperature using a Renishaw InVia system. Raman spectra detected the existence of certain Raman-active modes inside the samples. The Raman mode observed in a spectrum depends on the Raman selection rules, which consider the crystal orientation in relation to the direction and polarization of the incident and scattered light. This dependence is shown in Fig. 5.20 and Fig. 5.21.

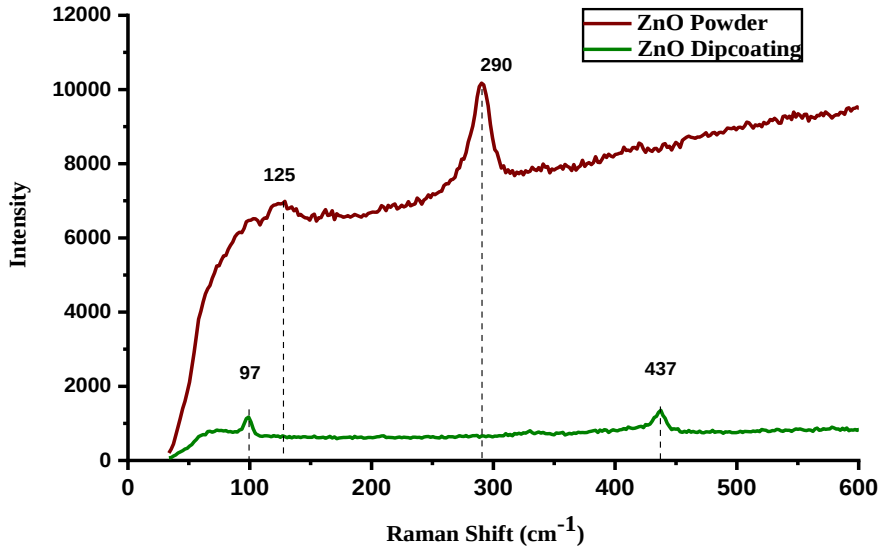

FIGURE 5.20 Raman spectroscopy of pure ZnO thin film and ZnO powder.

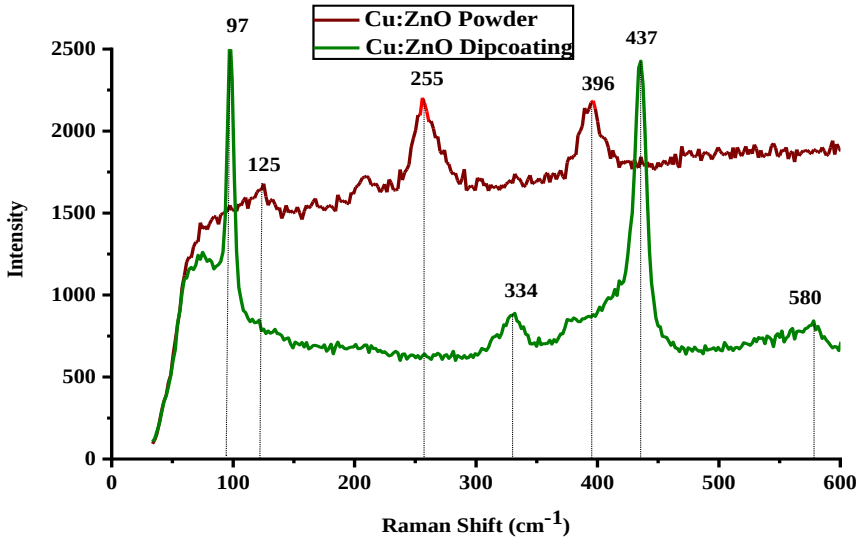

FIGURE 5.21 Raman spectroscopy of Cu doped ZnO thin film and powder.

Fig. 5.20 and Fig. 5.21 show the Raman spectra of pure and Cu doped ZnO thin film and their powder sample being excited at 532 nm. Raman spectrum of pure ZnO exhibits four prominent peaks at 97, 125, 290 and 437 cm^{-1}. Raman spectra of Cu doped samples exhibits peaks at 97, 125, 255, 396 and 437 cm^{-1}. The peaks 97 and 125 cm^{-1} corresponding to E_2 (low) optical phonon, while the peak 255, 290 and 437 cm^{-1} corresponding to E_1 (TO) and E_2 (high) optical phonon respectively. Optical phonon modes of pure ZnO 437 cm^{-1} peaks is E_2 (high) modes. Peaks of ZnO at 97 cm^{-1} and 437 cm^{-1} are relevant to multi-photon process and have been designated to the second-order Raman spectrum originating from the zone boundary phonons, E_2 (low) and E_2 (high) respectively [195]. Two peaks at about 97 and

437 cm^{-1} observed in ZnO vibrational modes confirms first-order Raman scattering, which can be designated to E_2 (low) and E_2 (high) optical phonons of the ZnO respectively [196]. The peak value was detected 437 cm^{-1} in E_2 (high) mode indicates the characteristic of wurtzite structure ZnO. The peaks are seen because the incident light is perpendicular to the c-axis of the samples. Overall from Raman analysis, Raman spectra detected the existence of Raman-active modes for both samples.

5.7 Discussion of results on pure and Cu doped ZnO thin films and their powder samples.

Pure and Cu-doped ZnO examined in the form of power as well as thin films prepared using dip coating method on glass substrates and detailed report is prepared as follow:

- UV-Vis spectroscopy reveals the gap of ZnO samples decreases with copper doping. The copper doping degenerate the impurity band and valence band of the ZnO system and the conduction band bottom moves towards the low energy. Doping decreases the forbidden band width and in turn the transition from the valence band to the conduction band for the electron requires less energy, and the light absorbed through a red shift phenomenon. These inclusive results indicate that copper-doped zinc oxide has better optical properties and smaller internal stress of the film, which is in favor of as a high-performance solar cell photo-anodic material.
- Effect of doping is observed to reduce the reflectance in all cases. Absorbance of Cu doped ZnO samples is improved. Refractive index and extinction coefficient increase with increase in wavelength of incident photon. The high values of extinction coefficient in the fundamental absorption region (low wavelength $\lambda <$ 400 nm) are observed due to the intrinsic absorption for the higher energy gap.
- The data obtained in the Raman spectra of pure and Cu doped ZnO thin films demonstrates that Cu ions successfully substituted Zn ions in the wurtzite hexagonal structure of ZnO. The strong red shift observed in E_2 (high) and A_1 (TO) modes of pure and doped ZnO and both can be attributed to the phonon confinement effect. The Raman spectra showed that intensity of the E_2 peak increased with doping of Cu. Raman modes in thin films indicated that Cu doping didn't change the wurtzite structure of ZnO. A peak associated to E_1(high) vibration mode of ZnO found at around 580 cm^{-1}. In addition, E_1 longitudinal optical (LO) mode generated due to Zn interstitial defects.

- Photoluminescence spectra of the Cu doped ZnO samples reveals prominent peaks corresponding to strong green emission in the visible region at room temperature which can be used for solar cell appliances and as a photo catalyst.
- Experimental studies ensured that the Cu doped ZnO thin films grown using dip coating method shows minimum band gap i.e. 3.35 eV and from PL it is 3.29 eV.

CHAPTER 6

Preparation of doped ZnO thin films (Cu: ZnO, K: ZnO and Na: ZnO) by CBD and their characterizations

6.1 Introduction

Zinc oxide (ZnO) is a multifunctional material with its distinctive physical and synthetic properties i.e. high chemical stability, high electrochemical coupling coefficient, wide scope of radiation absorption and high photo stability [197,198]. ZnO acts as an n-type semiconductor and excess zinc at interstitial positions is responsible for its electrical conductivity. Specific band gap (3.37 eV) and expansive exciton binding energy (60 meV) at room temperature makes ZnO a potential candidate for the optoelectronics, photonics, piezoelectric and solar cell applications.[199, 200]. ZnO exhibits variety of nanostructures. ZnO is the key material for various prospective applications such as photo detectors, laser diode, sensors, flexible and polymer based solar cells and an electrode in dye sensitized solar cells. Development of ZnO nanostructures based white light emitting diode (LED) attracting. Nowadays many researchers are working towards the development of ZnO nanostructures based white light emitting diode (LED) as it is an alternative source to enable bright and energy saving light sources [201–203]. ZnO thin films doped with materials like Cu are very useful for optoelectronic applications because of its extraordinary electrical properties [204] However, the formation of donor compensating point defects restrict its efficiency [205]. Coulomb interactions between dopant and acceptor-like defects, such as oxygen interstitial lead to bound complexes [206, 207]. The bending of p-type and n-type material lowers the recombination rate of photo generated electrons and holes [208].

We performed methodical Raman spectroscopy studies to examine the vibrational symmetry qualities of the pure doped ZnO films. Progress in metal doped ZnO works are effectively

encouraging possibility for spintronics and photonics applications because of their one of a kind properties [209, 210]. Raman spectra indicated a successful incorporation of K ions into the ZnO lattice [211]. Moreover, the Raman spectroscopy is a versatile technique to study the doping agent incorporation and impurity induced modes of ZnO nanoparticles doped with metals [212]. By introducing various ions in the crystal lattice of ZnO, its optical properties can be modified [213].

PL emission spectroscopy is a traditional technique to determine optical properties and internal defects of metal doped ZnO nanostructures [214]. ZnO is an n-type semiconductor. ZnO is expected to be p-doped by elements of IA group (such Li, Na, and K), IB group (such as Cu, Ag, Au), or V–A group (such as N, P, As, Sb) [215]. Electrical properties of ZnO vary significantly due to carrier concentration, mobility and resistivity. The Hall Effect is the most extensively used method to measure the electrical properties. Resistivity and Hall Measurements were made by the van der Pauw method [216, 217] to study the conductivity phenomena across square-shaped samples. Doping of various impurity elements in ZnO shows different functions and improved properties of semiconductor compounds such as electrical, optical and mechanical, which facilitate the development of many electronic and optoelectronic devices [218–220].

Many investigations are carried out to improve the characteristics of ZnO thin films by doping in it with various materials. However, investigations of Cu, Na and K doped ZnO thin films are very scarce, also to the best of our knowledge, there is no study which compares the effects of these dopants on electrical and optical properties of ZnO. Moreover, most studies are concentrated around the ZnO thin films developed by physical routes and little research has been done on the same developed by chemical route. Thus, it is of interest to us to investigate the influence of the Cu, Na and K dopant elements on the properties of ZnO thin films deposited by chemical routes. Therefore, we set out an easy, well-grounded and low-cost method for growing and doping ZnO with Cu, K and Na dopant using chemical bath deposition, in aqueous solution. Influence of doping on electrical and optical parameters like resistivity, conductivity, mobility, carrier concentration, band gap values and ionization energies of impurity levels were investigated.

6.2 Preparation of doped ZnO films

Pure ZnO thin films were developed via chemical bath deposition method following the same procedure as mentioned in section 4.2 [221]. But before mixing the aqueous ammonia

solution, For the preparation of copper doped ZnO (Cu:ZnO), sodium doped ZnO (Na:ZnO) and potassium doped ZnO (K:ZnO), 0.1 M 20 ml aqueous copper chloride solution, 0.1 M 20 ml aqueous sodium chloride solution and 0.1 M 20 ml aqueous potassium chloride solution were added to 0.1 M 60 ml zinc chloride solution respectively before mixing aqueous ammonia solution.

InVia Raman Microscope from Renishaw with a laser excitation source (λ = 514 nm) was utilized to report Raman scattering spectra at room temperature. PL (photoluminescence) spectrum of all the samples were reported at room temperature through a Shimadzu RF-5301 PC spectro-fluoro- photometer under an excitation wavelength of λ = 325 nm and the emission spectra was reported at the wavelength range of 350 – 550 nm. Eexcitation was taken place using ozone free xenon-quartz lamp of 150 W. Hall mobility, type of conduction mechanism and carrier concentration determined using van der Pauw configuration (DNE 21A) at room temperature. Electrical conductivity and activation energy determined by the two probe resistivity measurement performed on all the samples at the temperature range of room temperature to 200 ˚C.

6.3 Photoluminescence studies

Photoluminescence (PL) spectra of all the four thin films at room temperature indicates effect of doping on the optical properties. Also Emission PL spectra has been reported at 325nm excitation wavelength. There are two sectors in the emission spectrum of ZnO thin film: Excitonic near band edge (NBE) emission in the UV region, with energy about the band gap of ZnO and the deep level emission (DLE) in the visible region emerged from intrinsic defects as well as extrinsic impurities. The DLE exhibits multiple peaks related to the nature of intrinsic defects, their complexes and extrinsic impurities. Tranformation of the pattern and status of peaks with reference to position depends upon the concentration of these defects and impurities.

In the current research, the PL peak at 380 nm, 386 nm, 397 nm and 392 nm with respect to photon energy 3.27, 3.21, 3.12 and 3.16 eV for pure ZnO, Cu:ZnO, Na:ZnO and K:ZnO respectively are shorter than band gap of the ZnO at room temperature (3.37 eV) which is not as a consequence of the band-band transition but it is a near band emission (NBE) which are owing to the recombination of free excitons. Oxygen vacancies (V_o) in the compounds and zinc interstitials are mainly responsible for the deep level emission (DLE) peaks recorded at 484 – 486 nm. [226]. The oxygen related effects like zinc interstitials (Z_{ni}) and

oxygen vacancies (V_o) are accountable for the green band at 534 and 520 nm of pure ZnO and Cu doped ZnO thin films. The violet emission presumably resulted from a close relation with defects such as interstitial Zn atoms (Z_{ni}) and ions in the ZnO lattice. The origin of green peak at ~534 nm for pure ZnO is mainly because of oxygen vacancies. However, the particular mechanism of green emission in ZnO is still doubtful and energy levels of various defects declared in literature diverge markedly. Furthermore, several reports point out that oxygen vacancies and Cu impurities are accountable for the green emission in ZnO. Dingle specified that green luminescence in Cu–ZnO is because of the charge transfer from impurity states (Cu^{+2}) to concerned valence band.[227]. In addition to this model as put forward by Garces et al. [228], Cu may exhibit either Cu^{+} or Cu^{+2} state. It is specified that monovalent state (Cu^{+}) will deliver structure with less emission by virtue of donor–acceptor pair recombination in which shift from the copper acceptor to superficial donor impurity happens. In the current investigation, existence of constitutional defects may be accountable for the green luminescence in undoped ZnO. Moreover, slight possibility of oxygen vacancy in pure ZnO may be responsible for the green emission. However, equitable intensification in green emission in Cu: ZnO samples indicates the contribution of Cu in green emission. It also recommends that copper-impurities are mainly the factors of the improved green emission. Thus, enhancement in n-type conductivity (Table 6.2) and appearance of green emission after copper doping in ZnO confirms the Cu doping in ZnO lattice and its effect on green emission. CuO film is a effectual absorbing layer in the field of solar energy [229].

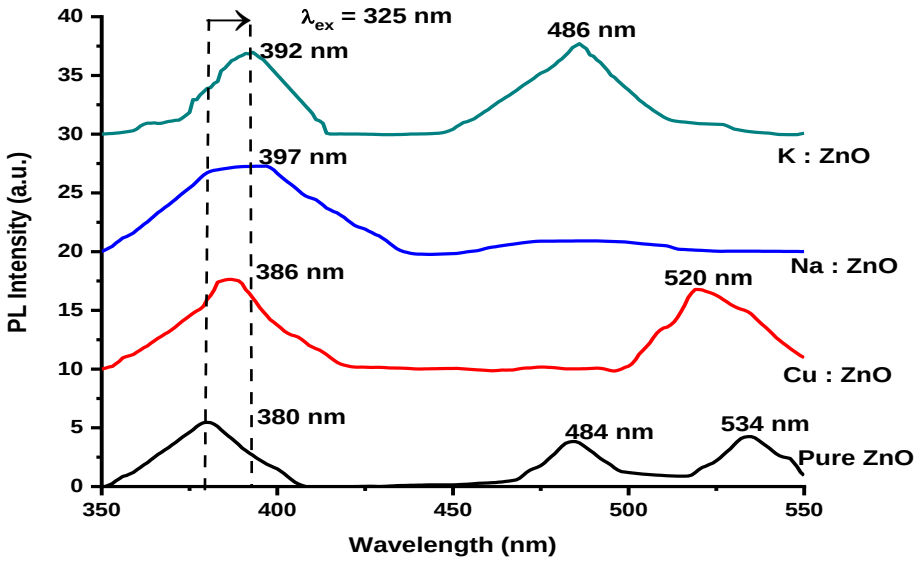

FIGURE 6.1 Red-shift of the UV peaks in PL spectra for the Cu-, Na- and K- doped ZnO compared to the undoped ZnO thin films.

TABLE 6.1 PL peak position of pure and doped samples

Thin Film	Peak position at wavelength λ_{ex} = 325 nm		
	NBE (Near band edge emission) Violet emission	DLE (Deep level emission) Blue emission	DLE (Deep level emission) Green emission
Pure ZnO	380 nm (3.27 eV)	484 nm (2.56 eV)	534 nm (2.32 eV)
Cu:ZnO	386 nm (3.21 eV)	—	520 nm (2.38eV)
Na:ZnO	397 nm (3.12 eV)	—	—
K:ZnO	392 nm (3.16 eV)	486 nm (2.55 eV)	—

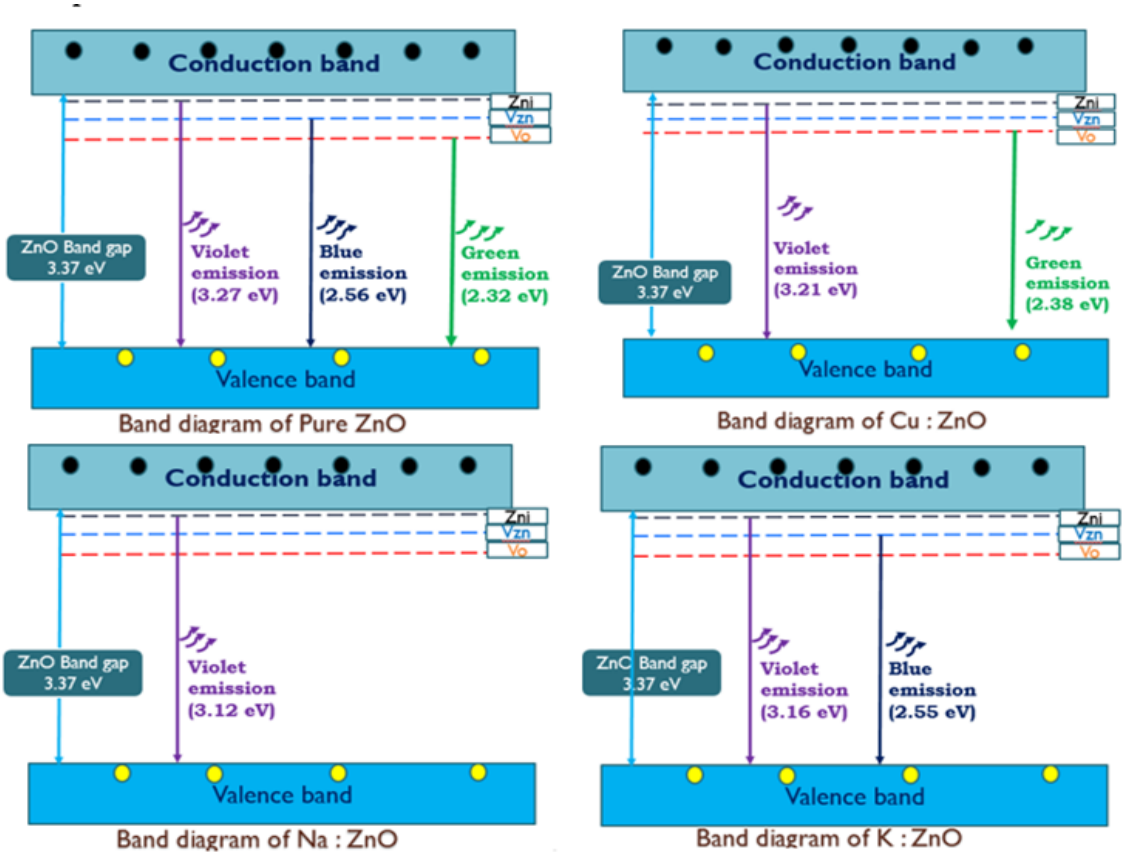

FIGURE 6.2 Band diagram of Pure ZnO and Cu, Na and K doped ZnO thin films.

6.4 Raman spectroscopy studies

Vibrational properties of pure and doped ZnO investigated to know the impact of doping of Cu, Na and K on ZnO. Fig. 6.3 shows Raman spectra for pure ZnO, Cu: ZnO, Na: ZnO and K: ZnO and results are compiled. Peaks at 138 cm^{-1}, 338 cm^{-1}, 439 cm^{-1} and 605 cm^{-1} represent E_{2L}, $2E_{MO}$, E_{2H} and A_{1LO} respectively, the fundamental modes of hexagonal ZnO. Polar mode $A_{1(LO)}$ exhibited at around 605 cm^{-1} was found in all doped samples and it is

transferred to lower energy. The scattering contributions outside the Brillouin zone center was observed in the shifting and broadening of phonon modes. The complexes having zinc interstitial defect and vacancy created by oxygen in ZnO lattice are accountable for $A_{1\,(LO)}$ mode of phonon. [222]. Significant structural disorder in ZnO observed as changes in the line width and position of the Raman peaks may be due to these interstitial incorporation of Cu, Na and K.

Fig. 6.3 shows Raman spectra in which E_2 (low), E_2 (high) – E_2 (low), E_2 (high), A_1 (LO) and 2(LO) vibration modes are observed 138 cm^{-1}, 338 cm^{-1}, 439 cm^{-1}, 605 cm^{-1} and 1123 cm^{-1} peaks respectively. The peak at 338 cm^{-1} was appropriate to second order phonon method owing to multiple phonon processes [223]. E_2 (high) mode of pure and doped ZnO indicates the band characteristic of wurtzite-structured ZnO and it is because of the good crystallinity of the films [224]. The first and second order of the LO phonons at the Γ center of the Brillouin zone are confirmed by the A_1 (LO) (605 cm^{-1}) and 2LO (1123 cm^{-1}, which is normally inactive in the infrared) modes respectively. These vibrations are strongly coupled to the lattice via Frohlich interactions and owing to localized excitations. They are shown to present a resonant profile. [225].

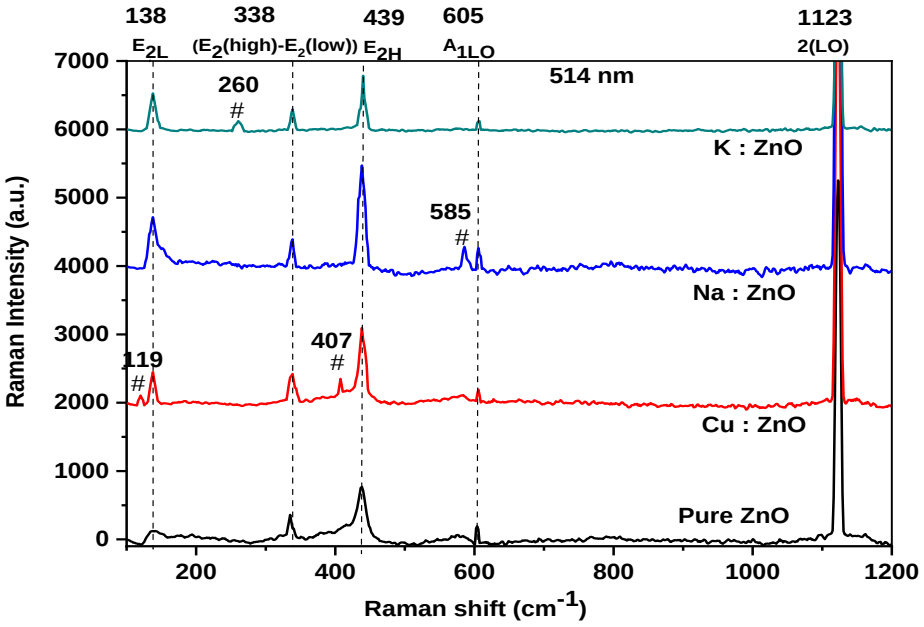

FIGURE 6.3 Raman spectra of undoped and doped ZnO films grown on glass. (The background has been removed, and the spectra have been vertically offset for clarity).

Conclusively, we point out that some of the additional peaks appear in the spectra of ZnO thin films with certain dopant species indicating host lattice defects in the ZnO structure only, which is shown with "#" such as the peak at 119 and 407 cm^{-1} for the Cu doped, at

585 cm^{-1} for the Na doped, and at 260 cm^{-1} for K doped thin films. These modes seem to be corresponded to the individual dopants and may be utilized as indication for their incorporation.

6.5 Study of electrical properties

6.5.1. Resistivity measurements

Temperature dependence of electrical resistivity of pure and doped ZnO thin films with different dopant concentrations was computed by two probe resistivity measurement method at constant temperature in the range of room temperature to ~200 ˚C. The resistivity (ρ) of the samples was quantified by using the formula:

$$\boldsymbol{\rho = \frac{RA}{l}} \tag{6.1}$$

Where R is the resistance, A is the cross sectional area and l is the distance between two probes on thin film. Resistivity of a 0.1 M Pure ZnO is 72.14 Ω cm but by increasing the precursor concentration from 0.1 to 0.5 M of Cu, Na and K doped ZnO, the resistivity value decreases as shown in Table 6.2. The higher resistivity of Cu and K doped ZnO thin films compared to pure ZnO at low concentration might be due to the capture of free electrons in ZnO lattice by the empty lower energy 3d Cu and 4s Na states respectively. Resistivity gets decreasing with increasing dopant concentration in all the samples. Electrical conductivity of Cu: ZnO, Na: ZnO and K: ZnO films depended on the oxygen vacancies and contribution from the Zn–Cu, Zn–Na and Zn–K interstitial atoms. The resistivity of the Cu: ZnO, Na: ZnO and K: ZnO films decreased from 78.57 to 15 Ω·cm, 72.14 to 22.86 Ω·cm and 78.57 to 20 Ω·cm as the doping concentration increased from 0.1 M to 0.5 M respectively.

6.5.2. Activation energy

Activation energy is the energy required to transfer charge from one primarily neutral species to another and denoted by Ea. This is uniform to the electrostatic binding energy of the charge to the species. Transmission from one species to another is taken place when these charge carriers are being excited and reached to atleast activation energy from the Fermi-level,. These species are termed crystals. The activation energy is related with film conductivity [227] and interconnected by this formula:

$$\boldsymbol{\sigma = \sigma_0 e^{-[E_a/2k_BT]}} \tag{6.2}$$

Where, σ_0 is conductivity at 0 ˚C, k_B is Boltzmann constant and T is absolute temperature. The equation can be written as:

$$\ln \sigma = \frac{-E_a}{2k_B T} + ln\sigma_0 \quad (6.3)$$

This equation is equivalent to a straight line equation, y = mx + c. So that can be determined from the slope of the straight line. From the graph of ln σ vs 1/T, can be calculated by using the relation:

$$E_a = \left(\frac{-\ln \sigma}{1/T}\right) \times 2k_B = \left(\frac{\ln \rho}{1/T}\right) \times 2k_B\,(eV) \quad (6.4)$$

The activation energy depicts the position of trap levels below the conduction band. In this research, activation energies of the pure and Cu, Na and K doped ZnO films were measured and reported in Table 6.2. The slopes of the fitting lines help in calculating the activation energy. Fig. 6.4 shows the graphical representation of the variation of log ρ with reciprocal of temperature for the Cu, Na and K doped ZnO thin film. Decrease in the resistance with increasing temperature indicates semiconducting nature of all the films. From the slopes of log ρ vs 1000/T plots the values of activation energies (As shown in Table 6.2) were calculated using the formula:

$$\text{Activation energy } E_a = 2.303 \times k_B \times 10^3 \times \text{slope}\ (\text{eV}) \quad (6.5)$$

Where $k_B = 8.602 \times 10^{-5}$ eV/K.

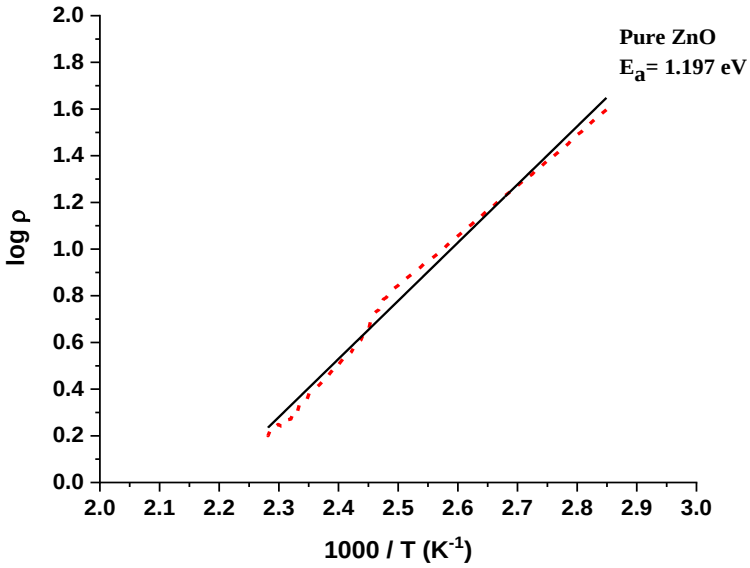
Pure ZnO
E_a= 1.197 eV
log ρ
1000 / T (K^{-1})

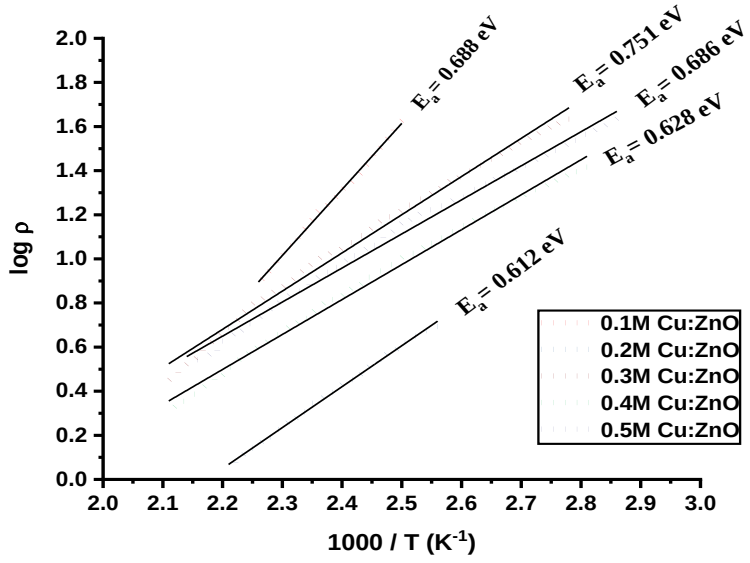
E_a= 0.688 eV
E_a= 0.751 eV
E_a= 0.686 eV
E_a= 0.628 eV
E_a= 0.612 eV
0.1M Cu:ZnO
0.2M Cu:ZnO
0.3M Cu:ZnO
0.4M Cu:ZnO
0.5M Cu:ZnO
log ρ
1000 / T (K^{-1})

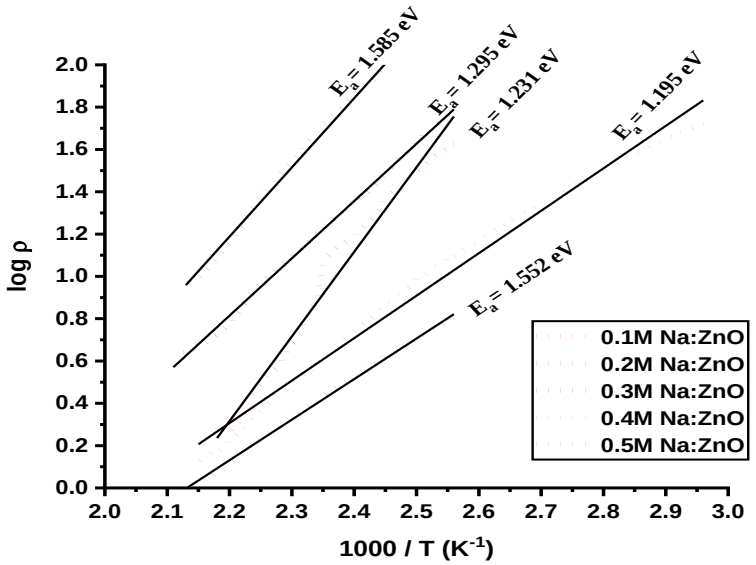
E_a= 1.585 eV
E_a= 1.295 eV
E_a= 1.231 eV
E_a= 1.195 eV
E_a= 1.552 eV
0.1M Na:ZnO
0.2M Na:ZnO
0.3M Na:ZnO
0.4M Na:ZnO
0.5M Na:ZnO
log ρ
1000 / T (K^{-1})

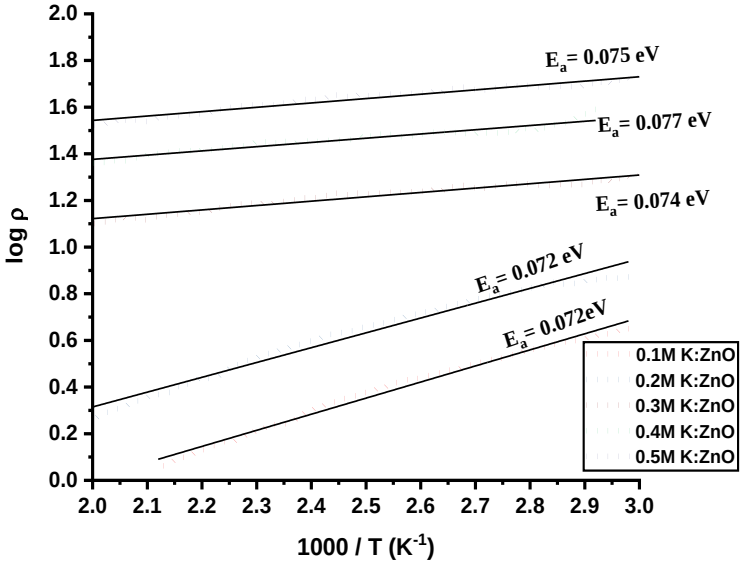

FIGURE 6.4 Curve between log ρ and 1000/T of pure and doped ZnO thin films.

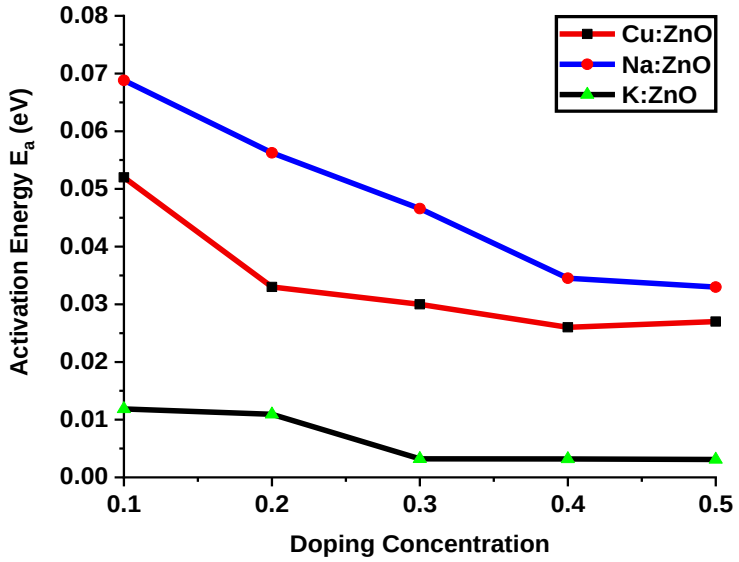

FIGURE 6.5 Variation in activation energy (E_a) of a Cu, Na and K doped ZnO thin films with variation in doping concentration from 0.1 to 0.5 M.

6.5.3. Measurements of Hall parameters

Hall measurements have been carried out at room temperature. In order to obtain p-type nature of films, it is necessary to provide the compensation of native donor defects such as oxygen vacancies and interstitial zinc atoms, by doping. The defects like Zinc interstitial and oxygen vacancy; and addition of the Cu, Na and K dopant produced carriers in doped ZnO films. Usually the concentration of defects in ZnO is very large, which demands very high concentration of acceptors to compensate them. Therefore P-type ZnO is difficult to obtain

due to low solubility of dopants in ZnO, wide band gap and low valence band energy. Self-compensation from donors and high ionization energy of acceptors are the two main problems hindering the enhancement of free hole concentration. Current limitations to p-doping limit electronic and optoelectronic applications of ZnO, which usually require pn-junctions. Known p-type dopants include group-I element: Li, Na, K; group-V elements: N, P and As; as well as copper and silver. However, many of these form deep acceptors and p-type conduction is not significant at room temperature [197]. Hall Effect study can be used to determine the type of carriers. Activation energy relies on the donor carrier concentration and energy levels of the impurity. An increment in donor carrier concentration brings the Fermi level up in the energy gap and results in the reduction of activation energy [230]. Hall Effect measurements were conducted on samples grown on glass substrate at different magnetic field ranging from 0.1 to 1.5T. Hall effect measurement is conducted for total sixteen thin films, one film of 0.1 M pure ZnO and five films of Cu, K and Na doped ZnO each, carrying different dopant concentration from 0.1 to 0.5 M. The Hall coefficient is defined as:

$$\mathbf{R_H} = \frac{\mathbf{V_H} \times \mathbf{t}}{\mathbf{I} \times \mathbf{B}} \tag{6.6}$$

Where R_H is Hall coefficient, V_H is Hall voltage, t is the thickness of the film, I is the current passing through the conductor and B is the magnetic field in Guass. The Hall coefficient reveals the nature of the charge carriers and their concentration. Formula of carrier concentration (ɳ) and mobility (μ) are:

$$\mathbf{R_H} = \frac{-\mathbf{1}}{\eta \times \mathbf{q}} \tag{6.7}$$

$$\boldsymbol{\mu} = \frac{\mathbf{R_H}}{\boldsymbol{\rho}} \tag{6.8}$$

Where n is the concentration of the carriers, q is the charge of a single carrier.

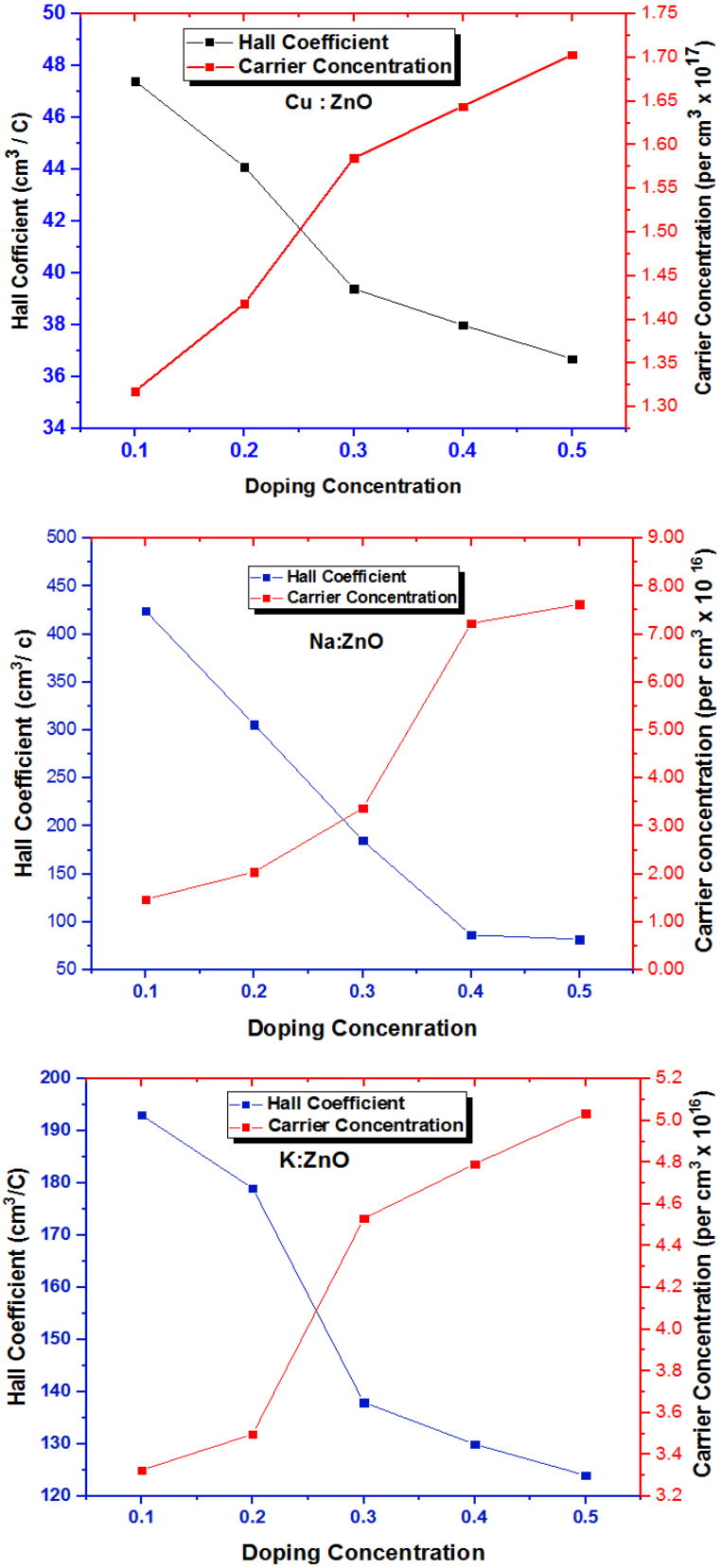

FIGURE 6.6 Variation in Hall coefficient and carrier concentration with different doping concentration of the Cu, Na and K doped ZnO thin films.

Figure 6.6 shows the variation in Hall coefficient and carrier concentration with different doping concentration of the Cu, Na and K doped ZnO thin films. The negative value of the Hall coefficient (R_H) for the pure ZnO film indicates its n-type conducting nature whereas; the positive values of R_H for all of the doped ZnO films signify their p-type conductivity. The carrier (electron) concentration for the undoped ZnO is found to be 1.651×10^{17} cm^3. On the other hand, both the carrier (hole) concentration and the carrier mobility in all doped ZnO films are found to increase gradually as we change the doping concentration from 0.1 to 0.5 M. The p-type conductivity mainly arises due to the doping of the alkali metals in ZnO. The substitution of monovalent alkali ions (Na^+ and K^+) at the Zn^{+2} ion sites can introduce holes into the system [231, 232].

Table 6.2 summarize the values of different electronic parameters of pure and doped ZnO thin films. It is conclude that in all samples, resistivity decreases with increasing doping concentration. Also carrier concentration increases with doping concentration.

Mobility of the pure ZnO film was found to be 0.525 cm^2 /V·s. In case of Cu and K doping, it seems to be increasing with doping concentration from 0.60 to 2.45 cm^2 /V·s and from 2.46 to 6.2 cm^2 /V·s respectively. But for Na doping mobility decreases from 5.88 cm^2 /V·s for 0.1 M concentration to 1.98 cm^2 /V·s for 0.4 M concentration and then it increases to 3.59 cm^2 /V·s for 0.5 M. Also the rate of the change of mobility is low in case of copper doping compared to Na and K doping.

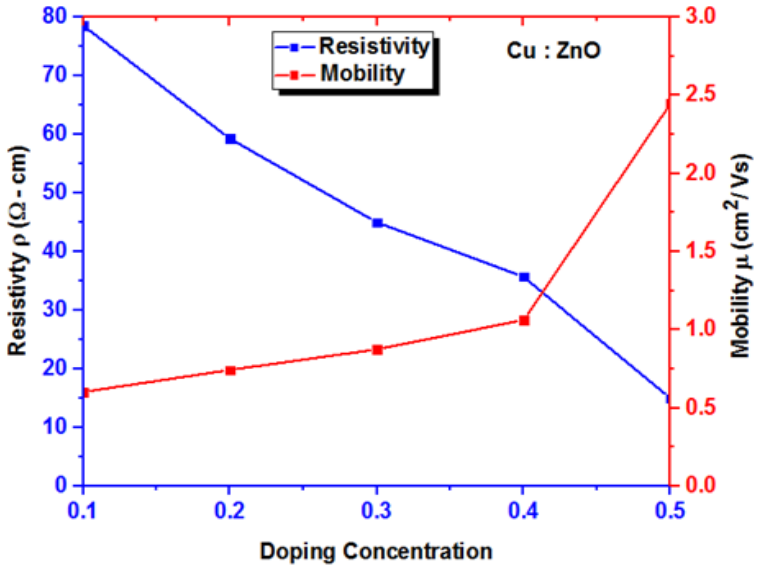

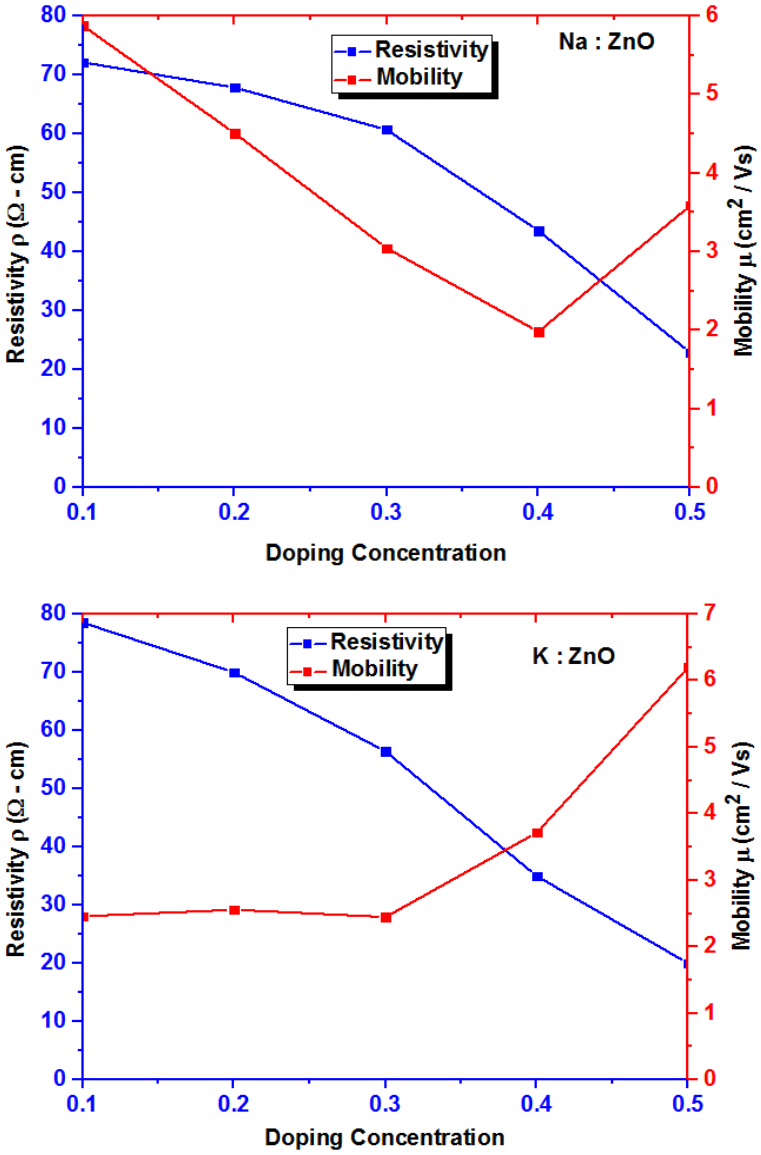

FIGURE 6.7 Variation in resistivity (ρ) and mobility (μ) Cu, Na and K doped ZnO thin films with variation in doping concentration from 0.1 to 0.5 M.

TABLE 6.2 Optical and electrical data of Pure ZnO and Cu, Na and K doped ZnO thin films deposited on glass substrate with various doping concentrations.

Sample	Resistivity ρ (Ω cm)	Conductivity σ (S/cm)	Mobility μ (cm^2/ Vs)	Hall Coefficient R_H (cm^3/C)	Carrier Concentration η (e^-/ cm^3)	Activation Energy E_a (eV)
Pure ZnO	72.14	0.0139	0.525	37.84	1.651×10^{17}	1.197
0.1M Cu:ZnO	78.57	0.0127	0.603	47.40	1.318×10^{17}	0.688
0.2M Cu:ZnO	59.29	0.0169	0.744	44.10	1.418×10^{17}	0.686
0.3M Cu:ZnO	45.00	0.0222	0.876	39.40	1.585×10^{17}	0.751
0.4M Cu:ZnO	35.71	0.0280	1.064	38.00	1.644×10^{17}	0.628

0.5M Cu:ZnO	15.00	0.0667	2.447	36.70	1.703×10^{17}	0.612
0.1M Na:ZnO	72.14	0.0139	5.877	424.00	1.473×10^{16}	1.231
0.2M Na:ZnO	67.86	0.0147	4.509	306.00	2.043×10^{16}	1.585
0.3M Na:ZnO	60.71	0.0165	3.047	185.00	3.375×10^{16}	1.295
0.4M Na:ZnO	43.57	0.0230	1.985	86.50	7.227×10^{16}	1.191
0.5M Na:ZnO	22.86	0.0438	3.588	82.00	7.620×10^{16}	1.552
0.1M K:ZnO	78.57	0.0127	2.456	193.00	3.236×10^{16}	0.072
0.2M K:ZnO	70.00	0.0143	2.557	179.00	3.498×10^{16}	0.072
0.3M K:ZnO	56.43	0.0177	2.446	138.00	4.531×10^{16}	0.074
0.4M K:ZnO	35.00	0.0286	3.714	130.00	4.792×10^{16}	0.077
0.5M K:ZnO	20.00	0.0500	6.200	124.00	5.033×10^{16}	0.075

The carrier concentration of pure ZnO is 1.651×10^{17} e^{-}/cm^3 and for Cu: ZnO, Na: ZnO and K: ZnO films is increased from 1.318×10^{17} to 1.703×10^{17} e^{-}/cm^3 , 1.473×10^{16} to 7.620×10^{16} e^{-}/cm^3 and 3.236×10^{16} to 5.033×10^{16} e^{-}/cm^3 as the doping concentration increased from 0.1 M to 0.5 M respectively.

6.6 Thermoelectric power studies

6.6.1 Thermoelectric power

The Seebeck coefficient (S) is an important parameter characterizing the thermoelectric properties of the thin films. The temperature dependence of this parameter in our study for pure and doped thin films is shown in Fig. 6.8 (Seebeck coefficient versus temperature characteristics). For pure ZnO and doped ZnO thin films, the values of 'S' linearly decrease with increasing temperatures. These linear variations are related to free electron model which is a temperature dependent phenomena. Comparing equation 3.12 and 3.13 with, y=mx+c we get y=S, x=1/T. By plotting a graph of S versus 1/T (Figure 6.8), slope m= $-\frac{E_c - E_f}{e}$ (For n-type) and slope m= $\frac{E_f - E_v}{e}$ (For p-type) can be obtained. It means ($E_c - E_f$ = -me) (For n-type) and ($E_f - E_v$ = me) (For p-type) and $A = \frac{ec}{k_B}$.

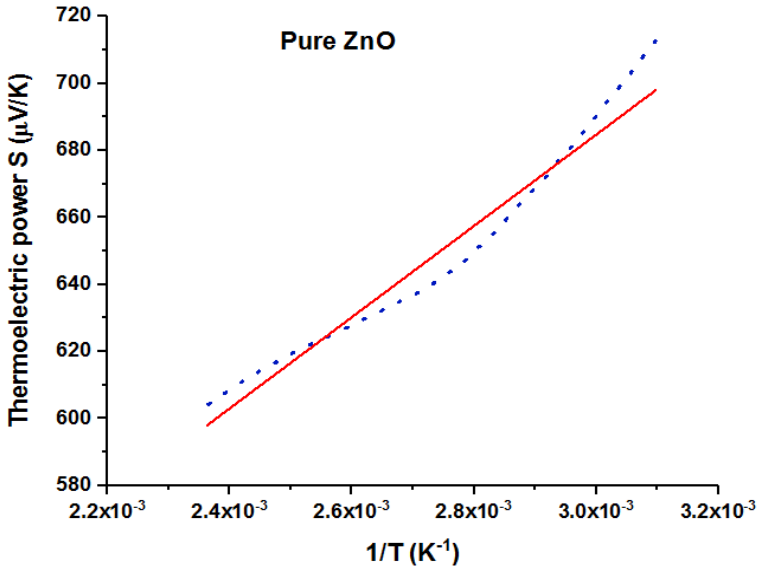
Pure ZnO
Thermoelectric power S (μV/K)
720
700
680
660
640
620
600
580
2.2x10-3
2.4x10-3
2.6x10-3
2.8x10-3
3.0x10-3
3.2x10-3
1/T (K-1)

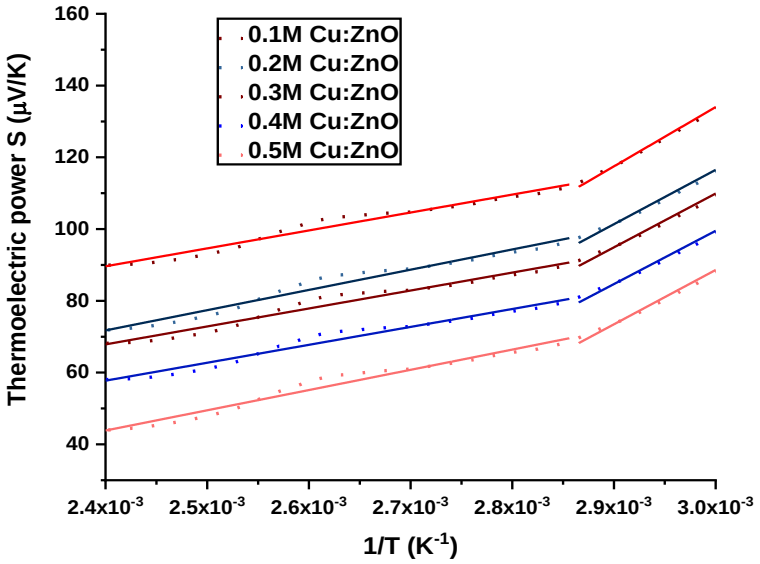
0.1M Cu:ZnO
0.2M Cu:ZnO
0.3M Cu:ZnO
0.4M Cu:ZnO
0.5M Cu:ZnO
Thermoelectric power S (μV/K)
160
140
120
100
80
60
40
2.4x10-3
2.5x10-3
2.6x10-3
2.7x10-3
2.8x10-3
2.9x10-3
3.0x10-3
1/T (K-1)

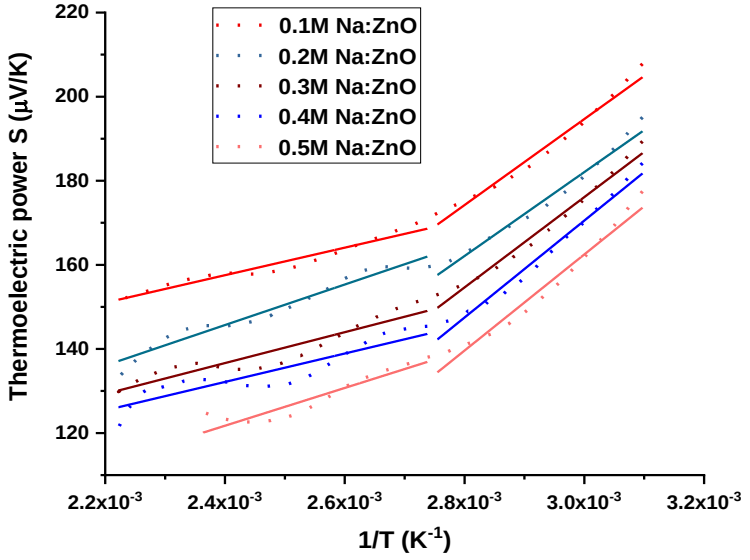
0.1M Na:ZnO
0.2M Na:ZnO
0.3M Na:ZnO
0.4M Na:ZnO
0.5M Na:ZnO
Thermoelectric power S (μV/K)
220
200
180
160
140
120
2.2x10-3
2.4x10-3
2.6x10-3
2.8x10-3
3.0x10-3
3.2x10-3
1/T (K-1)

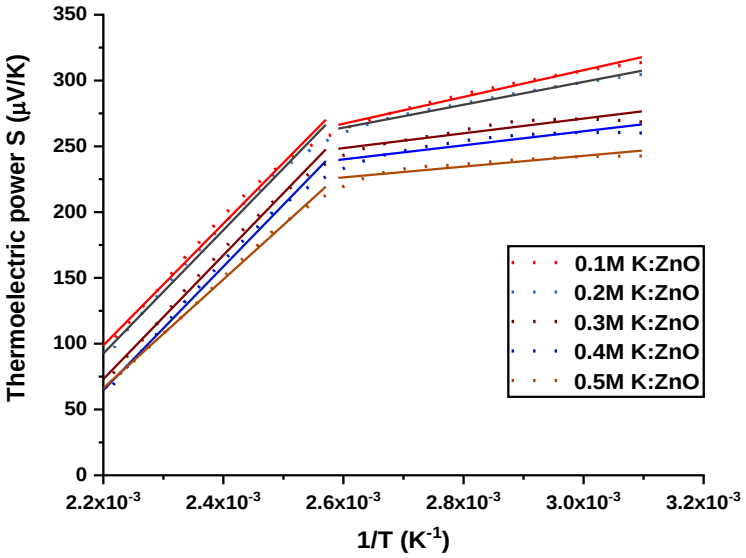

Figure 6.8 Thermoelectric power vs inverse temperature for pure ZnO, Cu: ZnO, Na: ZnO and K: ZnO thin films with variation in dopant concentration from 0.1M to 0.5M.

Hall effect measurement of pure ZnO shows n-type conductivity, whereas that of all doped samples shows p-type conductivity and for that the value of thermoelectric power should be negative and positive respectively [233]. In experimental studies using the setup shown in Fig. 6.8, values of thermoelectric power obtain negative for pure ZnO and positive for all doped thin films with variation in concentration from 0.1M to 0.5M. These values verify the n-type and p-type conductivity of the materials (Table 6.4). The carrier concentration of the samples as obtained from the Hall effect is of the order from 10^{16} to ~10^{17}cm^{-3} [233] and we feel it is logical to employ a nondegenerate model to analyze the thermoelectric power data. Harry et al. [234] have pointed out that A = (5/2) - r, where 'r' corresponds to the scattering index and is equal to - 0.5 for piezoelectric scattering and - 1.5 for ionized impurity scattering. Thus A=3 for piezoelectric scattering and 4 for ionized impurity scattering. From Equation 3.12 and 3.13 it is clear that 'A' corresponds to the value of the thermopower at infinite temperature limit. From the graph of thermopower S versus 1/T (Figure 6.8), the extrapolated tangent at the higher temperature region of the curves approximately gives a common intercept at the ordinate from which the value of 'A' has been obtained is 3.2 (Table 6.3). This value corresponds to the scattering index ≈ - 0.5 and is an indication that piezoelectric scattering is dominant in these ZnO films. This is in agreement with the fact that ZnO is a piezoelectric crystal [235]. Also charged impurity scattering [236] as well as neutral impurity scattering [236] in Cu doped ZnO thin films, optical mode lattice as well as neutral impurity scattering [236] in Na doped ZnO thin films and optical mode lattice [237]

as well as piezoelectric scattering [235] in K doped ZnO thin films grown using CBD method for the variation in concentration from 0.1M to 0.5M at different temperature are due to their transport coefficients as shown in Table 6.3.

6.6.2 Peltier coefficient

Comparing equation 3.18 and 3.19 with equation y = mx + c, we get $y = \pi$, $x =$ T, m = $\frac{\gamma - Ak_B}{e}$ for n-type whereas $m = \frac{Ak_B - \gamma}{e}$ for p-type and $c = \frac{-E_0}{e}$ for n-type whereas $c = \frac{E_0}{e}$ for p-type. The value of γ (Table 6.3) can be obtained from the slope of the graph Peltier coefficient (π) versus T. (Figure 6.9).

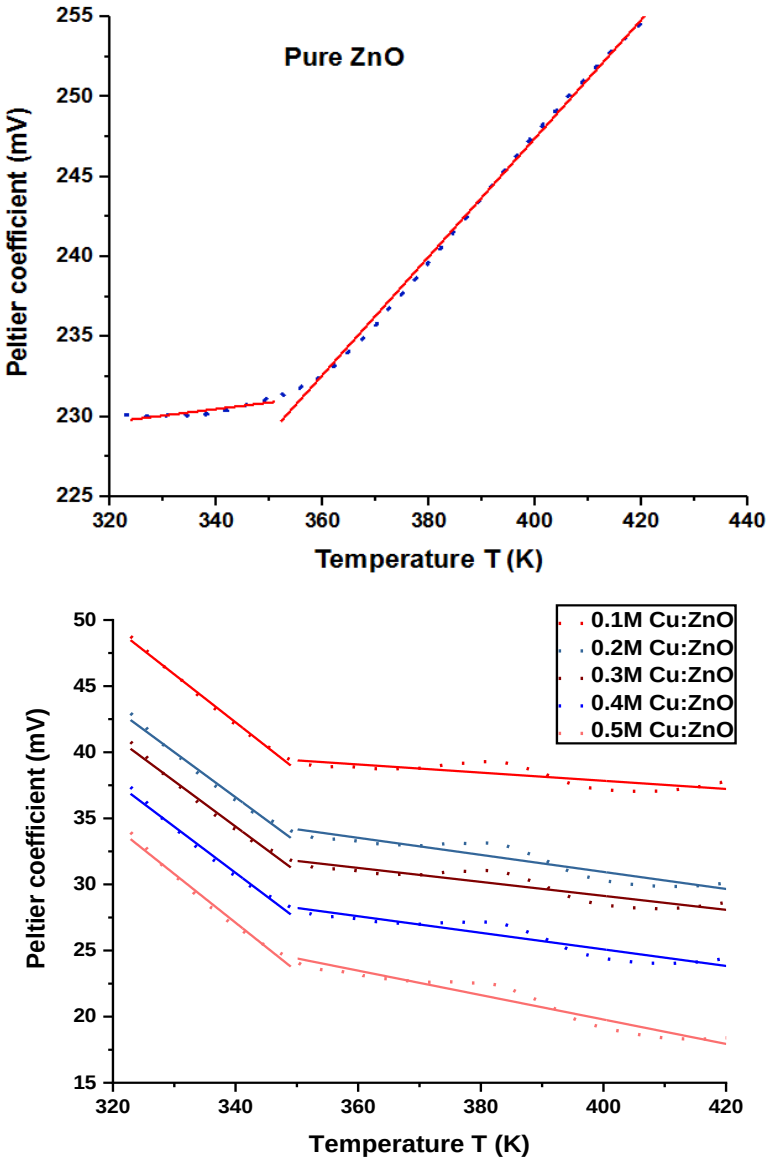

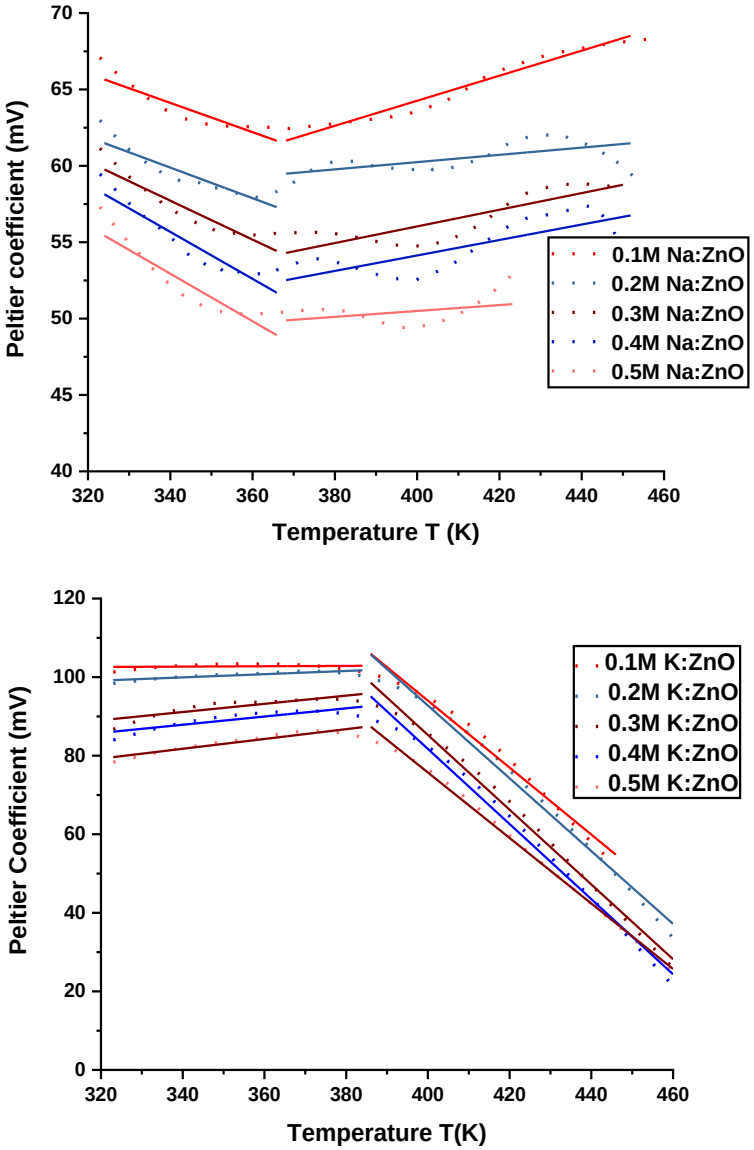

Figure 6.9 Peltier coefficient vs temperature for pure ZnO, Cu, Na and K doped ZnO with variation in concentration from 0.1M to 0.5M.

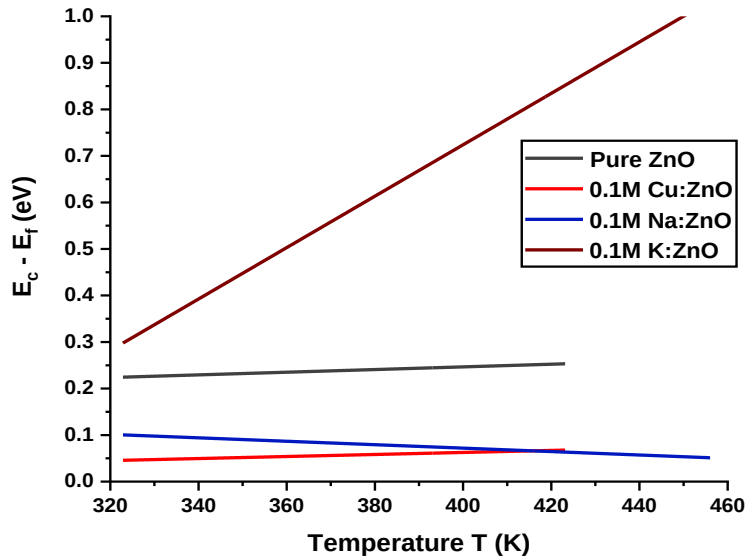
Pure ZnO
0.1M Cu:ZnO
0.1M Na:ZnO
0.1M K:ZnO
$E_c - E_f$ (eV)
Temperature T (K)

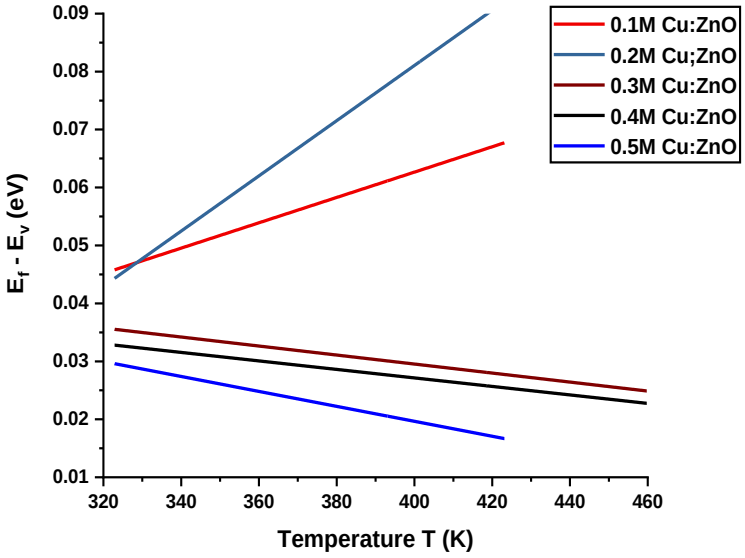
0.1M Cu:ZnO
0.2M Cu;ZnO
0.3M Cu:ZnO
0.4M Cu:ZnO
0.5M Cu:ZnO
$E_f - E_v$ (eV)
Temperature T (K)

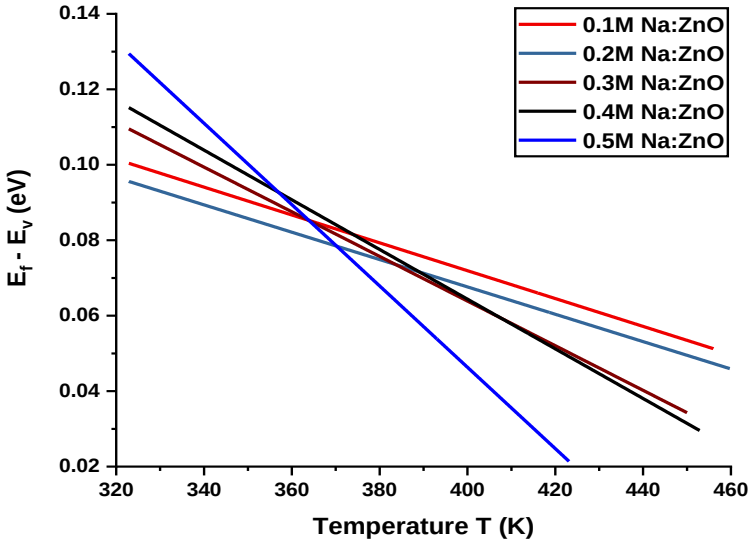
0.1M Na:ZnO
0.2M Na:ZnO
0.3M Na:ZnO
0.4M Na:ZnO
0.5M Na:ZnO
$E_f - E_v$ (eV)
Temperature T (K)

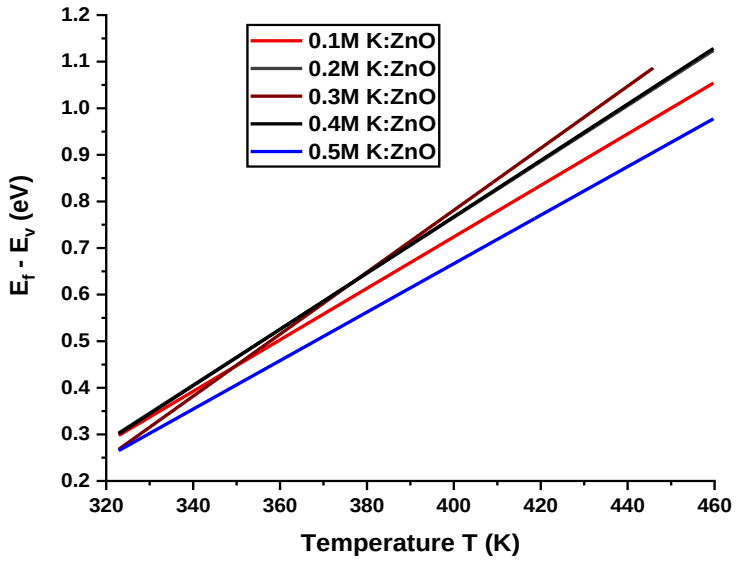

Figure 6.10 (E_c - E_f) vs temperature for Pure ZnO and (E_f - E_v) vs temperature for Cu, Na and K doped ZnO with variation in concentration from 0.1M to 0.5M.

From the Figure 6.10, the minimum value of (E_c - E_f) obtained from the graph of (E_c - E_f) versus T is 0.22 eV and is more than five times of k_BT. Thus our previous consideration for a ZnO as a nondegenerate model is justified (Table 6.4). The minimum values of (E_f - E_v) obtained from the graph (E_f - E_v) versus T are less than five times of k_BT for all Cu doped ZnO and Na doped ZnO thin films which show degenerate nature of the materials whereas that of pure ZnO and all K doped ZnO thin films are more than five times of k_BT which show nondegenerate type of materials. (Table 6.4).

6.6.3 Thermoelectric power factor

The power factors of the pure ZnO, Cu, Na and K doped ZnO thin films at different dopant concentration are illustrated in Figure 6.11 (power factor versus temperature) which were calculated by the formula (Equation 3.20) [238].

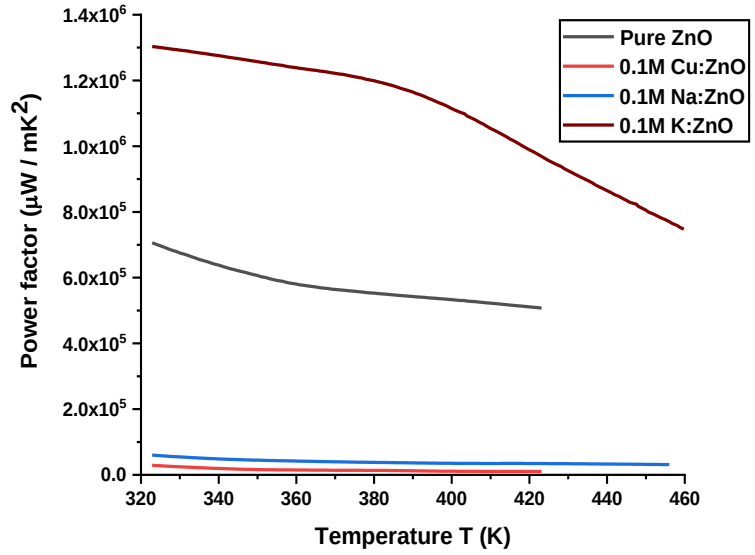
Pure ZnO
0.1M Cu:ZnO
0.1M Na:ZnO
0.1M K:ZnO
Power factor (μW / mK2)
Temperature T (K)

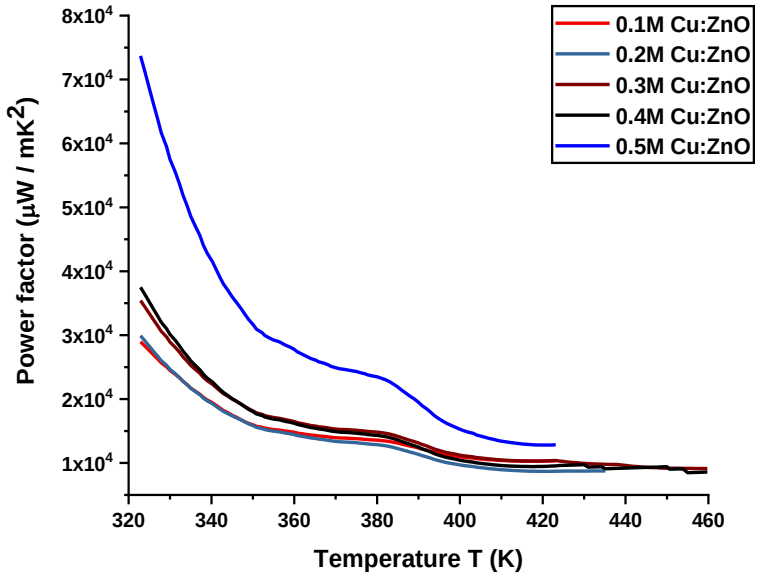
0.1M Cu:ZnO
0.2M Cu:ZnO
0.3M Cu:ZnO
0.4M Cu:ZnO
0.5M Cu:ZnO
Power factor (μW / mK2)
Temperature T (K)

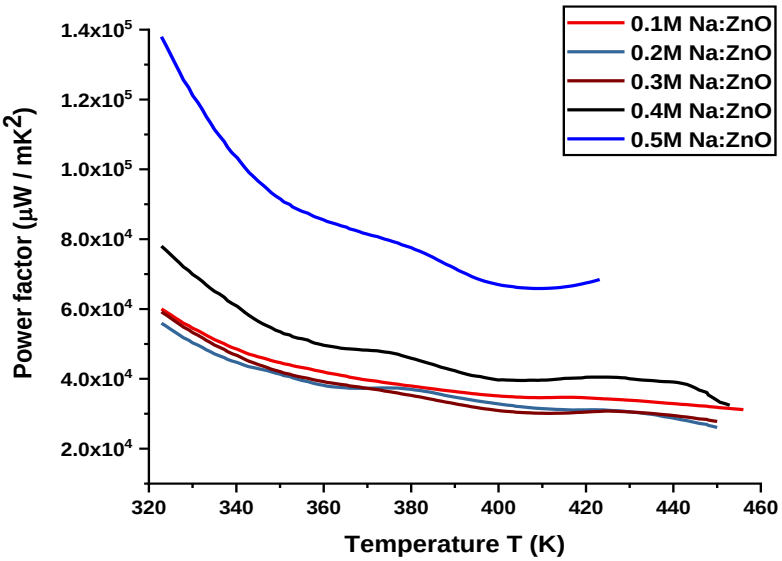
0.1M Na:ZnO
0.2M Na:ZnO
0.3M Na:ZnO
0.4M Na:ZnO
0.5M Na:ZnO
Power factor (μW / mK2)
Temperature T (K)

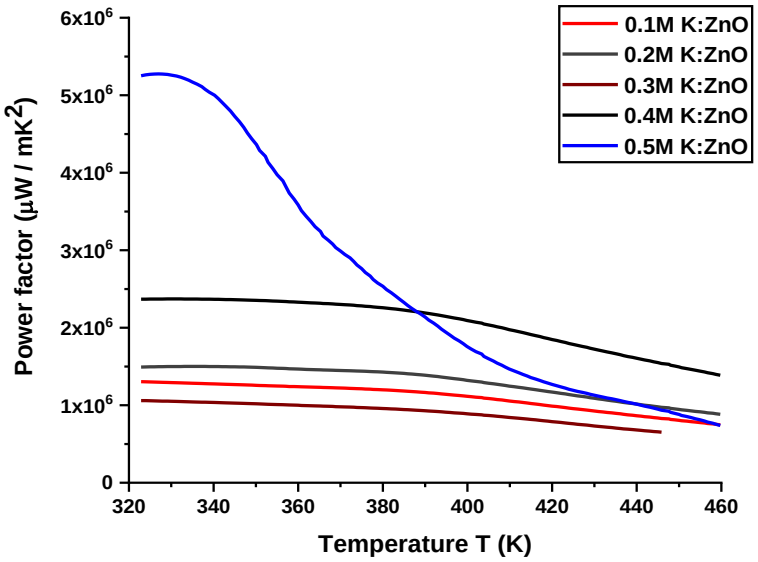

Figure 6.11 Power factor vs temperature for pure ZnO, Cu, Na and K doped ZnO with variation in concentration from 0.1M to 0.5M.

The graph of these quantity of power factors versus temperature is represented in Fig. 6.11 showing that the values of power factor decrease with the increasing temperatures.

6.6.4 Jonker analysis

The variation of the Seebeck coefficient with electron conductivity can also be represented by plotting the Seebeck coefficient as a function of the natural logarithm of electrical conductivity (a Jonker plot) [239].

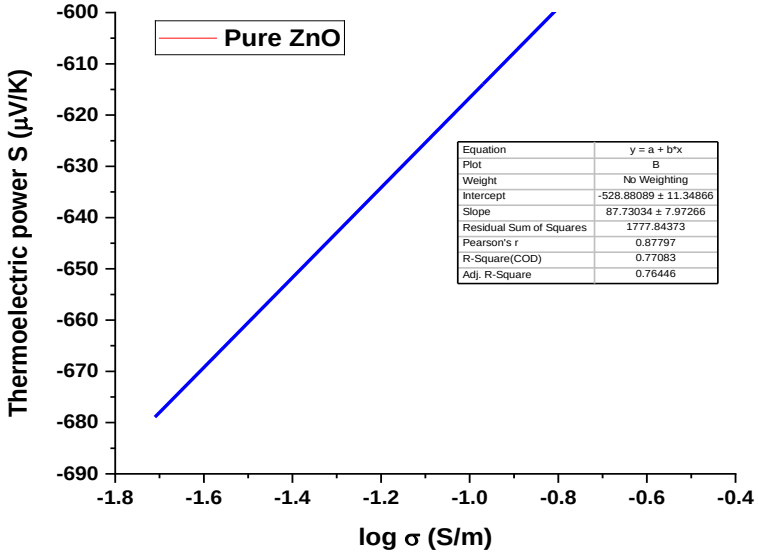

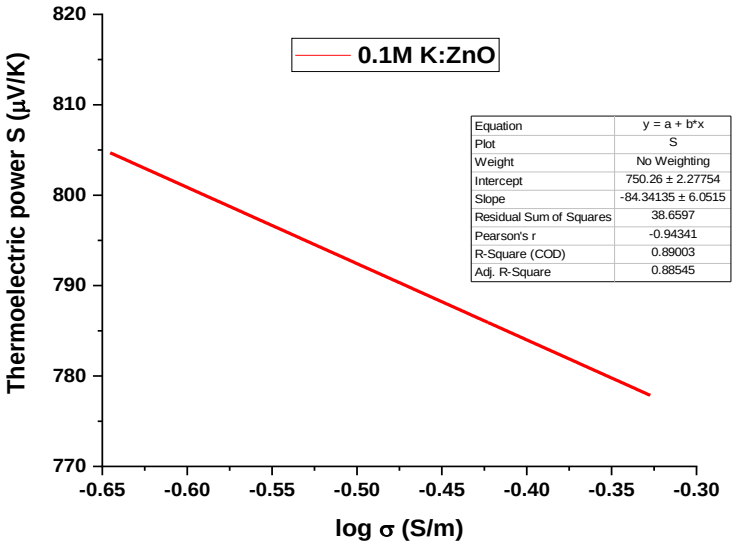

Equation	y = a + b*x
Plot	S
Weight	No Weighting
Intercept	750.26 ± 2.27754
Slope	-84.34135 ± 6.0515
Residual Sum of Squares	38.6597
Pearson's r	-0.94341
R-Square (COD)	0.89003
Adj. R-Square	0.88545

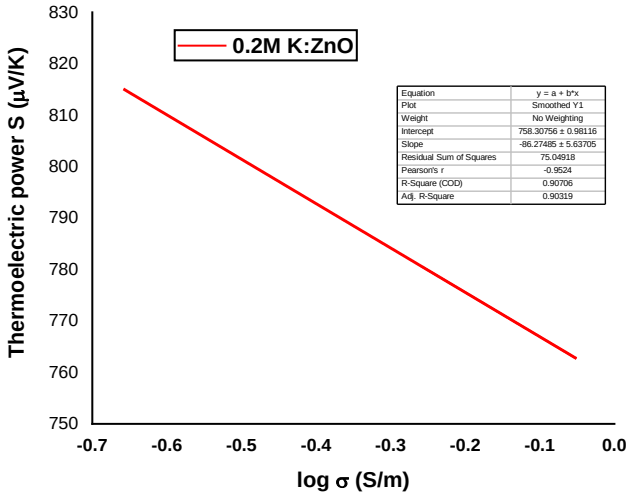

Equation	y = a + b*x
Plot	Smoothed Y1
Weight	No Weighting
Intercept	758.30756 ± 0.98116
Slope	-86.27485 ± 5.63705
Residual Sum of Squares	75.04918
Pearson's r	-0.9524
R-Square (COD)	0.90706
Adj. R-Square	0.90319

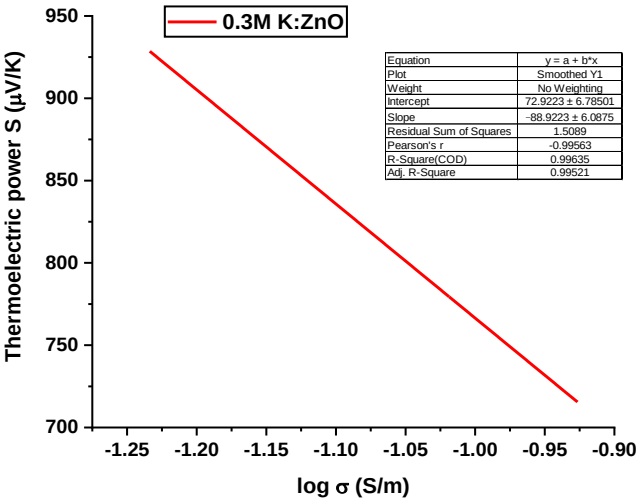

Equation	y = a + b*x
Plot	Smoothed Y1
Weight	No Weighting
Intercept	72.9223 ± 6.78501
Slope	-88.9223 ± 6.0875
Residual Sum of Squares	1.5089
Pearson's r	-0.99563
R-Square(COD)	0.99635
Adj. R-Square	0.99521

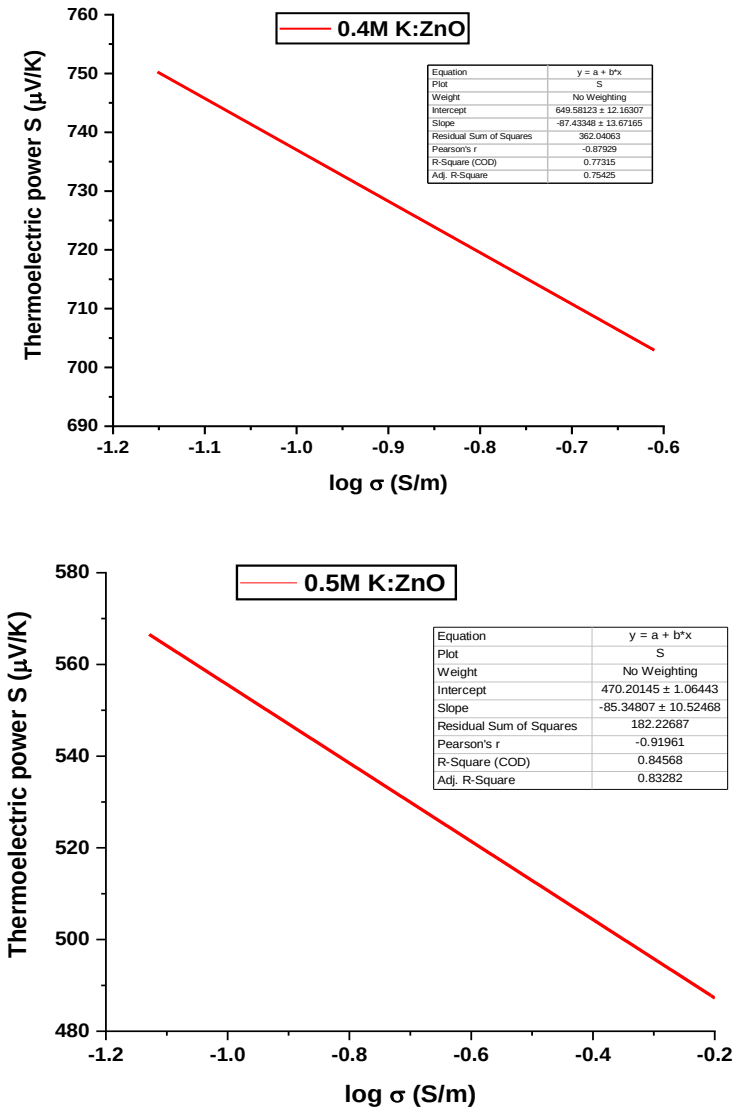

Figure 6.12 Jonker plot (Seebeck coefficient vs natural logarithm of electrical conductivity) for pure ZnO, 0.1M K;ZnO, 0.2M K;ZnO, 0.3M K;ZnO, 0.4M K;ZnO, and 0.5M K:ZnO.

The values of slope of the Jonker plot for pure ZnO and 0.1M to 0.5M K doped ZnO thin films are around k_B/e (86.15 μV/K), which indicates it is a non-degenerate material. But the values of slope of the Jonker plot for 0.1M to 0.5M Cu doped and 0.1M to 0.5M Na doped ZnO thin films are lower than k_B/e (86.15 μV/K), which is a degenerate material.

Table 6.3 Transport coefficient and types of scattering of pure ZnO and Cu, Na and K doped ZnO thin films with variation in concentration from 0.1M to 0.5M.

Sample	Transport Coefficient (A)		Type of Scattering		γ (eV/K)	
	300K to 460 K		300K to 460 K		300 K to 350 K	351 K to 460 K
Pure ZnO	3.2		Piezoelectric		5.59×10^{-5}	3.81×10^{-4}
Sample	**Transport Coefficient (A)**		**Type of Scattering**		**γ (eV/K)**	
	300 K to 350 K	**351 K to 460 K**	**300 K to 350 K**	**351 K to 460 K**	**300 K to 350 K**	**351 K to 460 K**
0.1M Cu:ZnO	4	0.35	Charged Impurity Scattering	Neutral Impurity Scattering	3.49×10^{-4}	3×10^{-5}
0.2M Cu:ZnO	3.91	0.73	Charged Impurity Scattering	Neutral Impurity Scattering	3.25×10^{-4}	6.49×10^{-5}
0.3M Cu:ZnO	3.94	0.6	Charged Impurity Scattering	Neutral Impurity Scattering	3.27×10^{-4}	5.29×10^{-5}
0.4M Cu:ZnO	4	0.72	Charged Impurity Scattering	Neutral Impurity Scattering	3.33×10^{-4}	6.29×10^{-5}
0.5M Cu:ZnO	4	1.06	Charged Impurity Scattering	Neutral Impurity Scattering	3.53×10^{-4}	9.29×10^{-5}
Sample	**Transport Coefficient (A)**		**Type of Scattering**		**γ (eV/K)**	
	300 K to 370 K	**371 K to 460 K**	**300 K to 370 K**	**371 K to 460 K**	**300 K to 370 K**	**371 K to 460 K**
0.1M Na:ZnO	1.3	0.90	Optical mode lattice Scattering	Neutral Impurity Scattering	8.19×10^{-5}	7.88×10^{-5}
0.2M Na:ZnO	1.36	0.35	Optical mode lattice Scattering	Neutral Impurity Scattering	7.79×10^{-5}	1.59×10^{-5}
0.3M Na:ZnO	1.69	0.56	Optical mode lattice Scattering	Neutral Impurity Scattering	10.8×10^{-5}	2.51×10^{-5}
0.4M Na:ZnO	2.03	0.59	Optical mode lattice Scattering	Neutral Impurity Scattering	12.7×10^{-5}	3.59×10^{-5}
0.5M Na:ZnO	2.09	0.15	Optical mode lattice Scattering	Neutral Impurity Scattering	13.1×10^{-5}	$2,59 \times 10^{-5}$
Sample	**Transport Coefficient (A)**		**Type of Scattering**		**γ (eV/K)**	
	300 K to 390 K	**391 K to 460 K**	**300 K to 390 K**	**391 K to 460 K**	**300 K to 390 K**	**391 K to 460 K**
0.1M K:ZnO	0.03	2.7	Optical mode lattice Scattering	Piezoelectric	2.80 x 10-5	8.57×10^{-4}
0.2M K:ZnO	0.42	2.9	Optical mode lattice Scattering	Piezoelectric	8.49 x 10-5	9.77×10^{-4}
0.3M K:ZnO	1.18	2.7	Optical mode lattice Scattering	Piezoelectric	8.99 x 10-5	9.37×10^{-4}
0.4M K:ZnO	1.17	2.9	Optical mode lattice Scattering	Piezoelectric	8.09 x 10-5	9.84×10^{-4}
0.5M K:ZnO	1.38	2.7	Optical mode lattice Scattering	Piezoelectric	10.2 x 10-5	8.49×10^{-4}

Table 6.4 Types of material and types of conductivity of pure ZnO and Cu, Na and K doped ZnO thin films with variation in concentration from 0.1M to 0.5M.

Sample	E_c - E_f (eV)	Types of material	E_0 (eV)	Types of conductivity
Pure ZnO	0.2292	Non degenerate	0.2111	n-type
0.1M Cu:ZnO	0.045	Degenerate	0.1613	p-type
0.2M Cu:ZnO	0.044	Degenerate	0.1473	p-type
0.3M Cu:ZnO	0.035	Degenerate	0.1459	p-type
0.4M Cu:ZnO	0.033	Degenerate	0.1444	p-type
0.5M Cu:ZnO	0.029	Degenerate	0.1473	p-type
0.1M Na:ZnO	0.100	Degenerate	0.0920	p-type
0.2M Na:ZnO	0.095	Degenerate	0.0866	p-type
0.3M Na:ZnO	0.120	Degenerate	0.0946	p-type
0.4M Na:ZnO	0.120	Degenerate	0.0988	p-type
0.5M Na:ZnO	0.130	Degenerate	0.0976	p-type
0.1M K:ZnO	0.298	Non degenerate	0.0905	p-type
0.2M K:ZnO	0.264	Non degenerate	0.0624	p-type
0.3M K:ZnO	0.271	Non degenerate	0.1058	p-type
0.4M K:ZnO	0.302	Non degenerate	0.0601	p-type
0.5M K:ZnO	0.312	Non degenerate	0.0470	p-type

6.7 Discussion of results on Cu: ZnO, Na: ZnO and K: ZnO thin films

- In summary, complete and careful comparison of pure ZnO and copper (Cu), potassium (K) and sodium (Na) doped ZnO thin films has been carried out. All three dopants improve film's optical and electrical properties compared to undoped ZnO.
- The Raman spectra shows that the intensity of the dominant peak changes with different dopant i.e. such as the peak at 119 cm^{-1} and 407 cm^{-1} for the Cu doped, at 585 cm^{-1} for the Na doped, and at 260 cm^{-1} for K doped thin films.; compared to the ZnO thin film, the shifting of peaks is due to lattice defects and lattice disorder.
- The synchronous Raman and photoluminescence examinations have the preferred standpoint to correspond with the changes observed in the optical property of the semiconducting materials.
- Hall effect results show that a growth condition is suitable for p-type doped ZnO thin films with high carrier concentration i.e. 1.651 x 10^{17} e^-/ cm^3. Also, chemical

bath deposition as a method to grow stabe p-type ZnO.

- The decrease in resistivity from 78.57 to 15.00 Ω·cm for Cu-ZnO, 72.14 to 22.86 Ω·cm for Na-ZnO and 78.57 to 20.00 Ω·cm for K-ZnO thin films prepared with different concentrations compared with pure ZnO films is attributed to the replacement of Zn^{+2} by Cu^{+2}, Na^{+} and K^{+} ions respectively. The resistivity of all doped thin films decrease with increase in doping concentration. As the concentration of impurity increases, both the conductivity and mobility of thin films increase.

- ZnO thin films doped with Cu, Na and K has the capability to increase its conductivity i.e. 0.0127 S/cm to 0.0667 S/cm, 0.0139 S/cm to 0.0438 S/cm and 0.0127 S/cm to 0.0500 S/cm respectively without adversely modifying other properties. The deposited films find suitable for photocells and solar cell gadgets.
- The influence of all dopant concentration on thermoelectric properties has been studied. Seebeck coefficient was found to be decreasing with increase in dopant concentration resulted in a high power factor. It resulted in the enhancement of Seebeck coefficient (151 μV/K for Cu, 207 μV/K for Na and 954 μV/K for K) and power factor (2.9×10^4 $\mu Wm^{-1}K^{-2}$ for Cu, 6×10^4 $\mu Wm^{-1}K^{-2}$ for Na, 1.3×10^4 $\mu Wm^{-1}K^{-2}$ for K respectively). Our study explores the thermoelectric properties of all doped zinc oxide thin films to pave a road for its thermoelectric applications.
- Jonker plots (Seebeck coefficient versus logarithm of conductivity) are useful for predicting the TCO properties (i.e., maximum achievable conductivity of TCO thin films). On the basis of these conclusions, it may be suggested that this material can be a potential choice soon for thermoelectric power generation applications.
- Highest value of power factor was obtained giving a possibility of industrial applications in thermoelectricity and solar cell devices.

CHAPTER 7

Summary, Conclusions and Scope of Future Work

7.1 Summary

Considering the present scenario of ZnO research, few issues were identified which have been the motivation of the present thesis work. ZnO; both pure and doped has a lot of practical applications in different devices. The aim of this work was to offer some understanding of the variation in precursor concentration, variation in number of coats as well as effect of doping on ZnO thin films.

Thin films having different number of layers were prepared by depositing ZnO layers on one after other. Influence of multiple layering of ZnO thin films on the structural, morphological and optical properties were studied by X-ray diffraction, scanning electron microscopy and UV-VIS-NIR transmittance and reflectance spectroscopy. Required annealing temperature for the as grown films is determined by TGA analysis of powder obtained by drying precursor solution.

Zinc oxide thin films were deposited on glass substrate from aqueous solution of $ZnCl_2$ and NH_3 by chemical bath deposition method (CBD). The films of various thicknesses, particle size and other useful analysis have been obtained by varying the concentration of $ZnCl_2$ from 0.1M, 0.2M, 0.3M, 0.4M and 0.5M. As the concentration of the precursor increases, thickness of the film increases and lattice strain also increases gradually. The crystallite size and band gap energy were found to depend on the concentration. The band gap increases as the crystallite size increases.

It is attracting attention to explore the impact of the Cu, Na and K dopants on the properties of ZnO thin films prepared through chemical routes. Keeping this in mind we lay out an easy, well-grounded and cost effective method to prepare doped ZnO with Cu, K and Na dopant using Chemical Bath Deposition in aqueous solution. Effect of doping on electrical and optical parameters like resistivity, conductivity, mobility, carrier concentration, band gap and ionization energies of impurity levels studied.

The positive value of Hall voltage of all doped thin films i.e. copper (Cu), potassium (K) and sodium (Na) doped ZnO thin films measured using Van der Pauw method with four point electrode fixture is in agreement with the red shift in PL spectra of p-type doping.

Seebeck coefficient, Peltier coefficient and power factor of pure and Cu, Na and K doped ZnO thin films grown using CBD method with variation in precursor concentration from 0.1M to 0.5M are found, which show results in very positive manner.

7.2 Conclusion

- In the current research, pure ZnO as well as doped ZnO thin films (with Cu, Na and K doping) on glass substrate as well as powder of ZnO have been prepared by colloidal solution route.
- In pure ZnO thin films, the optical and electrical properties strongly varied with the increasing precursor concentrations from 0.1M to 0.5M as well as by varying number of coat from single coat to quintuple coat of ZnO thin films. The transmittance, absorbance, reflectance, refractive index, extinction coefficient, band gap and the real as well as imaginary parts of dielectric constant for the variation in precursor concentration and variation in number of coat from single coat to quintuple coat of ZnO thin films were determined.
- Complete and careful comparison of pure ZnO and copper (Cu), potassium (K) and sodium (Na) doped ZnO thin films has been carried out. All three dopants improve the optical and electrical properties of thin films compared to undoped ZnO.
- The Raman spectra shows that the intensity of the dominant peak changes with different dopant compared to the ZnO thin film. The shifting of peaks is due to lattice defects and lattice disorder. The synchronous Raman and photoluminescence examinations have the preferred standpoint to correspond with the changes observed in the optical property of the semiconducting materials.

- The positive value of Hall voltage of all doped thin films measured using Van der pauw method with four point electrode fixture is in agreement with the red shift in PL spectra of p-type doping.
- The decrease in resistivity of copper doped thin films compared with ZnO films is attributed to the replacement of Zn^{2+} ions by Cu^{2+} ions while in sodium and potassium doped thin films decrease in resistivity is due to the interstitial localization of Na^{+} and K^{+} ions respectively in the adjacent of the oxygen and Zn atoms.
- The resistivity of all doped thin films decrease with increase in doping concentration. ZnO thin films doped with Cu, Na and K has the capability to increase its conductivity without adversely modifying other properties.
- Increase in doping material will reduce the Seebeck coefficient. The values of slope of the Jonker plot for pure ZnO and 0.1M to 0.5M K doped ZnO thin films are around k_B/e (86.15 μV/K), which indicates it is a non-degenerate material. But the values of slope of the Jonker plot for 0.1M to 0.5M Cu doped and 0.1M to 0.5M Na doped ZnO thin films are lower than k_B/e (86.15 μV/K), which is a degenerate material.
- Power factor of Cu, Na and K doped thin films increases as the variation in concentration increases from 0.1M to 0.5M. Power factor which determines the performance of the thermoelectric energy convertor.

7.3 Scope of future Work

In order to improve the quality of the thin film of this material and their characterization more work is required, for example:

- Characterization of pure and doped ZnO thin films synthesized by changing other deposition parameters.
- The chemical bath deposition method has been optimized for pure and doped ZnO films of Cu, Na and K. The technique can be extended to prepare and characterize other metal doped ZnO films. Apart from being a cost-effective and simple technique, the method uses milder reaction conditions than those employed by most chemical methods proposed in the literature. Doping of different metals in ZnO may be particularly suitable by this method.
- ZnO thin films have been broadly observed due to its potential application in various field i.e. piezoelectric, photovoltaic, optoelectronic utilization. These aspects at

recent advances in the preparation of ZnO based thin films with variable doped materials and factors that control the electrical and optical properties would be investigated. e.g. variation in annealing temperature, deposition speed and coating time etc.

- Measurement of temperature dependent Hall effect would be a better scope for electronic devices.

List of References

[1] D. S. Dhawale and C. D. Lokhande, “Chemical route to synthesis of mesoporous ZnO thin films and their liquefied petroleum gas sensor performance,” J. Alloys Compd., vol. 509, no. 41, pp. 10092–10097, 2011, doi: 10.1016/j.jallcom.2011.08.046.

[2] W. Zeng, T. Liu, and Z. Wang, “Enhanced gas sensing properties by SnO2 nanosphere functionalized TiO 2 nanobelts,” J. Mater. Chem., vol. 22, no. 8, pp. 3544 –3548, 2012, doi: 10.1039/c2jm15017d.

[3] Q. A. Drmosh, Z. H. Yamani, and M. K. Hossain, “Hydrogen gas sensing performance of low partial oxygen-mediated nanostructured zinc oxide thin film,” Sensors Actuators, B Chem., vol. 248, pp. 868–877, 2017, doi: 10.1016/ j. snb. 2017. 01.082.

[4] R. R. Salunkhe, D. S. Dhawale, D. P. Dubal, and C. D. Lokhande, “Sprayed CdO thin films for liquefied petroleum gas (LPG) detection,” Sensors Actuators, B Chem., vol. 140, no. 1, pp. 86–91, 2009, doi: 10.1016/j.snb.2009.04.046.

[5] Y. Zhang and J. Mu, “Controllable synthesis of flower- and rod-like ZnO nanostructures by simply tuning the ratio of sodium hydroxide to zinc acetate,” Nanotechnology, vol. 18, no. 7, 2007, doi: 10.1088/0957-4484/18/7/075606.

[6] Ü. Özgür et al., “A comprehensive review of ZnO materials and devices,” Journal of Applied Physics, vol. 98, no. 4. pp. 1–103, Aug. 15, 2005, doi: 10.1063/1.1992666.

[7] D. S. Dhawale, D. P. Dubal, A. M. More, T. P. Gujar, and C. D. Lokhande, “Room temperature liquefied petroleum gas (LPG) sensor,” Sensors Actuators, B Chem., vol. 147, no. 2, pp. 488–494, 2010, doi: 10.1016/j.snb.2010.02.063.

[8] J. Chen, J. Li, J. Li, G. Xiao, and X. Yang, “Large-scale syntheses of uniform ZnO nanorods and ethanol gas sensors application,” J. Alloys Compd., vol. 509, no. 3, pp. 740–743, 2011, doi: 10.1016/j.jallcom.2010.09.043.

[9] L. Huang and H. Fan, “Room-temperature solid state synthesis of ZnO/α-Fe 2O 3 hierarchical nanostructures and their enhanced gas-sensing properties,” Sensors Actuators, B Chem., vol. 171–172, pp. 1257–1263, 2012, doi: 10.1016/j. snb. 2012. 06.068.

[10] K. M. Kim, H. R. Kim, K. Il Choi, H. J. Kim, and J. H. Lee, “Design of highly sensitive C2H5oH sensors using self-assembled ZnO nanostructures,” Sensors, vol. 11, no. 10, pp. 9685–9699, Oct. 2011, doi: 10.3390/s111009685.

[11] K. M. Kim, H. R. Kim, K. Il Choi, H. J. Kim, and J. H. Lee, “ZnO hierarchical nanostructures grown at room temperature and their C 2H5OH sensor applications,”

Sensors Actuators, B Chem., vol. 155, no. 2, pp. 745–751, 2011, doi: 10.1016/j.snb.2011.01.040.

[12] X. Wang, W. Cai, G. Wang, and C. Liang, “Standing porous ZnO nanoplate-built hollow microspheres and kinetically controlled dissolution/crystal growth mechanism,” J. Mater. Res., vol. 27, no. 6, pp. 951–958, 2012, doi: 10.1557/jmr.2012.15.

[13] D. Dimova-Malinovska, “Nanostructured ZnO thin films: Properties and applications,” NATO Sci. Peace Secur. Ser. B Phys. Biophys., vol. 16, no. 4, pp. 157–166, 2011, doi: 10.1007/978-94-007-0903-4_16.

[14] X. Wang, W. P. Carey, and S. S. Yee, “Monolithic thin-film metal-oxide gas-sensor arrays with application to monitoring of organic vapors,” Sensors Actuators B. Chem., vol. 28, no. 1, pp. 63–70, 1995, doi: 10.1016/0925-4005(94)01531-L.

[15] Y. Natsume and H. Sakata, “Zinc oxide films prepared by sol-gel spin-coating,” Thin Solid Films, vol. 372, no. 1, pp. 30–36, 2000, doi: 10.1016/S0040-6090(00)01056-7.

[16] T. Negami, Y. Hashimoto, and S. Nishiwaki, “Cu(In,Ga)Se2 thin-film solar cells with an efficiency of 18%,” Sol. Energy Mater. Sol. Cells, vol. 67, no. 1–4, pp. 331–335, 2001, doi: 10.1016/S0927-0248(00)00300-7.

[17] K. Arshak and I. Gaidan, “Development of a novel gas sensor based on oxide thick films,” Mater. Sci. Eng. B Solid-State Mater. Adv. Technol., vol. 118, no. 1–3, pp. 44–49, 2005, doi: 10.1016/j.mseb.2004.12.061.

[18] R. Ghosh, S. Fujihara, and D. Basak, “Studies of the optoelectronic properties of ZnO thin films,” J. Electron. Mater., vol. 35, no. 9, pp. 1728–1733, 2006, doi: 10.1007/s11664-006-0226-6.

[19] N. Shakti and P. S. Gupta, “Structural and Optical Properties of Sol-gel Prepared ZnO Thin Film,” Appl. Phys. Res., vol. 2, no. 1, pp. 19–28, 2010, doi: 10.5539/ apr.v2n1p19.

[20] E. I. A and O. N. A, “Effects of Ligand on the Absorbance and Transmittance of Chemical Bath Deposited Zinc Sulphide Thin Film,” Pelagia Res. Libr. Adv. Appl. Sci. Res., vol. 3, no. 5, pp. 2821–2825, 2012, [Online]. Available: www. pelagiaresearchlibrary.com.

[21] S. Tewari and A. Bhattacharjee, “Structural, electrical and optical studies on spray-deposited aluminium-doped ZnO thin films,” Pramana - J. Phys., vol. 76, no. 1, pp. 153–163, 2011, doi: 10.1007/s12043-011-0021-7.

[22] H. Yin et al., “A comparative study of the physical and chemical properties of nano-sized ZnO particles from multiple batches of three commercial products,” J. Nanoparticle Res., vol. 17, no. 2, pp. 1–19, 2015, doi: 10.1007/s11051-014-2851-y.

[23] K. Joshi, M. Rawat, S. K. Gautam, R. G. Singh, R. C. Ramola, and F. Singh, “Band gap widening and narrowing in Cu-doped ZnO thin films,” J. Alloys Compd., vol. 680, pp. 252–258, 2016, doi: 10.1016/j.jallcom.2016.04.093.

[24] G. Malik, S. Mourya, J. Jaiswal, and R. Chandra, “Effect of annealing parameters on optoelectronic properties of highly ordered ZnO thin films,” Mater. Sci. Semicond. Process., vol. 100, no. April, pp. 200–213, 2019, doi: 10.1016/j.mssp.2019.04.032.

[25] P. Rong, S. Ren, and Q. Yu, “Fabrications and Applications of ZnO Nanomaterials in Flexible Functional Devices-A Review,” Crit. Rev. Anal. Chem., vol. 49, no. 4, pp. 336–349, 2019, doi: 10.1080/10408347.2018.1531691.

[26] H. Ennaceri et al., “Deposition of multifunctional TiO2 and ZnO top-protective coatings for CSP application,” Surf. Coatings Technol., vol. 298, pp. 103–113, 2016, doi: 10.1016/j.surfcoat.2016.04.048.

[27] P. Steiger, J. Zhang, K. Harrabi, I. A. Hussein, J. M. Downing, and M. A. McLachlan, “Hydrothermally grown ZnO electrodes for improved organic photovoltaic devices,” Thin Solid Films, vol. 645, pp. 417–423, 2018, doi: 10.1016/j.tsf.2017.11.021.

[28] D. C. Look, J. W. Hemsky, and J. R. Sizelove, “Residual native shallow donor in ZnO,” Phys. Rev. Lett., vol. 82, no. 12, pp. 2552–2555, 1999, doi: 10.1103/PhysRevLett.82.2552.

[29] D. C. Look, G. C. Farlow, P. Reunchan, S. Limpijumnong, S. B. Zhang, and K. Nordlund, “Evidence for native-defect donors in n-type ZnO,” Phys. Rev. Lett., vol. 95, no. 22, pp. 1–4, 2005, doi: 10.1103/PhysRevLett.95.225502.

[30] C. G. Van De Walle, “Hydrogen as a cause of doping in zinc oxide,” Phys. Rev. Lett., vol. 85, no. 5, pp. 1012–1015, 2000, doi: 10.1103/PhysRevLett.85.1012.

[31] S. Zh, E. S. Marstein, and A. Holt, “S. Zh. Karazhanov, E. S. Marstein, and A. Holt,” J. Appl. Phys., no. 105, pp. 1–15, 2009.

[32] S. B. Zhang, S. H. Wei, and A. Zunger, “Intrinsic n-type versus p-type doping asymmetry and the defect physics of ZnO,” Phys. Rev. B - Condens. Matter Mater. Phys., vol. 63, no. 7, pp. 1–7, 2001, doi: 10.1103/PhysRevB.63.075205.

[33] D. C. Look and B. Claflin, “P-type doping and devices based on ZnO,” Phys. Status Solidi Basic Res., vol. 241, no. 3, pp. 624–630, 2004, doi: 10.1002/pssb.200304271.

[34] S. Ning, P. Zhan, Q. Xie, Z. Li, and Z. Zhang, “Room-temperature ferromagnetism in un-doped ZrO2 thin films,” J. Phys. D. Appl. Phys., vol. 46, p. 44504, 2013, doi: 10.1088/0022-3727/46/44/445004.

[35] D. Chakraborti, J. Narayan, and J. T. Prater, “Room temperature ferromagnetism in Zn1-xCuxO thin films,” Appl. Phys. Lett., vol. 90, no. 6, p. 062504, 2007, doi: 10.1063/1.2450652.

[36] J. Ding, H. Chen, X. Zhao, and S. Ma, “Effect of substrate and annealing on the structural and optical properties of ZnO:Al films,” J. Phys. Chem. Solids, vol. 71, no. 3, pp. 346–350, 2010, doi: 10.1016/j.jpcs.2009.12.088.

[37] S. Muthukumaran and R. Gopalakrishnan, “Structural, FTIR and photoluminescence studies of Cu doped ZnO nanopowders by co-precipitation method,” Opt. Mater. (Amst)., vol. 34, no. 11, pp. 1946–1953, Sep. 2012, doi: 10.1016/j.optmat.2012.06.004.

[38] D. Behera, J. Panigrahi, and B. S. Acharya, “Probing the effect of nitrogen gas on electrical conduction phenomena of ZnO and Cu-doped ZnO thin films prepared by spray pyrolysis,” Ionics (Kiel)., vol. 17, no. 8, pp. 741–749, 2011, doi: 10.1007/s11581-011-0564-0.

[39] P. M. Martin, John Wiley & Sons, 2011.

[40] F. Quaranta, A. Valentini, F. R. Rizzi, and G. Casamassima, “Dual-ion-beam sputter deposition of ZnO films,” J. Appl. Phys., vol. 74, no. 1, pp. 244–248, 1993, doi: 10.1063/1.354152.

[41] V. Craciun, J. Elders, J. G. E. Gardeniers, and I. W. Boyd, “Characteristics of high quality ZnO thin films deposited by pulsed laser deposition,” Appl. Phys. Lett., vol. 65, no. 23, pp. 2963–2965, 1994, doi: 10.1063/1.112478.

[42] C. K. Ong and S. J. Wang, “In situ RHEED monitor of the growth of epitaxial anatase TiO 2 thin films,” Appl. Surf. Sci., vol. 185, no. 1–2, pp. 47–51, 2001, doi: 10.1016/S0169-4332(01)00589-X.

[43] M. Yoneta, Y. Kamiura, and F. Hashimoto, “Chemical etching-induced defects in phosphorus-doped silicon,” J. Appl. Phys., vol. 70, no. 3, pp. 1295–1308, 1991, doi: 10.1063/1.349586.

[44] Y. Natsume, H. Sakata, T. Hirayama, and H. Yanagida, “Low-temperature conductivity of ZnO films prepared by chemical vapor deposition,” J. Appl. Phys., vol. 72, no. 9, pp. 4203–4207, 1992, doi: 10.1063/1.352231.

[45] A. J. C. Fiddes, K. Durose, A. W. Brinkman, J. Woods, P. D. Coates, and A. J. Banister, “Preparation of ZnO films by spray pyrolysis,” J. Cryst. Growth, vol. 159, no. 1–4, pp. 210–213, 1996, doi: 10.1016/0022-0248(95)00707-5.

[46] E. Pascual, E. Martínez, J. Esteve, and A. Lousa, “Boron carbide thin films deposited by tuned-substrate RF magnetron sputtering,” Diam. Relat. Mater, vol. 8, no. 2–5, pp. 402–405, 1999, doi: 10.1016/s0925-9635(98)00274-x.

[47] K. Koski, J. Hölsä, and P. Juliet, “Voltage controlled reactive sputtering process for aluminium oxide thin films,” Thin Solid Films, vol. 326, no. 1–2, pp. 189–193, 1998, doi: 10.1016/S0040-6090(98)00546-X.

[48] D. Perednis and L. J. Gauckler, “Thin film deposition using spray pyrolysis,” J. Electroceramics, vol. 14, no. 2, pp. 103–111, 2005, doi: 10.1007/s10832-005-0870-x.

[49] D. P. Dubal, R. Holze, and P. Gomez-Romero, “Development of hybrid materials based on sponge supported reduced graphene oxide and transition metal hydroxides for hybrid energy storage devices,” Sci. Rep., vol. 4, pp. 1–10, 2014, doi: 10.1038/srep07349.

[50] T. R. Society and R. Society, “On the Properties of Silicic Acid and other Analogous Colloidal Substances Author (s): Thomas Graham Source : Proceedings of the Royal Society of London , Vol . 13 (1863 - 1864), pp . 335-341 Published by : The Royal Society Stable URL : http://www.js,” R. Soc., vol. 13, no. May, pp. 335–341, 2010.

[51] D. J. Shaw, “Colloid and Surface Chemistry,” Butterworth, vol. 4, p. 115, 1992.

[52] H. C. Hamaker, “General theory of lyophobic colloids. ,vol. 1015, 1936.

[53] A. Wei, C. Xu, X. W. Sun, W. Huang, and G. Q. Lo, “Field emission from hydrothermally grown ZnO nanoinjectors,” IEEE/OSA J. Disp. Technol., vol. 4, no. 1, pp. 9–12, 2008, doi: 10.1109/JDT.2007.901569.

[54] D. C. Look, D. C. Reynolds, J. W. Hemsky, R. L. Jones, and J. R. Sizelove, “Production and annealing of electron irradiation damage in ZnO,” Appl. Phys. Lett., vol. 75, no. 6, pp. 811–813, 1999, doi: 10.1063/1.124521.

[55] A. Hernández Battez et al., “CuO, ZrO2 and ZnO nanoparticles as antiwear additive in oil lubricants,” Wear, vol. 265, no. 3–4, pp. 422–428, 2008, doi: 10.1016/j.wear.2007.11.013.

[56] P. Wagner and R. Helbig, “Halleffekt und anisotropie der beweglichkeit der elektronen in ZnO,” J. Phys. Chem. Solids, vol. 35, no. 3, pp. 327–335, 1974, doi: 10.1016/S0022-3697(74)80026-0.

[57] Zinc Oxide Bulk, Thin Films and Nanostructures. 2006.

[58] M. A. Abdulsattar, “Capped ZnO (3, 0) nanotubes as building blocks of bare and H passivated wurtzite ZnO nanocrystals,” Superlattices Microstruct., vol. 85, pp. 813–819, 2015, doi: 10.1016/j.spmi.2015.07.015.

[59] N. F. Saniee, “Structural and optical properties of Transparent Conducting Si-doped ZnO Thin Films Grown by Pulsed Laser Deposition,” Appl. Phys. Rev., vol. 98, no. 1, p. 041301, 2005, [Online]. Available: http://www.nanoarchive.org/7248/.

[60] Ü. Özgür et al., “A comprehensive review of ZnO materials and devices,” Journal of Applied Physics, vol. 98, no. 4. pp. 1–103, Aug. 15, 2005, doi: 10.1063/1.1992666.

[61] R. Serhane et al., “Pulsed laser deposition of piezoelectric ZnO thin films for bulk acoustic wave devices,” Appl. Surf. Sci., vol. 288, pp. 572–578, 2014, doi: 10.1016/j.apsusc.2013.10.075.

[62] M. R. Parra and F. Z. Haque, “Aqueous chemical route synthesis and the effect of calcination temperature on the structural and optical properties of ZnO nanoparticles,” Integr. Med. Res., vol. 3, pp. 363–369, 2014, doi: 10.1016/j.jmrt.2014.07.001.

[63] S. Siva Kumar, P. Venkateswarlu, V. R. Rao, and G. N. Rao, “Synthesis, characterization and optical properties of zinc oxide nanoparticles,” Int. Nano Lett., vol. 3, no. 30, pp. 1–6, 2013, doi: https://doi.org/10.1186/2228-5326-3-30.

[64] S. M. Huang et al., “One-step growth of structured ZnO thin films by chemical bath deposition in aqueous ammonia solution,” J. Phys. D Appl. Phys. J. Phys. D Appl. Phys, vol. 42, no. 42, pp. 55412–6, 2009, doi: 10.1088/0022-3727/42/5/055412.

[65] H. Khallaf et al., “Investigation of chemical bath deposition of ZnO thin films using six different complexing agents,” J. Phys. D Appl. Phys. J. Phys. D Appl. Phys, vol. 42, no. 42, 2009, doi: 10.1088/0022-3727/42/13/135304.

[66] I. Nkrumah, F. K. Ampong, B. Kwakye-Awuah, R. K. Nkum, and F. Boakye, “Synthesis and characterization of zno thin films deposited by chemical bath technique,” Int. J. Res. Eng. Technol., vol. 2, no. 12, pp. 809–812, 2013, [Online]. Available: http://hdl.handle.net/123456789/12634.

[67] P. B. Taunk, R. Das, D. P. Bisen, R. K. Tamrakar, and N. Rathor, “Synthesis and optical properties of chemical bath deposited ZnO thin film,” Karbala Int. J. Mod. Sci., vol. 1, no. 3, pp. 159–165, 2015, doi: 10.1016/j.kijoms.2015.11.002.

[68] D. Acharyya and P. Bhattacharyya, “An efficient BTX sensor based on ZnO nanoflowers grown by CBD method,” Solid. State. Electron., vol. 106, pp. 18–26, 2015, doi: 10.1016/j.sse.2014.12.027.

[69] S. Rezabeigy, M. Behboudnia, and N. Nobari, “Growth of ZnO Nanorods on Glass Substrate by Chemical Bath Deposition,” Procedia Mater. Sci., vol. 11, pp. 364–369, 2015, doi: 10.1016/j.mspro.2015.11.130.

[70] S. Ilican, Y. Caglar, and M. Caglar, “Preparation and characterization of ZnO thin films deposited by sol-gel spin coating method,” J. Optoelectron. Adv. Mater., vol. 10, no. 10, pp. 2578–2583, 2008.

[71] N. V Kaneva and C. D. Dushkin, “Preparation of nanocrystalline thin films of ZnO by sol-gel dip coating,” Bulg. Chem. Commun., vol. 43, no. 2, pp. 259–263, 2011.

[72] M. Sahal, B. Hartiti, A. Ridah, M. Mollar, and B. Marí, “Structural, electrical and optical properties of ZnO thin films deposited by sol-gel method,” Microelectronics J., vol. 39, no. 12, pp. 1425–1428, 2008, doi: 10.1016/j.mejo.2008.06.085.

[73] J. Petersen et al., “Optical properties of ZnO thin films prepared by sol-gel process,” Microelectronics J., vol. 40, no. 2, pp. 239–241, 2009, doi: 10.1016/j.mejo.2008.07.061.

[74] A. J. Hashim, M. S. Jaafar, A. J. Ghazai, and N. M. Ahmed, “Fabrication and characterization of ZnO thin film using sol-gel method,” Optik (Stuttg)., vol. 124, no. 6, pp. 491–492, 2013, doi: 10.1016/j.ijleo.2011.12.059.

[75] S. Benramache, B. Benhaoua, F. Chabane, and A. Guettaf, “A comparative study on the nanocrystalline ZnO thin films prepared by ultrasonic spray and sol-gel method,” Optik (Stuttg)., vol. 124, no. 18, pp. 3221–3224, 2013, doi: 10.1016/j.ijleo.2012.10.001.

[76] K. Omri, I. Najeh, R. Dhahri, J. El Ghoul, and L. El Mir, “Effects of temperature on the optical and electrical properties of ZnO nanoparticles synthesized by sol-gel method,” Microelectron. Eng., vol. 128, pp. 53–58, 2014, doi: 10.1016/j.mee.2014.05.029.

[77] M. Heshmat, H. Abdizadeh, and M. R. Golobostanfard, “Sonochemical Assisted Synthesis of ZnO Nanostructured thin Films Prepared by Sol-gel Method,” Procedia Mater. Sci., vol. 11, no. 2014, pp. 486–490, 2015, doi: 10.1016/j.mspro.2015.11.070.

[78] S. Aydemir and S. Karakaya, “Effects of withdrawal speed on the structural and optical properties of sol-gel derived ZnO thin films,” J. Magn. Magn. Mater., vol. 373, pp. 33–39, 2015, doi: 10.1016/j.jmmm.2014.01.077.

[79] T. Ates, C. Tatar, and F. Yakuphanoglu, “Preparation of semiconductor ZnO powders by sol-gel method: Humidity sensors,” Sensors Actuators, A Phys., vol. 190, pp. 153–160, 2013, doi: 10.1016/j.sna.2012.11.031.

[80] Y. H. Hwang, S. J. Seo, and B. S. Bae, “Fabrication and characterization of sol-gel-derived zinc oxide thin-film transistor,” J. Mater. Res., vol. 25, no. 4, pp. 695–700, 2010, doi: 10.1557/JMR.2010.0103.

[81] R. K. Shukla, A. Srivastava, N. Kumar, A. Pandey, and M. Pandey, “Optical and sensing properties of Fe doped ZnO nanocrystalline thin films,” Mater. Sci. Pol., vol. 34, no. 2, pp. 354–361, 2016, doi: 10.1515/msp-2016-0039.

[82] M. Sajjad, I. Ullah, M. I. Khan, J. Khan, M. Y. Khan, and M. T. Qureshi, “Structural and optical properties of pure and copper doped zinc oxide nanoparticles,” Results Phys., vol. 9, pp. 1301–1309, Jun. 2018, doi: 10.1016/j.rinp.2018.04.010.

[83] E. Bhawani, G. S. Harish, and S. R. P, “Effect of Cu doping on Electrical, Photoluminescene and Band Gap Engineering of Mg Doped ZnO Nanoparticles,” Am. J. Eng. Res., vol. 6, no. 7, pp. 30–35, 2017.

[84] A. Ghosh, N. Kumari, and A. Bhattacharjee, “Influence of Cu doping on the structural, electrical and optical properties of ZnO,” Pramana - J. Phys., vol. 84, no. 4, pp. 621–635, 2015, doi: 10.1007/s12043-014-0851-1.

[85] M. Bedir, “Charecterization of undoped and Cu-doped thin film deposited on glass substrates by spray pyrolysis,” Chinese Phys. Soc., vol. 23, no. 4, pp. 939–942, 2006.

[86] J. S. C. Licurgo, G. R. de Almeida Neto, and H. R. Paes Junior, “Structural, electrical and optical properties of copper-doped zinc oxide films deposited by spray pyrolysis,” Ceramica, vol. 66, no. 379, pp. 284–290, 2020, doi: 10.1590/0366-69132020663792877.

[87] B. El Filiali, T. T. V., A. I. Díaz Cano, and M. Morales Rodiguez, “Structural and raman scattering studies of ZnO-Cu nanocrystals grown by spray pyrolysis,” Rev. Mex. Ing. Química, vol. 11, no. 1, pp. 23–43, 2015.

[88] P. Jongnavakit, P. Amornpitoksuk, S. Suwanboon, and N. Ndiege, “Preparation and photocatalytic activity of Cu-doped ZnO thin films prepared by the sol-gel method,” Appl. Surf. Sci., vol. 258, no. 20, pp. 8192–8198, 2012, doi: 10.1016/j.apsusc.2012.05.021.

[89] D. Verma Atul, “Effect of copper doping sol-gel ZnO thin films: physical properties and sensitivity to ethanol vapor,” Mater. Res. Express, vol. 4, no. 10, pp. 1–19, 2017, doi: https://doi.org/10.1088/2053-1591/aa8cff.

[90] K. Chongsri, S. Aunpang, W. Techitdheera, and W. Pecharapa, “Preparation and characterization of cu-doped ZnO sol-gel derived optical thin films,” Adv. Mater. Res., vol. 802, pp. 124–128, 2013, doi: 10.4028/www.scientific.net/AMR.802.124.

[91] D. Q. G. Rswr et al., “_Structural and opto-electrical analysis of Cu doped ZnO thin films by sol-gel method,” Cenasic, vol. 19, no. 8, pp. 233–236, 2019.

[92] N. H. Erdogan, T. Kutlu, N. Sedefoglu, and H. Kavak, “Effect of Na doping on microstructures, optical and electrical properties of ZnO thin films grown by sol-gel method,” J. Alloys Compd., vol. 881, p. 160554, 2021, doi: 10.1016/j.jallcom.2021.160554.

[93] Y. Li, C. Lin, X. Zhou, J. Ma, and X. Zhu, “Electrical and optical properties of Na+-doped ZnO thin films prepared by sol-gel method,” Sixth Int. Conf. Thin Film Phys. Appl., vol. 6984, p. 69840U, 2008, doi: 10.1117/12.792359.

[94] J. Lv et al., “Optical constants of Na-doped ZnO thin films by sol-gel method,” Opt. Commun., vol. 284, no. 12, pp. 2905–2908, 2011, doi: 10.1016/j.optcom.2011.01.075.

[95] L. W. Wang et al., “Effects of Na content on structural and optical properties of Na-doped ZnO thin films prepared by sol-gel method,” J. Alloys Compd., vol. 623, pp. 367–373, 2015, doi: 10.1016/j.jallcom.2014.11.055.

[96] J. Lü, K. Huang, J. Zhu, X. Chen, X. Song, and Z. Sun, “Preparation and characterization of Na-doped ZnO thin films by sol-gel method,” Phys. B Condens. Matter, vol. 405, no. 15, pp. 3167–3171, 2010, doi: 10.1016/j.physb.2010.04.045.

[97] H. Shen, X. Zhao, L. Duan, R. Liu, H. Li, and B. Wang, “Effect of NaZn/Nai ratio on structural, optical, and electrical properties of Na-doped ZnO thin films,” J. Appl. Phys., vol. 121, no. 15, 2017, doi: 10.1063/1.4980172.

[98] S. Kumar and R. Thangavel, “Structural and optical properties of Na doped ZnO nanocrystalline thin films synthesized using sol-gel spin coating technique,” J. Sol-Gel Sci. Technol., vol. 67, no. 1, pp. 50–55, 2013, doi: 10.1007/s10971-013-3049-y.

[99] D. Wang and S. Gao, “Influence of Annealing Condition on The Structure and Optical Properties of Na-doped ZnO Thin Films Prepared by Sol-Gel Method,” J. Alloys Compd., vol. 476, no. 1–2, pp. 925–928, 2009, doi: 10.1016/j.jallcom.2008.09.127.

[100] A. Chelouche et al., “Na doping effects on the structural, conduction type and optical properties of sol–gel ZnO thin films,” J. Mater. Sci. Mater. Electron., vol. 28, no. 2, pp. 1546–1554, 2017, doi: 10.1007/s10854-016-5694-8.

[101] H. Fan, Z. Yao, C. Xu, X. Wang, and Z. Yu, “Effects of Na Doping on Structural, Optical, and Electronic Properties of ZnO Thin Films Fabricated by Sol–Gel Technique,” J. Electron. Mater., vol. 47, no. 7, pp. 3847–3854, 2018, doi: 10.1007/s11664-018-6258-x.

[102] J. Lü, J. Dai, J. Zhu, X. Song, and Z. Sun, “Effect of Na concentrations on microstructure and optical properties of ZnO films,” J. Wuhan Univ. Technol. Mater. Sci. Ed., vol. 26, no. 1, pp. 23–27, 2011, doi: 10.1007/s11595-011-0160-1.

[103] W. Wang, W. Meng, M. Liu, and X. Wang, “Effect of Na-doped concentration on the structure and optical properties of ZnO thin films,” Adv. Mater. Res., vol. 430–432, pp. 310–314, 2012, doi: 10.4028/www.scientific.net/AMR.430-432.310.

[104] G. Shanmuganathan, I. B. S. Banu, S. Krishnan, and B. Ranganathan, “Influence of K-doping on the optical properties of ZnO thin films grown by chemical bath deposition method,” J. Alloys Compd., vol. 562, pp. 187–193, 2013, doi: 10.1016/j.jallcom.2013.01.184.

[105] P. V. Athma, N. Johns, E. I. Anila, and T. A. Safeera, “Structural and optical characterization of potassium doped zinc oxide nanosheets,” Opt. Mater. (Amst)., vol. 38, pp. 223–227, 2014, doi: 10.1016/j.optmat.2014.10.034.

[106] G. Shanmuganathan and I. B. S. Banu, “Influence of Codoping on the Optical Properties of ZnO Thin Films Synthesized on Glass Substrate by Chemical Bath Deposition Method,” Adv. Condens. Matter Phys., vol. 2014, pp. 1–9, 2014, doi: 10.1155/2014/761960.

[107] S. Kahraman, H. M. Çakmak, S. Çetinkaya, F. Bayansal, H. A. Çetinkara, and H. S. Güder, “Characteristics of ZnO thin films doped by various elements,” J. Cryst. Growth, vol. 363, pp. 86–92, 2013, doi: 10.1016/j.jcrysgro.2012.10.018.

[108] G. Shanmuganathan and I. B. Shameem Banu, “Room temperature optical and magnetic properties of (Cu, K) doped ZnO based diluted magnetic semiconductor thin films grown by chemical bath deposition method,” Superlattices Microstruct., vol. 75, pp. 879–889, 2014, doi: 10.1016/j.spmi.2014.08.024.

[109] J. Xu, S. Shi, X. Zhang, Y. Wang, M. Zhu, and L. Li, “Structural and optical properties of (Al, K)-co-doped ZnO thin films deposited by a sol-gel technique,” Mater. Sci. Semicond. Process., vol. 16, no. 3, pp. 732–737, 2013, doi: 10.1016/j.mssp.2012.12.016.

[110] I. Ji et al., “K-doping effects on the characteristics of ZnO thin films synthesized by using a spin-coating method,” J. Korean Phys. Soc., vol. 64, no. 10, pp. 1581–1585, 2014, doi: 10.3938/jkps.64.1581.

[111] B. W. C. Au and K. Y. Chan, “Sodium and potassium doped P-type ZnO films by sol-gel spin-coating technique,” Appl. Phys. A Mater. Sci. Process., vol. 123, no. 7, pp. 1–9, 2017, doi: 10.1007/s00339-017-1099-7.

[112] R. Vettumperumal, S. Kalyanaraman, and R. Thangavel, “Effect of Er concentration on surface and optical properties of K doped ZnO sol-gel thin films,” Superlattices Microstruct., vol. 83, pp. 237–250, 2015, doi: 10.1016/j.spmi.2015.03.028.

[113] L. Xu, X. Li, and J. Yuan, “Effect of K-doping on structural and optical properties of ZnO thin films,” Superlattices Microstruct., vol. 44, no. 3, pp. 276–281, 2008, doi: 10.1016/j.spmi.2008.04.004.

[114] L. Xu, F. Gu, J. Su, Y. Chen, X. Li, and X. Wang, “The evolution behavior of structures and photoluminescence of K-doped ZnO thin films under different annealing temperatures,” J. Alloys Compd., vol. 509, no. 6, pp. 2942–2947, 2011, doi: 10.1016/j.jallcom.2010.11.164.

[115] S. Azara Hussain and A. Jabbar Radi, “Study the effect of film thickness on the structural and optical of (ZnO) thin film prepared by pulsed laser deposition,” J. Phys. Conf. Ser., vol. 1294, no. 2, pp. 7–12, 2019, doi: 10.1088/1742-6596/1294/2/022001.

[116] C. Klingshirn, “ZnO: From basics towards applications,” Phys. Status Solidi Basic Res., vol. 244, no. 9, pp. 3027–3073, 2007, doi: 10.1002/pssb.200743072.

[117] D. C. Look, J. W. Hemsky, and J. R. Sizelove, “Residual native shallow donor in ZnO,” Phys. Rev. Lett., vol. 82, no. 12, pp. 2552–2555, 1999, doi: 10.1103/PhysRevLett.82.2552.

[118] A. Janotti and C. G. Van De Walle, “Hydrogen multicentre bonds,” Nat. Mater., vol. 6, no. 1, pp. 44–47, 2007, doi: 10.1038/nmat1795.

[119] H. Absalan and F. E. Ghodsi, “Comparative study of ZnO thin films prepared by different sol-gel route,” Iran. J. Phys. Res., vol. 11, no. 4, p. 67, 2012, doi: 10.1016/j.spmi.2005.07.003.

[120] J. F. Muth, R. M. Kolbas, A. K. Sharma, S. Oktyabrsky, and J. Narayan, “Excitonic structure and absorption coefficient measurements of ZnO single crystal epitaxial films deposited by pulsed laser deposition,” J. Appl. Phys., vol. 85, no. 11, pp. 7884–7887, 1999, doi: 10.1063/1.370601.

[121] K. Vanheusden, C. H. Seager, W. L. Warren, D. R. Tallant, and J. A. Voigt, “Correlation between photoluminescence and oxygen vacancies in ZnO phosphors,” Appl. Phys. Lett., vol. 403, no. 1996, p. 403, 1995, doi: 10.1063/1.116699.

[122] C. Klingshirn, R. Hauschild, H. Priller, M. Decker, J. Zeller, and H. Kalt, “ZnO rediscovered - Once again!?,” Superlattices Microstruct., vol. 38, no. 4–6, pp. 209–222, 2005, doi: 10.1016/j.spmi.2005.07.003.

[123] M. A. Borysiewicz, “ZnO as a functional material, a review,” Crystals, vol. 9, no. 10, 2019, doi: 10.3390/cryst9100505.

[124] P. Wu et al., “Correlation between photoluminescence and oxygen vacancies in In 2O3, SnO2 and ZnO metal oxide nanostructures,” J. Phys. Conf. Ser., vol. 188, pp. 1–8, 2009, doi: 10.1088/1742-6596/188/1/012054.

[125] A. Van Dijken, E. A. Meulenkamp, D. Vanmaekelbergh, and A. Meijerink, “The Kinetics of the Radiative and Nonradiative Processes in Nanocrystalline ZnO Particles upon Photoexcitation,” J. Phys. Chem. B, vol. 104, no. 8, pp. 1715–1723, 2000, doi: 10.1021/jp993327z.

[126] A. B. Djurišić et al., “Green, yellow, and orange defect emission from ZnO nanostructures: Influence of excitation wavelength,” Appl. Phys. Lett., vol. 88, no. 10, pp. 28–31, 2006, doi: 10.1063/1.2182096.

[127] D. C. Reynolds, D. C. Look, B. Jogai, and H. Morkoç, “Similarities in the bandedge and deep-centre photoluminescence mechanisms of ZnO and GaN,” Solid State Commun., vol. 101, no. 9, pp. 643–646, 1997, doi: 10.1016/S0038-1098(96)006977.

[128] D. C. Reynolds, D. C. Look, B. Jogai, J. E. Van Nostrand, R. Jones, and J. Jenny, “Source of the yellow luminescence band in GaN grown by gas-source molecular beam epitaxy and the green luminescence band in single crystal ZnO,” Solid State Commun., vol. 106, no. 10, pp. 701–704, 1998, doi: 10.1016/S0038-1098(98)000489.

[129] A. Janotti and C. G. Van De Walle, “Native point defects in ZnO,” Phys. Rev. B - Condens. Matter Mater. Phys., vol. 76, no. 16, p. 165202, 2007, doi: 10.1103/PhysRevB.76.165202.

[130] F. A. Chaves and D. Jiménez, “Ac ce d M us pt,” Nanotechnology, vol. 29, no. 27, pp. 1–13, 2018.

[131] Z. Ma, F. Ren, X. Ming, Y. Long, and A. A. Volinsky, “Cu-doped ZnO electronic structure and optical properties studied by first-principles calculations and experiments,” Materials (Basel)., vol. 12, no. 1, pp. 1–12, Jan. 2019, doi: 10.3390/ma12010196.

[132] R. Swapna and M. C. Santhosh Kumar, “Deposition of Na-N dual acceptor doped p-type ZnO thin films and fabrication of p-ZnO:(Na, N)/n-ZnO:Eu homojunction,” Mater. Sci. Eng. B Solid-State Mater. Adv. Technol., vol. 178, no. 16, pp. 1032–1039, 2013, doi: 10.1016/j.mseb.2013.06.010.

[133] J. J. Lai et al., “Effects of Na content on the luminescence behavior, conduction type, and crystal structure of Na-doped ZnO films,” J. Appl. Phys., vol. 110, no. 1, p. 013704, 2011, doi: 10.1063/1.3603033.

[134] G. Shanmuganathan, I. B. S. Banu, S. Krishnan, and B. Ranganathan, “Influence of K-doping on the optical properties of ZnO thin films grown by chemical bath deposition method,” J. Alloys Compd., vol. 562, pp. 187–193, 2013, doi: 10.1016/j.jallcom.2013.01.184.

[135] S. Aksoy, Y. Caglar, S. Ilican, and M. Caglar, “Sol-gel derived Li-Mg co-doped ZnO films: Preparation and characterization via XRD, XPS, FESEM,” J. Alloys Compd., vol. 512, no. 1, pp. 171–178, 2012, doi: 10.1016/j.jallcom.2011.09.058.

[136] C. H. Park, S. B. Zhang, and S. H. Wei, “Origin of p-type doping difficulty in ZnO: The impurity perspective,” Phys. Rev. B - Condens. Matter Mater. Phys., vol. 66, no. 7, pp. 1–3, 2002, doi: 10.1103/PhysRevB.66.073202.

[137] M. J. S. Spencer, “Gas sensing applications of 1D-nanostructured zinc oxide: Insights from density functional theory calculations,” Prog. Mater. Sci., vol. 57, no. 3, pp. 437–486, 2012, doi: 10.1016/j.pmatsci.2011.06.001.

[138] C Jagadish; S J Pearton, Zinc oxide bulk, thin films and nanostructures : processing, properties and applications. Amsterdam ; London : Elsevier, 2006.

[139] L. I. Berger, Semiconductor Materials, 1st ed. CRC Press, 1996.

[140] X. W. Sun and H. S. Kwok, “Optical properties of epitaxially grown zinc oxide films on sapphire by pulsed laser deposition,” J. Appl. Phys., vol. 86, no. 1, pp. 408–411, 1999, doi: 10.1063/1.370744.

[141] Y. S. Park, Index of Refraction of ZnO. 1968.

[142] V. Srikant and D. R. Clarke, “On the optical band gap of zinc oxide,” J. Appl. Phys., vol. 83, no. 10, pp. 5447–5451, 1998, doi: 10.1063/1.367375.

[143] Ü. Ö. Hadis Morkoç, Zinc Oxide: Fundamentals, Materials and Device Technology. WILEY, 2009.

[144] G. S. & K. S. Noboru Yamazoe, “Oxide Semiconductor Gas Sensors,” Springer, vol. 7, pp. 63–75, 2003, doi: https://doi.org/10.1023/A:1023436725457.

[145] Pearton SJ et al. Recent progress in processing and properties of ZnO. Progress in Materials Science. 2005;50:293-340. doi: 10.1016/j.pmatsci.2004.04.001.

[146] W. H. Bragg and W. L. Bragg, Nature, vol. 17, no. 1, pp. 428–438, 1913. doi.org/ 10.1098 /rspa.1913.0040.

[147] P. Scherrer, “Bestimmung der inneren Struktur und der Größe von Kolloidteilchen mittels Röntgenstrahlen,” Kolloidchem. Ein Lehrb., vol. 277, no. 1916, pp. 387–409, 1912, doi: 10.1007/978-3-662-33915-2_7.

[148] B. Martínez, F. Sandiumenge, L. Balcells, J. Arbiol, F. Sibieude, and C. Monty, "Structure and magnetic properties of Co-doped ZnO nanoparticles," Phys. Rev. B - Condens. Matter Mater. Phys., vol. 72, no. 16, pp. 1–8, 2005, doi: 10.1103 / PhysRevB.72.165202.

[149] P. A. J. Sasanka Deka, "Synthesis and magnetic properties of Mn doped ZnO nanowires," Solid State Commun., vol. 142, no. 4, pp. 190–194, 2007, doi: 10.1016 /j.ssc.2007.02.017.

[150] Pankove, J.I. (1971) Optical Processes in Semiconductors. Dover, New York, 93.

[151] E. H. Hall, "On a New Action of the Magnet on Electric Currents," Johns Hopkins Univ. Press, vol. 2, no. 3, pp. 287–292, 1879.

[152] D. H. Petersen, O. Hansen, R. Lin, and P. F. Nielsen, "Micro-four-point probe Hall effect measurement method," J. Appl. Phys., vol. 104, no. 1, p. 013710, 2008, doi: 10.1063/1.2949401.

[153] S. C. Moulzolf, D. J. Frankel, and R. J. Lad, "In situ four-point conductivity and Hall effect apparatus for vacuum and controlled atmosphere measurements of thin film materials," Rev. Sci. Instrum., vol. 73, no. 6, p. 2325, Jun. 2002, doi: 10.1063 /1. 1475349.

[154] E. A. Davis, "Book Renews," Educ. Rev., vol. 32, no. 1, pp. 95–115, 1980, doi: 10. 1080/0013191800320108.

[155] K. Mahmood et al., "Modulation of thermoelectric properties of Mg2GeO4 thin films by controlling the growth process," Ceram. Int., vol. 45, no. 15, pp. 18701–18703, 2019, doi: 10.1016/j.ceramint.2019.06.095.

[156] Jonker G, "Giant thermoelectric Seebeck coefficient of a two-dimensional electron gas in SrTiO3," Philips Res. Rep, vol. 23, no. 2, p. 131, 1968.

[157] C. A. Domenicali, "Irreversible thermodynamics of thermoelectric effects in inhomogeneous, anisotropic media," Phys. Rev., vol. 92, no. 4, pp. 877–881, 1953, doi: 10.1103/PhysRev.92.877.

[158] X. L. Chen, X. H. Geng, J. M. Xue, D. K. Zhang, G. F. Hou, and Y. Zhao, "Temperature-dependent growth of zinc oxide thin films grown by metal organic chemical vapor deposition," J. Cryst. Growth, vol. 296, no. 1, pp. 43–50, 2006, doi: 10.1016/j.jcrysgro.2006.08.028.

[159] K.Savarimuthu. G. Rajamanickam "Experimental Study on Flexible ZnO Based Nanogenerator Using Schottky Contact for Energy Harvesting Applications," IEEE

Trans. Nanotechnol., vol. 16, no. 3, pp. 469–476, 2017, doi: 10.1109/ TNANO. 2017. 2688337.

[160] L. F. Koao, F. B. Dejene, and H. C. Swart, "Properties of flower-like ZnO nanostructures synthesized using the chemical bath deposition," Mater. Sci. Semicond. Process., vol. 27, no. 1, pp. 33–40, 2014, doi: 10.1016/j.mssp.2014.06.009.

[161] P. Kathirvel, D. Manoharan, and S. Mohan, "Spectral Investigations of Chemical Bath Deposited Zinc Oxide Thin Films – Ammonia Gas Sensor," J Optoelectron Biomed Mater, vol. 1, no. 1, pp. 25–33, 2009,

[162] P. K. Kalita, B. K. Sarma, and H. L. Das, "Photoresponse characteristics of vacuum evaporated ZnTe thin films," Indian J. Pure Appl. Phys., vol. 37, no. 12, pp. 885–890, 1999.

[163] A. G. Shikalgar and S. H. Pawar, "Photoconducting properties of cadmium sulphide-lithium thin films formed by the chemical bath deposition method," Thin Solid Films, vol. 61, no. 3, pp. 313–320, 1979, doi: 10.1016/0040-6090(79)90475-9.

[164] Jacques I. Pankove1 and David A. Kiewit, "Optical Processes in Semiconductors," J. Electrochem. Soc., vol. 119, no. 5, p. 1338, 1972.

[165] V. Srikant and D. R. Clarke, "Optical absorption edge of ZnO thin films: The effect of substrate," Journal of Applied Physics, vol. 81, no. 9, p. 6357- 6364, 1997, doi: 10.1063/1.364393

[166] A. M. Tauc, J., "States in the gap," J. Non. Cryst. Solids, vol. 8–10, pp. 569–585, 1972, doi: 10.1016/0022-3093(72)90194-9.

[167] P. P. Sahay, S. Tewari, and R. K. Nath, "Optical and electrical studies on spray deposited ZnO thin films," Cryst. Res. Technol., vol. 42, no. 7, pp. 723–729, 2007, doi: 10.1002/crat.200610895.

[168] M. R. Islam and J. Podder, "Optical properties of ZnO nano fiber thin films grown by spray pyrolysis of zinc acetate precursor," Cryst. Res. Technol., vol. 44, no. 3, pp. 286–292, 2009, doi: 10.1002/crat.200800326.

[169] M. Caglar, S. Ilican, and Y. Caglar, "Influence of dopant concentration on the optical properties of ZnO: In films by sol-gel method," Thin Solid Films, vol. 517, no. 17, pp. 5023–5028, 2009, doi: 10.1016/j.tsf.2009.03.037.

[170] A. R. Forouhi and I. Bloomer, "Optical dispersion relations for amorphous semiconductors and amorphous dielectrics," Phys. Rev. B, vol. 34, no. 10, pp. 7018–7026, 1986, doi: 10.1103/PhysRevB.34.7018.

[171] A. K. Walton and T. S. Moss, “Determination of refractive index and correction to effective electron mass in PbTe and PbSe,” Proc. Phys. Soc., vol. 81, no. 3, pp. 509–513, 1963, doi: 10.1088/0370-1328/81/3/319.

[172] F. F. Oliveira, M. P. Proenca, J. P. Araújo, and J. Ventura, “Electrodeposition of ZnO thin films on conducting flexible substrates,” J. Mater. Sci., vol. 51, no. 12, pp. 5589–5597, 2016, doi: 10.1007/s10853-016-9850-6.

[173] T. Morita et al., “Fabrication of Transparent ZnO Thick Film with Unusual Orientation by the Chemical Bath Deposition,” Cryst. Growth Des., vol. 15, no. 7, pp. 3150–3156, 2015, doi: 10.1021/cg501729w.

[174] M. Suja, S. B. Bashar, M. M. Morshed, and J. Liu, “Realization of Cu-doped p-type ZnO thin films by molecular beam epitaxy,” ACS Appl. Mater. Interfaces, vol. 7, no. 16, pp. 8894–8899, 2015, doi: 10.1021/acsami.5b01564.

[175] A. Zawadzka, P. Płóciennik, Y. El Kouari, H. Bougharraf, and B. Sahraoui, “Linear and nonlinear optical properties of ZnO thin films deposited by pulsed laser deposition,” J. Lumin., vol. 169, pp. 483–491, 2016, doi: 10.1016/j.jlumin.2015.04.020.

[176] J. Bin Lee, S. H. Kwak, and H. J. Kim, “Effects of surface roughness of substrates on the c-axis preferred orientation of ZnO films deposited by r.f. magnetron sputtering,” Thin Solid Films, vol. 423, no. 2, pp. 262–266, 2003, doi: 10.1016/S0040-6090(02)00977-X.

[177] J. Ye et al., “The growth and annealing of single crystalline ZnO films by low-pressure MOCVD,” J. Cryst. Growth, vol. 243, no. 1, pp. 151–156, 2002, doi: 10. 1016/S0022-0248 (02)01474-4.

[178] N. Kalyani, Y. C. Ching, and N. Azizi, “Structural and optical properties of ZnO thin films obtained by spray pyrolysis,” Mater. Res. Innov., vol. 18, no. March, pp. S6-126-S6-130, 2014, doi: 10.1179/1432891714Z.0000000001013.

[179] H. Bahadur et al., “Nano-structured ZnO films by sol-gel process,” Indian J. Pure Appl. Phys., vol. 45, no. 4, pp. 395–399, 2007.

[180] Z. R. Khan, M. S. Khan, M. Zulfequar, and M. Shahid Khan, “Optical and Structural Properties of ZnO Thin Films Fabricated by Sol-Gel Method,” Mater. Sci. Appl., vol. 02, no. 05, pp. 340–345, 2011, doi: 10.4236/msa.2011.25044.

[181] M. L. Addonizio, A. Aronne, S. Daliento, O. Tari, E. Fanelli, and P. Pernice, “Sol-gel synthesis of ZnO transparent conductive films: The role of pH,” Appl. Surf. Sci., vol. 305, pp. 194–202, 2014, doi: 10.1016/j.apsusc.2014.03.037.

[182] H. Nian, S. H. Hahn, K. K. Koo, E. W. Shin, and E. J. Kim, “Sol-gel derived N-doped ZnO thin films,” Mater. Lett., vol. 63, no. 26, pp. 2246–2248, 2009, doi: 10.1016/ j. matlet.2009. 07. 038.

[183] J. Li, J. Xu, Q. Xu, and G. Fang, “Preparation and characterization of Al doped ZnO thin films by sol-gel process,” J. Alloys Compd., vol. 542, pp. 151–156, 2012, doi: 10. 1016/j. jallcom. 2012.07.075.

[184] C. A. ARGUELLo et al., “Physics and Chemistry of II-VI ComPounds,” W. A. Benjamin, Inc, 1955.

[185] D. Dey, T. Maitra, U. V. Waghmare, and A. Taraphder, “Phonon dispersion, Raman spectra, and evidence for spin-phonon coupling in MnV2 O4 from first principles,” Phys. Rev. B, vol. 101, no. 20, p. 205132, 2020, doi: 10.1103/PhysRevB.101.205132.

[186] S. Ben Yahia, L. Znaidi, A. Kanaev, and J. P. Petitet, “Raman study of oriented ZnO thin films deposited by sol-gel method,” Spectrochim. Acta - Part A Mol. Biomol. Spectrosc., vol. 71, no. 4, pp. 1234–1238, Dec. 2008, doi: 10.1016/j.saa.2008.03.032.

[187] Jacques I. Pankove and David A. Kiewit, “Optical Processes in Semiconductors,” Electrochem. Soc., vol. 119, no. 5, p. 1338, 1972.

[188] M. A. Tauc J, “States in the gap,” J. Non. Cryst. Solids, vol. 8–10, no. 1, pp. 569–585, 1972, doi: 10.1016/0022-3093(72)90194-9.

[189] M. R. Islam and J. Podder, “Optical properties of ZnO nano fiber thin films grown by spray pyrolysis of zinc acetate precursor,” Cryst. Res. Technol., vol. 44, no. 3, pp. 286–292, 2009, doi: 10.1002/crat.200800326.

[190] A. R. Forouhi and I. Bloomer, “Optical dispersion relations for amorphous semiconductors and amorphous dielectrics,” Phys. Rev. B, vol. 34, no. 10, pp. 7018–7026, 1986, doi: 10.1103/PhysRevB.34.7018.

[191] C. KITTEL, "Elementary Solid State Physics", 1962, p. 339.

[192] B. Lin, Z. Fu, and Y. Jia, “Green luminescent center in undoped zinc oxide films deposited on silicon substrates,” Appl. Phys. Lett., vol. 79, no. 7, pp. 943–945, 2001, doi: 10.1063/1.1394173.

[193] P. Misra, T. K. Sharma, and L. M. Kukreja, “Temperature dependent photoluminescence processes in ZnO thin films grown on sapphire by pulsed laser deposition,” Curr. Appl. Phys., vol. 9, no. 1, pp. 179–183, 2009, doi: 10.1016/j.cap.2008.01.007.

[194] S. Chackrabarti, R. A. Zargar, A. Aziz, and A. K. Hafiz, “Structural and optical characteristics of transparent conducting yttrium doped ZnO films using screen

printing technology," J. Mater. Sci. Mater. Electron., vol. 27, no. 5, pp. 5271–5276, 2016, doi: 10.1007/s10854-016-4424-6.

[195] K. Samanta, P. Bhattacharya, R. S. Katiyar, W. Iwamoto, P. G. Pagliuso, and C. Rettori, "Raman scattering studies in dilute magnetic semiconductor Zn1-x Cox O," Phys. Rev. B - Condens. Matter Mater. Phys., vol. 73, no. 24, 2006, doi: 10.1103/PhysRevB.73.245213.

[196] D. Luković Golić et al., "Structural characterization of self-assembled ZnO nanoparticles obtained by the sol-gel method from Zn(CH3COO)22H2O," Nanotechnology, vol. 22, no. 39, 2011, doi: 10.1088/0957-4484/22/39/395603.

[197] D. Segets, J. Gradl, R. K. Taylor, and V. Vassilev, "Absorbance Spectra for the Determination of ZnO Nanoparticle Size Distribution, Solubility," ACS Nano, vol. 3, no. 7, pp. 1703–1710, 2009, doi: 10.1021/nn900223b.

[198] A. Kolodziejczak-Radzimska and T. Jesionowski, "Zinc oxide-from synthesis to application: A review," Materials (Basel)., vol. 7, no. 4, pp. 2833–2881, 2014, doi: 10. 3390 /ma7042833.

[199] J. X. Wang et al., "Free-standing ZnO-CuO composite nanowire array films and their gas sensing properties," Nanotechnology, vol. 22, no. 32, Aug. 2011, doi: 10.1088/0957-4484/22/32/325704.

[200] A. Janotti and C. G. Van De Walle, "Fundamentals of zinc oxide as a semiconductor," Reports Prog. Phys., vol. 72, no. 12, 2009, doi: 10.1088/0034-4885/72/12/126501.

[201] Z. L. Wang, "Zinc oxide nanostructures: growth, properties and applications," J. Phys. Condens. Matter, vol. 16, no. 25, pp. R829–R858, Jun. 2004, doi: 10.1088/0953-8984/16/25/R01.

[202] J. L. Gomez and O. Tigli, "Zinc oxide nanostructures: From growth to application," Journal of Materials Science, vol. 48, no. 2. pp. 612–624, Jan. 2013, doi: 10.1007/s10853-012-6938-5.

[203] L. Schmidt-Mende and J. L. Macmanus-Driscoll, "ZnO : nanostructures, defects, and devices," vol. 10, no. 5, pp. 40–48, Jun. 2019 [Online]. Available: http://nbn-resolving. de/ urn:nbn:de:bsz:352-251979.

[204] V. S. Rana, J. K. Rajput, T. K. Pathak, and L. P. Purohit, "Cu sputtered Cu/ZnO Schottky diodes on fluorine doped tin oxide substrate for optoelectronic applications," Thin Solid Films, vol. 679, pp. 79–85, Jun. 2019, doi: 10.1016/j.tsf.2019.04.019.

[205] M. K. Hamza Taha et al., “Control of the compensating defects in Al-doped and Ga-doped ZnO nanocrystals for MIR plasmonics,” RSC Adv., vol. 7, no. 46, pp. 28677–28683, 2017, doi: 10.1039/c7ra03697c.

[206] D. Sett and D. Basak, “Toward understanding the role of VZn defect on the photoconductivity of surface-passivated ZnO NRs,” J. Phys. Chem. C, vol. 121, no. 39, 2017, doi: 10.1021/acs.jpcc.7b06393.

[207] S. Ghosh, A. Mallick, B. Dou, M. F. A. M. van Hest, S. M. Garner, and D. Basak, “A novel blanket annealing process to achieve highly transparent and conducting Al doped ZnO thin films: Its mechanism and application in perovskite solar cells,” Sol. Energy, vol. 174, pp. 815–825, Nov. 2018, doi: 10.1016/j.solener.2018.09.017.

[208] J. Varghese and R. Vinodkumar, “Effect of CuO on the photoluminescence quenching and photocatalytic activity of ZnO multilayered thin films prepared by sol-gel spin coating technique,” Mater. Res. Express, vol. 6, no. 10, p. 106405, Aug. 2019, doi: 10.1088/2053-1591/ab3596.

[209] S. J. Pearton et al., “Transition Metal Doped ZnO for Spintronics,” 2007.

[210] M. Silambarasan, S. Saravanan, and T. Soga, “Mn-doped ZnO nanoparticles prepared by solution combustion method,” in e-Journal of Surface Science and Nanotechnology, Jun. 2014, vol. 12, pp. 283–288, doi: 10.1380/ejssnt.2014.283.

[211] M. Sajjad, I. Ullah, M. I. Khan, J. Khan, M. Y. Khan, and M. T. Qureshi, “Structural and optical properties of pure and copper doped zinc oxide nanoparticles,” Results Phys., vol. 9, pp. 1301–1309, Jun. 2018, doi: 10.1016/j.rinp.2018.04.010.

[212] R. Y. Sato-Berrú, A. Vázquez-Olmos, A. L. Fernández-Osorio, and S. Sotres-Martínez, “Micro-Raman investigation of transition-metal-doped ZnO nanoparticles,” J. Raman Spectrosc., vol. 38, no. 9, pp. 1073–1076, Sep. 2007, doi: 10.1002/jrs.1658.

[213] P. Bhattacharyya, P. K. Basu, C. Lang, H. Saha, and S. Basu, “Noble metal catalytic contacts to sol–gel nanocrystalline zinc oxide thin films for sensing methane,” Sensors Actuators B, vol. 129, pp. 551–557, 2008, doi: 10.1016/j.snb.2007.09.001.

[214] L. Wu, Y. Wu, and W. Lü, “Preparation of ZnO Nanorods and optical characterizations,” Phys. E Low-Dimensional Syst. Nanostructures, vol. 28, no. 1, pp. 76–82, Jun. 2005, doi: 10.1016/j.physe.2005.02.005.

[215] P. Khosravi, F. Karimzadeh, and H. R. Salimijazi, “Investigation of structural and optical properties of ZnO:Cu co-sputtered thin films,” Mater. Res. Express, vol. 6, no. 11, 2019, doi: 10.1088/2053-1591/ab4493.

[216] D. H. Petersen, O. Hansen, R. Lin, and P. F. Nielsen, “Micro-four-point probe Hall effect measurement method,” J. Appl. Phys., vol. 104, no. 1, p. 013710, 2008, doi: 10.1063/1.2949401.

[217] S. C. Moulzolf, D. J. Frankel, and R. J. Lad, “In situ four-point conductivity and Hall effect apparatus for vacuum and controlled atmosphere measurements of thin film materials,” Rev. Sci. Instrum., vol. 73, no. 6, p. 2325, Jun. 2002, doi: 10.1063/1.1475349.

[218] V. Bhosle, A. Tiwari, and J. Narayan, “Electrical properties of transparent and conducting Ga doped ZnO,” J. Appl. Phys., vol. 100, no. 3, 2006, doi: 10.1063/1.2218466.

[219] V. Postica et al., “Multifunctional Materials: A Case Study of the Effects of Metal Doping on ZnO Tetrapods with Bismuth and Tin Oxides,” Adv. Funct. Mater., vol. 27, no. 6, Feb. 2017, doi: 10.1002/adfm.201604676.

[220] I. Tiginyanu et al., “Strong light scattering and broadband (UV to IR) photoabsorption in stretchable 3D hybrid architectures based on Aerographite decorated by ZnO nanocrystallites,” Sci. Rep., vol. 6, Sep. 2016, doi: 10.1038/srep32913.

[221] V. Shukla, A. Patel “Influence of Multiple Layers on Chemical Bath Deposited Zno Thin Films,” Int. J. Res. Appl. Sci. Eng. Technol., vol. 6, no. 3, pp. 268–274, Mar. 2018, doi: 10.22214/ijraset.2018.3042.

[222] R. N. Gayen, K. Sarkar, S. Hussain, R. Bhar, and A. K. Pal, “ZnO films prepared by modified sol-gel technique,” Indian J. Pure Appl. Phys., vol. 49, no. 7, pp. 470–477, 2011.

[223] H. Zhou et al., “Raman studies of ZnO: Co thin films,” in Physica Status Solidi (A) Applications and Materials Science, Jan. 2007, vol. 204, no. 1, pp. 112–117, doi: 10.1002/pssa.200673019.

[224] X. Liu, M. Afzaal, T. Badcock, P. Dawson, and P. O’Brien, “Conducting ZnO thin films with an unusual morphology: Large flat microcrystals with (0 0 0 1) facets perpendicular to the plane by chemical bath deposition,” Mater. Chem. Phys., vol. 127, no. 1–2, pp. 174–178, 2011, doi: 10.1016/j.matchemphys.2011.01.054.

[225] T. Livneh and E. Sterer, “Effect of pressure on the resonant multiphonon Raman scattering in UO2,” Phys. Rev. B - Condens. Matter Mater. Phys., vol. 73, no. 8, pp. 1–9, 2006, doi: 10.1103/PhysRevB.73.085118.

[226] A. K. Singh, V. Viswanath, and V. C. Janu, “Synthesis, effect of capping agents, structural, optical and photoluminescence properties of ZnO nanoparticles,” J. Lumin., vol. 129, no. 8, pp. 874–878, Aug. 2009, doi: 10.1016/j.jlumin.2009.03.027.

[227] R. Dingle, “Luminescent transitions associated with divalent copper impurities and the green emission from semiconducting zinc oxide,” Phys. Rev. Lett., vol. 23, no. 11, pp. 579–581, 1969, doi: 10.1103/PhysRevLett.23.579.

[228] N. Y. Garces, L. Wang, L. Bai, N. C. Giles, L. E. Halliburton, and G. Cantwell, “Role of copper in the green luminescence from ZnO crystals,” Appl. Phys. Lett., vol. 81, no. 4, pp. 622–624, 2002, doi: 10.1063/1.1494125.

[229] D. S. Permyakov, S. I. Rembeza, T. G. Menshikova, V. E. Polkovnikov, and M. A. Belykh, “Influence of Annealing on the Electrophysical Properties of Copper Oxide (II) Thin Film, Prepared by Sol-Gel Method,” Nano Hybrids Compos., vol. 28, pp. 48–52, 2020, doi: 10.4028/www.scientific.net/nhc.28.48.

[230] R. Kumar and N. Khare, “Temperature dependence of conduction mechanism of ZnO and Co-doped ZnO thin films,” Thin Solid Films, vol. 516, no. 6, pp. 1302–1307, 2008, doi: 10.1016/j.tsf.2007.06.121.

[231] C. H. Park, S. B. Zhang, and S. H. Wei, “Origin of p-type doping difficulty in ZnO: The impurity perspective,” Phys. Rev. B - Condens. Matter Mater. Phys., vol. 66, no. 7, pp. 1–3, 2002, doi: 10.1103/PhysRevB.66.073202.

[232] C. Rauch et al., “Lithium related deep and shallow acceptors in Li-doped ZnO nanocrystals,” J. Appl. Phys., vol. 107, no. 2, 2010, doi: 10.1063/1.3275889.

[233] H. B. Kwok and R. H. Bube, “Thermoelectric and photothermoelectric effects in semiconductors: CdS single crystals,” J. Appl. Phys., vol. 44, no. 1, pp. 138–144, 1973, doi: 10.1063/1.1661848.

[234] V. J. Shukla, A. J. Patel, “Effect of doping concentration on optical and electrical properties of intrinsic n-type ZnO (i-ZnO) and (Cu, Na and K) doped p-type ZnO thin films grown by chemical bath deposition method,” Nanosyst. Physics, Chem. Math., vol. 11, no. 4, pp. 391–400, 2020, doi: 10.17586/2220-8054-2020-11-4-391-400.

[235] A. P. Roth and D. F. Williams, “Properties of zinc oxide films prepared by the oxidation of diethyl zinc,” J. Appl. Phys., vol. 52, no. 11, pp. 6685–6692, 1981, doi: 10.1063/1.328618.

[236] A. Kyunghan Ahn “Thermoelectric Properties of the Compounds AgPbmLaTem+2,” ACS Publ., vol. 22, no. 3, pp. 876–882, 2010, doi: 10.1021/cm901668h.

[237] S. S. Devlin, M. Aven and J. S. Prener (eds.), “Physics and Chemistry of II-Vl Compounds,” Wiley, vol. 77, p. 561, 1967, doi: 10.1016/j.ando.2016.07.950.

[238] K. Mahmood et al., “Modulation of thermoelectric properties of Mg2GeO4 thin films by controlling the growth process,” Ceram. Int., vol. 45, no. 15, pp. 18701–18703, 2019, doi: 10.1016/j.ceramint.2019.06.095.

[239] G. H. Jonker, “The application of combined con_ductivity and Seebeck-effect plots for the analysis of semiconductor properties,” Philips Res. Reports, vol. 23, no. 2, pp. 131–138, 1968.

List of Publications

1. A paper title “Synthesis and Characterization of ZnO by Chemical Bath Deposition” published International Science Symposium on Recent Trends in Science and Technology Organized by Christ College, Rajkot & Sponsored by DST, Govt. of India, 2017.
2. A paper title “Effect of concentration of TEA and annealing temperature on band gap of ZnO: A review” published in International Journal of Research in Modern Engineering and Emerging Technology. 2017: 5(9), 100-106.
3. A paper title “Influence of Precursor Concentration on CBD grown ZnO Thin Films” published in International Journal of Scientific Research and Reviews. 2018: 7(1), 446-457.
4. A paper title “Influence of Multiple Layers on Chemical Bath Deposited ZnO Thin Films” published in International Journal for Research in Applied Science & Engineering Technology. 2018: 6(3), 268-274.
5. A paper title “Growth, synthesis, structural and optical properties of pure ZnO by colloidal solution route” published in Journal of Emerging Technologies and Innovative Research 2019: 6(1), 693-699.
6. A paper title “Effect of doping concentration on optical and electrical properties of intrinsic n-type ZnO (i-ZnO) and (Cu, Na and K) doped p-type ZnO thin films grown by chemical bath deposition method” published in Nanosystems Physics, Chemistry, Mathematics, 2020, 11 (4), 391–400.
7. A paper title "Synthesis, optical and photoluminescence properties of undoped and Cu-Doped ZnO thin films by colloidal solution route” published in Molecular Crystals and Liquid Crystals, 2020, 712 (1), 62-75.